UNIVERSITY OF SOUTHAMPTON

FACULTY OF MATHEMATICAL STUDIES
MATHEMATICS

NUMERICAL INVESTIGATION OF FILM COOLING IN A SUPERSONIC MAIN FLOW AND HEAT TRANSFER PHENOMENA IN A SUBSONIC ENVIRONMENT

by
Vassilios Stefanidis

Thesis submitted for the degree of Master of Philosophy

February 1998

UNIVERSITY OF SOUTHAMPTON

ABSTRACT

FACULTY OF MATHEMATICAL STUDIES
MATHEMATICS

Master of Philosophy

NUMERICAL INVESTIGATION OF FILM COOLING IN A SUPERSONIC MAIN FLOW AND HEAT TRANSFER PHENOMENA IN A SUBSONIC ENVIRONMENT

by Vassilios Stefanidis

In this thesis we describe research work that was carried out on the problem of turbine blade film cooling in a supersonic environment. Also we consider a numerical investigation of heat transfer effects on the wall of a turbine blade when the main flow is subsonic. In both cases the flow is considered to be irrotational, incompressible and time independent.

In chapter two we review previous research work that was carried out in order to understand and improve the efficiency of the film cooling method.

In chapter three turbo–jet engines are considered. Their working cycle and the existing methods for cooling their various components are described.

Chapter four deals with the supersonic case of film cooling. It is an extension of work performed by Fitt et al (1985). This is described at the beginning of the chapter together with a discussion of results produced from the subsonic case. Then the supersonic problem is stated together with the analytical and numerical methods used and an extensive discussion on the results produced is also provided.

The heat transfer problem for a subsonic main flow is stated in chapter five. The numerical schemes used to solve the equations are discussed, together with the results obtained.

Finally, chapter six provides an overall discussion on both problems, the results produced and various suggestions for further future work on both cases.

LIST OF CONTENTS

CHAPTER 4

FILM COOLING IN A SUPERSONIC MAIN FLOW

CHAPTER 5

THE HEAT TRANSFER PROBLEM

LIST OF FIGURES

LIST OF TABLES

ACKNOWLEDGEMENT

I would like to thank my supervisor Dr. A. D. Fitt for his guidance, help and encouragement all these years. I also want to thank all the people, staff and students, in the Mathematics Department for making these 3 years very enjoyable. Furthermore, I am very grateful to Dr. J. K. Liakos for the useful comments and remarks during the completion of my thesis. I also want to thank my closest friends for showing me that they believed in me and helping me all the difficult moments. Last but not least I would like to thank my family for being with me all the way all these years of my studies. My sister Terrie for supporting me psychologically and financially the last 2 years, my father Evangelos for his moral and financial help and finally my mother who will always be with me.

CHAPTER 1
INTRODUCTION

1.1. INTRODUCTION

The protection of solid surfaces exposed to high temperatures is a problem that has been investigated thoroughly for many decades. In many cases the high–temperature environments are gaseous. A particularly interesting problem concerns the case where the surfaces which need protection are components of aircraft turbo–jet engines. Many methods have been used for this but one of the most effective is film cooling.

In film cooling air is passed from the engine compressor to the turbine blades and injected into the main stream through slots. Such secondary air has a lower temperature than the free stream and is used not only for cooling the turbine disks and blades, but also to seal any turbine cavities and other internal components from hot gases. This process of maintaining an acceptable temperature in the turbine is very critical due to the fact that higher pressures, temperatures and rotation rates are needed in order to increase the efficiency of an engine. Thus it is imperative for engineers to have an accurate way to predict sealing requirements in order to achieve minimum fuel consumption and better designed long lasting engines and engine components.

The present work deals with the prediction of the mass flow of the injected secondary air in a supersonic environment. It is based on previous work carried out by Fitt et al (1985) for a subsonic main stream. Furthermore, the problem of heat transfer in a subsonic flow and the calculation of the temperature of the wall downstream of the slot, when the injected flow has formed a thin film above the solid

surface has also been considered.

The second chapter of this thesis describes research work performed during the previous decades. Some theoretical models for film cooling are mentioned, together with experimental work. Numerical investigations in both supersonic and subsonic environments are also discussed.

The third chapter considers the turbo–jet engine. Since the scope of this thesis is not to investigate completely a jet engine, it has been decided to provide only information that will be beneficial to the reader and help him/her to become familiarized with the problems that we have looked into. The various parts of the engine, the way it operates and also the different types of turbo–jet engines that have been developed during the years are mentioned here. Finally, different ways of protecting the turbine and its components are also considered. The chapter finishes with a section about the techniques of convection cooling, impingement cooling, transpiration and film cooling. More emphasis, of course, has been given to the last method, since this is the one that has been looked at to more detail in the later chapters.

In chapter four the work carried out by Fitt et al (1985) is extended. The subsonic problem, together with the formulation of the model and the numerical scheme used to solve it are discussed. A summary of the results obtained from the above investigation is also stated. The main part of this chapter consists of the research work performed for the supersonic case. All the theoretical work, the construction of the model, the different methods used to solve the problem and the results produced are discussed.

Chapter five deals with the heat transfer problem. A description of the problem and numerical schemes used together with the calculations are stated. Also the results from the model are analyzed and useful conclusions are drawn.

Finally, chapter six contains all the conclusions from both problems and suggestions are given to the reader for further research in areas that were not touched upon by the present, or previous investigations.

CHAPTER 2
LITERATURE REVIEW

2.1. LITERATURE REVIEW ON BOTH PROBLEMS

Many structural elements of gas turbines, such as nozzle guide vanes (NGVs) and turbine disks are subjected to substantial thermal stresses due to very high temperatures in the turbine (often as high as 2000K). These extreme temperatures, in combination with high rotational speeds, result in large magnitude stresses on the components of the turbine, especially on the blades of the stator. (For a better understanding of the above engine terms the reader should refer to the next chapter and figures 3.1 and 3.2, where a diagram of a turbo–jet engine and a turbine are presented.)

An efficient means of protecting the above components is thus necessary if such stresses are to be minimized, and the safety, reliability, efficiency and operating lifetimes of gas turbines are to be maximized. Thus, in order to maintain the turbine at a moderate temperature the introduction of a protective coolant into the main flow must be used.

The method of film cooling is used extensively in commercial and military applications, particularly on turbine blades, turbine walls, combustion chambers and afterburners. Different methods of film cooling have been developed through the years, but the main ones are the injection of coolant through a single slot, arrays of slots, or a single array of slots. The holes may be either perpendicular to the main flow, or inclined at an angle. A more thorough investigation into film cooling and cooling in general, may be seen in the following chapter, where a simple analysis of

the structure of the turbine and how it works is carried out.

Many researchers have been involved in the study of rotating disks, rim seals, disk–cavity heat transfer and film cooling over the past several decades. Much of the work has been experimental, but one can also find many theoretical approaches to the problem of film cooling and in the investigation of ways to produce techniques to improve the effectiveness of the coolant and to reduce the heat transfer along a turbine blade. In recent years due to the increase and improvements of computers many investigations have been performed by using Computational Fluid Dynamics (CFD) packages, or various numerical methods, such as Finite Element Methods (FEM), or Finite Difference Methods (FDM). All these contemporary techniques (especially CFD methods) have been utilized and proved to be quite successful in predicting with accuracy the film cooling effectiveness of various arrangements and to produce trustworthy references for further investigation into the difficult problems of secondary flow injection and film cooling. In the following pages a literature review of various film cooling methods and heat transfer problems in the turbine are mentioned.

Cole and Aroesty (1968) produced a theory for an inviscid fluid injected from a slot into a main hyper/supersonic stream. The assumption of continuity of the pressure across the dividing streamline created by the main stream and the secondary fluid, was assumed. By matching the outer and inner pressure, the shape of the stream line was found together with the injectant mass flow and the flow downstream of the slot. A similar technique was used to find the shape of the stream line and to calculate the mass flow for the supersonic case that is described in chapter 4.

Experimental work by Metzger and Fletcher (1971) proved that the technique of slot film cooling is more effective than hole injection (array of holes), since the space between the coolant holes allows the hot stream to penetrate through the coolant and reduces the cooling effectiveness.

Metzger et al (1972) followed a different way to investigate film cooling in a subsonic surrounding. They developed a finite difference scheme to predict film cooling and heat transfer downstream from a 2–dimensional slot at 20^o angle, where the fluid is injected into the main stream. They observed flow separation at the end of the slot and came to the conclusion that the length of the flow separation occurring down-

stream from the cavity depends on the angle of injection and that for small injection angles the separation region is smaller. A good prediction of the downstream temperature and velocity was achieved by their numerical scheme and, finally, the heat flow downstream from the slot could be calculated and gave a good agreement when compared with experimental data.

From the theoretical work of Brown et al (1988) the assumption that the pressure inside the airfoil was of magnitude $h << 1$ (where h is the thickness ratio of the airfoil) was used to formulate the supersonic problem (see chapter 4). They suggested a model with typical dimensions for the airfoil: l (length of the chord) and width $O(h)$. A nonlinear flow in the airfoil is assumed with typical velocities: $u = O(h^{\frac{1}{2}})$, $v = O(h^{\frac{3}{2}})$, and $x = O(1)$, where $y = O(h)$. The results produced were compared with experiments and gave good agreement.

Another approach to the problem of film cooling in a supersonic main stream was followed by O'Connor and Haji–Sheikh (1992).They used CFD methods and showed that their approaches were a good approximation to the process of film cooling by comparing their numerical results with experimental ones. They also showed that the cooling effectiveness is very high even a long distance downstream from the slot, due to the separation between the supersonic main stream and the coolant.

Similar results were obtained from a numerical study by Rizzetta (1992). He used a two–equation turbulence model ($\kappa - \varepsilon$) for the same problem (slot injection in a supersonic main stream with a Mach number of 3.7 and a Reynolds number $5.83\text{x}10^6$). His numerical results were compared with experimental data and good agreement between the two investigations was found.

Finally, Cho and Goldstein (1995) conducted experiments to obtain heat and mass transfer coefficients and film cooling effectiveness for a single hole and an array of holes. The results for a single slot arrangement showed that the mass transfer around the slot is affected by the main flow. When the array of holes was used the results obtained were very similar to those from the one hole injection. The cooling effectiveness was very high and almost uniform in the direction of the flow, but not in the lateral direction, across the holes.

The problem of cooling the turbine blade is not the only one that has been under constant investigation for the last few decades. Various other parts of the turbine also need cooling, thus a lot of research has been carried out in order to find ways to improve their protection from the high operating temperatures of the turbine. In the following pages we review a small fraction of previous research work on various turbine components, such as rim seals, NGVs, blade disks and blade tails.

Ito et al (1971) conducted experiments in order to examine the effectiveness of film cooling by a row of jets by measuring the mass transfer from the row. The density and the pressure of the coolant was greater than the main flow and it was found that the film cooling effectiveness was affected a great deal by the blade–wall curvature.

Sinha et al (1991) carried out experimental flow measurements downstream from a second row of holes located 40 hole diameters behind a first row. It was found that a thicker boundary layer existed above the second row of holes, which caused a greater penetration to the main flow. The velocity gradients in the shear layer and consequently the turbulence generated were altered, becoming slightly lower. Finally, it was found that the temperature of the blade at the free stream, due to the injected flow penetration, was lower at the second row of holes which would cause a greater pressure gradient on the layer.

Boyle (1991) compared experimental results of pressure surface and heat transfer against numerical results. The comparisons were for different turbine vane and blade geometries, with separated and unseparated flow, for a range of Reynolds numbers and turbulence intensities. The numerical solution method used was different from the conventional boundary layer method, because in the latter the solution domain was included in the boundary layer region and marching–type methods were used. In the numerical analysis a small fraction of the blade to blade mesh was in the boundary layer region and this requires the solution of the whole flow domain to be carried out in an iterative way. The results for the surface pressure from the numerical scheme showed good agreement with experimental data for many different blades. However, a more refined mesh was needed each time there was an abrupt pressure change. The numerical method predicted very accurately the heat transfer for various turbine blades downstream of the separation and in the turbulent region.

Daniels et al (1992) conducted experiments to determine the aerodynamic properties and sealing characteristics of various seals typical of those found on the downstream side of a rotor in a gas turbine. By measuring the mass transfer across the slots the film cooling effectiveness was determined. Their experimental results were in good agreement with those of other scientists. Also, on decreasing the radial gap width of the overlapping radial seal, the cooling effectiveness was increased significantly. However, the increase of the axial overlap of the seal did not improve the situation a lot.

Dadkhah et al (1992) studied experimentally two rim seals with an external flow present. The first seal had an overlapping upstream stator and the second had an upward stator lip downstream. They found that the interaction of the coolant with the main flow had an important influence on the effectiveness of the cooling air. On the other hand, when the pressure difference across the slot was zero, it gave a high estimate of the minimum mass flow required to seal the cavity.

Harasgama and Burton (1992) performed heat transfer experiments and flow visualization experiments on annular cascade or turbine NGVs with and without hole film cooling. The NGVs were operated at the correct non–dimensional gas turbine temperatures, Reynolds number and Mach number. The results indicated that high cooling effectiveness can be achieved when the holes are placed along an iso–Mach line. Also the Nusselt number ($Nu = \frac{hl}{k}$ where h is the heat transfer coefficient, l the NGV chord and k the thermal conductivity of air) is reduced by up to 75% in the regions close to the slots, but in other areas the reduction does not exceed 50%. Finally, by increasing the blowing rate of the film cooling gas, or reducing the coolant temperature, the heat transfer to the end wall was reduced significantly.

Chew et al (1994) conducted a CFD investigation into a slot injection model with a subsonic main stream, finding that their results were in good agreement with experimental measurements.

McMillin and Lau (1994) performed experimental investigations to study the distribution of the local heat transfer coefficient in the internal cooling area near the tail of a turbine blade. Mass transfer measurements were conducted in a test channel which had arrays of holes at the bottom wall and whose inner regions were exposed

to naphthalene, in order to obtain a uniform temperature. An analogy between heat transfer and mass transfer was used to calculate the distribution of the local heat transfer coefficient for the surface of the channel. The experimental results showed that the local heat/mass transfer coefficients were higher than the corresponding local wall heat/mass transfer coefficients. In experiments with side wall flow injection, a small part of the injection flow turned back and exited from the holes, which reduced the cooling mass flow in the channel. Thus it was found that the amount of cooling air coming out from the test surface had to be increased in order to compensate for the lateral mass flow loss and to cool the blade efficiently.

Finally, Amono et al (1994) performed a numerical study for the estimation of the temperature in a rotating disk and in the cavities between the nozzle and blade disk. This study was conducted to understand better the heat transfer at the rotating disks and the turbulence region in the gas turbine, by using computational methods and finite volume techniques. The Navier–Stokes (N/S) equations together with the modelled energy equation for incompressible fluids were used. In order to calculate the turbulent stresses the turbulence model $\kappa - \varepsilon$ was used. Also the technique of "segregation" was used where each part of the solution domain was computed separately. The results obtained showed the interaction of the injected secondary flow and the main gas flow in the form of temperature distributions (contours) and velocity vectors through the disk. It was shown that the "segregation" method was an efficient method to use since it used smaller meshes, i.e. fewer grid points, which required less CPU time and storage. Finally, the computational method used could be easily adapted to calculate optimum cooling conditions for any rotating blade disks in a turbine.

The problem of determining the optimum mass flow needed for efficient film cooling of a turbine blade in a sub/supersonic domain and of heat transfer in the presence of film cooling are two closely related existing problems. The literature which is available for both problems is really vast and it would have been impossible to include it all, or a large part of it, in this thesis. Thus only a small number of previous published research work has been discussed.

CHAPTER 3
THE TURBO–JET ENGINE AND THE PROCESS OF COOLING TURBINE COMPONENTS

3.1. INTRODUCTION

The mechanical arrangement of a turbo–jet engine is relatively simple, for it consists only of two main rotating parts (a compressor and a turbine) one or more combustion chambers and an exhaust system. Figure 3.1 shows a typical turbo–jet engine.

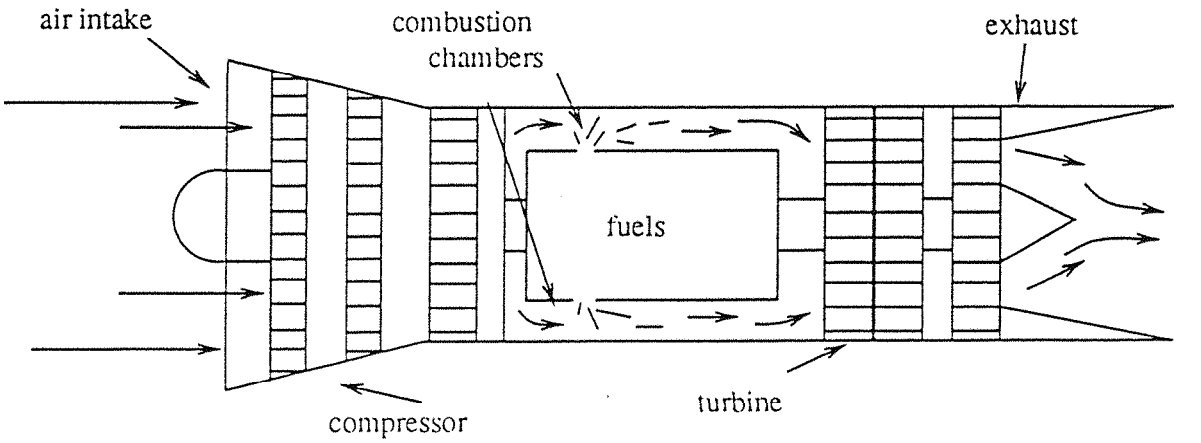

FIGURE 3.1. A typical turbo–jet engine

In a commonly used turbo–jet engine air enters the inlet and it is compressed as it passes through a number of blade rows which are stationary and rotating. The collection of rotating blades is referred to as the rotor and the arrangement of stationary blades as the stator. After the air is compressed, it leaves the compressor section and enters the combustion chambers where fuel is injected through nozzles into the compressed air and the resulting fuel–air mixture is burned. It has been found that only 25% of the compressed air is used for combustion. The remainder bypasses the fuel nozzles and mixes downstream of the combustion section with the mainstream gases in order to cool these hot gases before entering the turbine. The mixture, at a very high temperature, expands in the turbine and a small part of it is driven to the exhaust of the engine, where it is discharged to the atmosphere. In this way the exhaust system provides the gas momentum required to produce the thrust to move the aircraft. The remaining air is used by the turbine to extract shaft energy and drive the compressor.

In the following sections we discuss briefly the various components of a turbo–jet engine together with the working cycle of a typical engine and the methods of protecting the turbine from the hot operating gases. The reader is referred to Kerrebrock (1977) and to the book published by the Rolls–Royce Co. (1966) for further details.

3.1.1. The Compressor

The compressor, or diffuser, and the turbine are the two parts of the jet engine that consist of rows of rotating blades (rotor) and stationary ones (stator) to accelerate and diffuse the air.

The compressor controls the pressure ratio of the engine (especially at low Mach numbers) thus has a dominant influence on the gas turbine engine. It is one of the most difficult parts of the engine to design and develop, since it involves complex aerodynamics, design and testing. All of these are time–consuming and expensive procedures, thus in the last decade it has received extended emphasis at both research and development levels.

As the air enters the engine, it is diffused and compressed together with the fuel at high pressure and in large quantities it passes to the combustion chambers.

There are two types of compressors: axial and radial flow respectively. In the former the air passes parallel to the rotational axis of the engine, through a number of blade rows that are alternately rotating and stationary. Most modern engines use this particular compressor configuration.

Early gas turbine engines used a radial compressor. The air is turned radially outwards by the rotating blade row near the centre. As the air flows out of the rotor, it acquires a tangential velocity component and is compressed. A scroll, or radial diffuser collects the compressed air and feeds it back to the combustion chambers. Centrifugal (radial) compressors were used in early jet engines and nowadays for automotive applications.

3.1.2. The Combustion Chamber(s)

After the compressed air leaves the compressor section, it enters the combustion section, where the mixture of the compressed air and fuel is burned. Typically the ratio of air to kerosene fuel (by weight) is 60:1. However, as it is already mentioned, only 25% of the air is used to support combustion. The remaining is used to reduce the temperature of the hot gases entering the turbine, or to protect the turbine components.

In order for the fuel to be burned efficiently a flame tube, called a combustion liner, is used to monitor the airflow distribution in the chamber. The resulting heat accelerates the expanded air in such a way that it creates a smooth stream of heated gas. The whole process of combustion must be achieved with minimum pressure loss and with maximum heat release. Under these conditions the mixture can reach temperatures of up to 1500°C.

3.1.3. The Turbine

Everything that has been mentioned about the compressor applies equally well to the turbine, but two factors make the major differences between the turbine and the compressor. Firstly, the high gas temperature and pressure cause material problems to the turbine components that are much more serious than those in the compressor. However, the high temperature leads to lower tangential Mach numbers for the

turbine blades compared with the compressor blades of the same size, which causes fewer aerodynamic problems. Secondly, though the pressure drops in the turbine it increases in the compressor. This pressure decrease thins the boundary layer, reducing separation problems and making the aerodynamic design less critical.

The turbine is the second rotating part of a jet engine. It provides the power for driving the compressor. It consists of a row of nozzle guide vanes, air seals, a rotor and a stator; figure 3.2, shows the cross–section of the turbine as the air from the compressor enters the turbine (normal to the air flow).

The nozzle vanes are used to turn the expanded gas flow around the axis of the engine and at the same time to drop the pressure and the temperature in the turbine while raising the Mach number. In this way the turbine is able to provide the power and the energy for driving the compressor, (which is 75% of the combustion energy) and 25% represents the kinetic energy of the exhaust which provides the thrust. Finally, the air seals provide the internal cooling of the turbine.

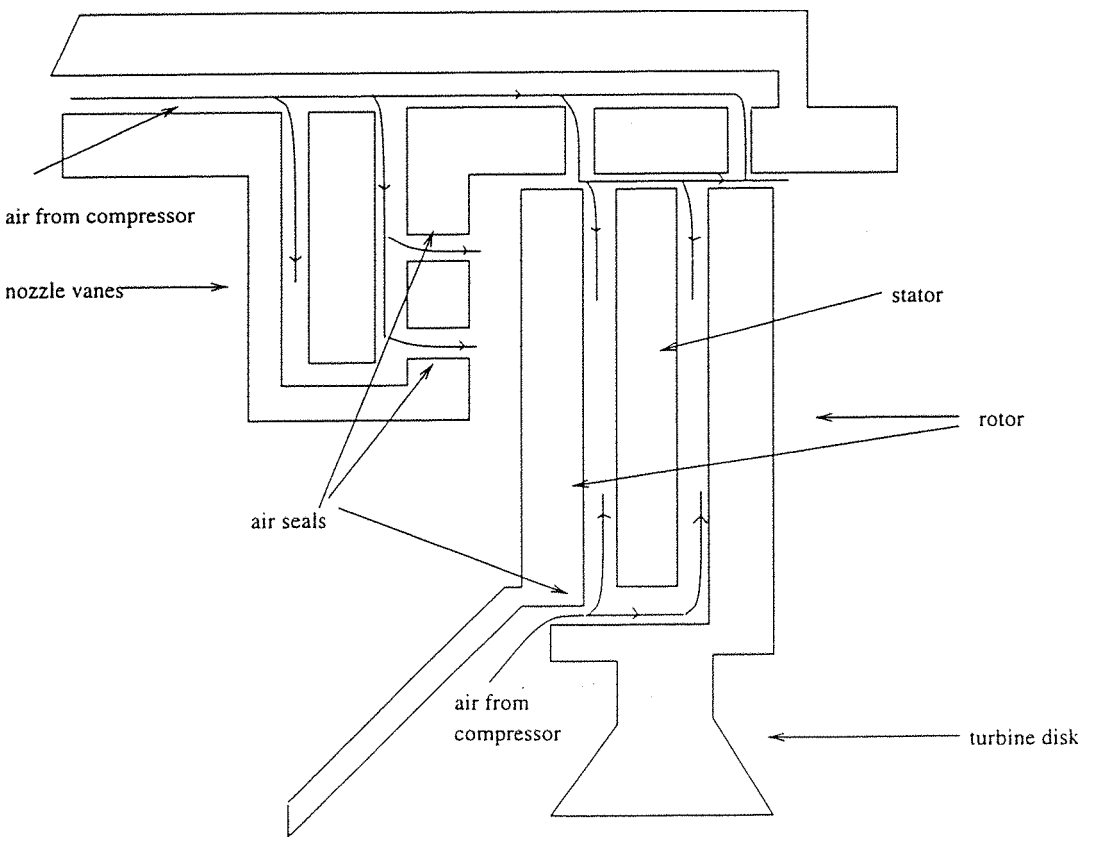

FIGURE 3.2. The cross–section of a turbine

3.1.4. The Exhaust System

The turbo–jet engine has an exhaust system which passes the discharged gases from the turbine to the atmosphere at high velocity and pressure. In this way the required thrust to move the aircraft is produced.

The exhaust can influence the performance of the engine, since the design of the exhaust system affects the turbine entry temperature, the mass flow of the air entering and exiting the exhaust and the velocity and pressure of the outcoming jet.

3.1.5. The Afterburner

Many jet engines have an additional component at the end of the turbine: the afterburner.

As mentioned before, only 25% or so of the air is used to support combustion, thus there is sufficient oxygen in the turbine exhaust to support additional burning. An afterburner is simply a large pipe placed near to the rear of the engine. Fuel is injected from a row of fuel nozzles, called spray bars, into the front area of the afterburner and is ignited. This heat expands the exhaust, providing an increase in the exhaust velocity and consequently in the thrust. Afterburning can more than double the thrust of a gas turbine engine, but with an increase in fuel consumption.

The jet engine uses the basic principles of propulsion. Jet propulsion is a practical application of Newton's third law of motion which states that *'for every force acting on a body there is an opposite and equal reaction'*. In aerodynamic terms, the 'body' is the atmospheric air which is accelerated as it passes through the engine. The force required to give this acceleration has an equal and opposite effect on the apparatus producing the acceleration.

A jet engine produces thrust in a similar way to the propeller/engine combination but whilst the latter gives a small acceleration to a large weight of air, the former gives a large acceleration to a small weight of air.

3.2. THE OPERATION OF A JET ENGINE

The turbo–jet engine operates on the 'working cycle' that is described in the book published by the Rolls–Royce Co. (1966) and will also be discussed in this section.

The engine draws air from the atmosphere and after compressing and heating it the energy and momentum given to the air forces it out of the propelling nozzle at velocities that can reach up to 1400 mph. On its way through the engine the air gives up some of its energy and momentum to drive the turbine that powers the compressor. The working cycle of the turbine engine consists of four continuous processes: induction, compression, combustion and exhaust. This continuous cycle gives a smoother running engine and enables more energy to be released for a given engine size. The working cycle of the gas turbine engine is an example of a Carnot cycle and is represented in figure 3.3.

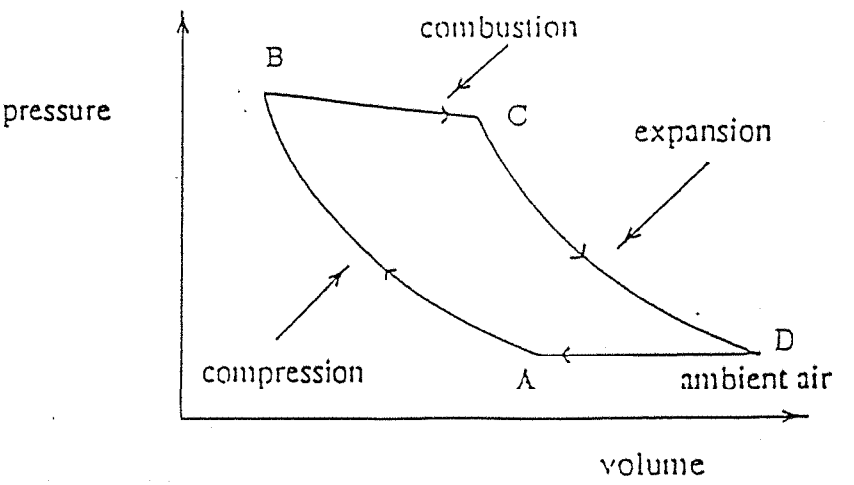

FIGURE 3.3. The working cycle of a turbo–jet engine

At point A the air at atmospheric pressure enters the engine. Along the line AB the pressure and the temperature are increased and at the same time its volume is decreased. In the compression process the pressure can be increased up to about 229 N/m^2. At the same time the velocity falls to under 160 m/sec., whereas the temperature goes up to about 300°C. During combustion, line BC, fuel is added to the air and burnt. This increases the volume and temperature of the air considerably.

The temperature increases to about 900°C and the velocity drops slightly. There is a small loss of pressure in the combustion chambers, indicated by the slope of the line BC. From C to D the gases expand through the turbine and exit the engine from the exhaust, back to atmosphere. In the expansion stage the pressure drops abruptly to less than 90 N/m^2. The temperature also falls, but the velocity and volume of the gases are increased considerably. During this part of the cycle some of the energy of the expanding gases is turned into mechanical power by the turbine and the remainder is discharged to the atmosphere, providing the propulsive jet. Finally, the exhaust gases return to atmospheric pressure, illustrated by the isobaric line DA.

3.3. DIFFERENT TYPES OF TURBO–JET ENGINE

For a number of decades variations of the gas turbine jet engine have been developed. Each type has its own characteristics and uses. Nevertheless, the general concepts and the design remain the same. In this section we will state, briefly, some characteristics and advantages and disadvantages of each engine. For a more detail discussion the reader is referred to Kerrebrock (1977).

3.3.1. The Ramjet Engine

The ramjet engine is the simplest of all, because it consists only of a diffuser (compressor), a combustion chamber and an exhaust nozzle. The design of the ramjet has made it suitable for supersonic aircrafts, because air can enter the compressor in hypersonic flow and can be diffused to supersonic speed before it is driven to the combustion chambers where fuel is added to the air. Thus the mixture can exit the engine at supersonic speed. Due to high temperatures developed in the engine the walls of the combustion chambers must always be kept much cooler than the main flow temperature by introducing a layer of cool air next to them. Thus the relatively high temperature allows operations at high flight Mach numbers.

A disadvantage of the ramjet engine is that the pressure ratio is limited by flight speed and diffuser performance. This means that a ramjet engine cannot develop static thrust (cannot accelerate a vehicle from a standing position). Furthermore, it is very difficult to design an efficient diffuser, due to the presence of shocks (unavoidable

in supersonic operation). Thus the development of a large supersonic diffuser with performance is difficult and at present extensive experimental work and testing are still being conducted.

3.3.2. The Turbofan Engine

The turbofan engine can increase the thrust efficiency of the engine, for a given fuel–consumption rate, by increasing the air flow. This is achieved by introducing a second turbine downstream from the main compressor–drive turbine. With the generated power a fan is used to extract energy from the main hot flow, thus reducing the velocity and the temperature of the exiting gases. This energy is supplied by the fan to a secondary flow to bypass the combustion chamber and the turbine and mix with the mainstream flow before the two flows are discharged through a common exhaust system to the atmosphere. A turbofan can also be modified to include an afterburner.

Since the speed of the expanded gases is lower than of those of the other engines, the turbofan can achieve a reduction in noise. Finally, the decrease in the temperature of the hot gases before the exhaust nozzle means that the discharged jet of air is less detectable to infrared scanning, that is possibly why turbofan engines are widely used in high–performance military aircrafts.

3.3.3. The Turboprop and Turboshaft engine

A turboprop engine produces a small amount of jet thrust in comparison to the shaft power that it can develop. The largest amount of the hot gases from the combustion chambers is extracted by the turbine to use it to provide shaft power to turn a propeller situated in the front section of the engine. The turbine is mechanically independent of the gas generator rotor components; this arrangement is called a free-turbine configuration and has the advantage of flexibility in meeting a range of performance requirements. This flexibility comes as a result of the variation of the pitch of the propeller. By changing the pitch the efficiency (defined as the ratio of the propulsive to the supplied power) can be maintained at a constant level over a large speed range.

The main disadvantage of the turboprop is that at higher subsonic Mach numbers (above 0.5) its performance deteriorates and the engine becomes very noisy. This is because at high speeds the velocity of the propeller tips become supersonic and compressibility effects reduce the engine efficiency. However, high speeds may be achieved if propellers with many blades turn slowly. Another disadvantage of the turboprop is that it is heavy due to the additional weight of the mechanical components of the propeller.

Since the generated thrust from the exiting gases is low a turboprop engine can only be used for small aircrafts of some special purpose, i.e. petrol aircrafts, or for long flights where high speeds are not essential.

A turboshaft engine may be defined as a gas turbine engine that is used to provide only shaft power. It is very similar to a turboprop engine, except that it incorporates a free turbine that is independent of any compressor stage. Hot gases are expanded to a lower pressure in the turbine, providing greater shaft power and little exhaust velocity. A turboshaft engine is ideal for helicopters and also electric utilities that have to meet peak power load demands.

3.4. THE COOLING OF THE TURBINE

Although the concept of the jet engine is simple, complex thermodynamic and aerodynamic problems may occur which can destroy the whole engine. They result from the high operating temperatures, (typically 900°C–1000°C), of the combustion chambers and turbine, the effects of varying flows across the compressor and turbine blades, and the design of the exhaust system through which the gases are ejected to form the propulsive jet.

High turbine inlet temperatures have great advantages for the turbine engines of aircraft, since they produce higher thrust. Thus they can increase the power and the efficiency of the whole turbine. Nevertheless, these high gas temperatures that exist in the turbine may cause serious structural problems, even to high–temperature resisting materials. These problems and the necessity to provide high efficiency at high temperatures have led engineers to investigate possible solutions for protecting

the turbine. Studies of the cooling of the turbine and its parts were first performed in the late 1940s and the research continued in the 1950s, as indicated by Oates (1985). Around 1960 turbine cooling was first introduced in commercial aircraft engines. Since then higher operating temperatures have been used, making the process of cooling even more important.

Usually, during the cooling process a part of the discharged compressor flow is used as coolant fluid. This large quantity of flow reduces some of the advantages of using high turbine temperatures. The air used for cooling reduces the capability of the turbine to drive the compressor because of the lower temperature at which it enters the turbine, which means that there are pressure losses. Also the cooling air mixes with the main stream air of the turbine and aerodynamic losses are caused. The gas losses associated with the cooling are: profile losses (due to viscous shear on the blade surfaces), secondary flow losses, losses due to the vorticity of the main stream and the viscous effects as the gas passes the blade tips (the boundary layer increases) which affects the engine efficiency, and losses due to air leakage past the blade tips.

The leakage in the turbines is more critical than that happening in the compressors due to the pressure difference across a blade row. In the case of estimating secondary losses, the existing methods are still under development. The profile losses in the turbine can be caused either by the local supersonic boundary layer losses (shock waves), or by an adverse pressure gradient (when the pressure gradient changes from a low to a high pressure): the pressure increases rapidly and the boundary layer thickens (since the boundary layer fluid is decelerated), the flow in the layer stops following the direction of the surface, separates, and the transition happens earlier on the suction surface. These effects described above are important. Therefore, a lot of work has been done in this area in order to minimize them by minimizing the quantity of the cooling air, whilst at the same time retaining the cooling effectiveness at the required levels. If an efficient way of cooling the blades and the other parts of the turbine is provided then higher operating temperatures may be used, which means more power and efficiency.

Although many methods have been suggested for cooling the turbine, only direct

air cooling has been sufficiently successful. With this method air, which is cooler than the operating hot gases, passes from the compressor and is introduced into the turbine blades. As the air enters the turbine, it also cools the turbine disc and the nozzle vanes. From the air seals the cooler air is carried outwards at high pressure, across the turbine, to the exhaust gas flow, which is at low pressure, and prevents the hot gases from flowing inwards into other primary components of the engine.

The cooling air can also be used in the following ways singly, or in combination, (see figure 3.4).

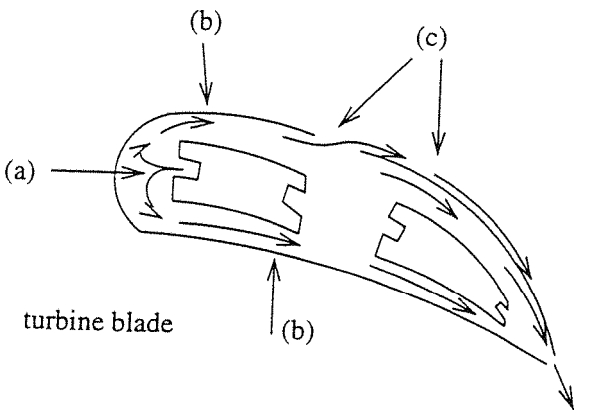

FIGURE 3.4. Diagram of an air–cooled turbine blade with three different types of cooling: (a)impingement, (b) convection and (c) film cooling

Convection cooling: cooling air flows inside the turbine vane, or blade passes through complex paths and geometries and exits through the blade tip, or through holes in the trailing edge. This form of cooling is limited to blades and vanes in the area where the gas temperature is not that high. Also, convection can be used only when the cooling effectiveness levels are about 0.5, Oates (1985). This is due to the fact that the supplied air pressure is limited and if better cooling is required then a higher pressure supply must be used.

Impingement cooling: is a form of convection cooling accomplished by directing cooling air against the inside surface of the airfoil through small, internal, high–velocity air jets. Impingement cooling is concentrated at critical sections of the turbine, such as the leading edges of the vanes and the blades.

Transpiration cooling: the coolant enters the main stream from a porous surface. It is a quite effective method, since it can protect the wall from heat transfer effects by injecting the cooling air exactly where the heat transfer is higher. Nevertheless, it is difficult to introduce this air with such a fine distribution, since sometimes the holes of the porous media may be blocked, or clogged, which could lead to inadequate cooling. Thus, in practice transpiration cooling is not very effective.

Film cooling: is the process in which a layer of cooling air is introduced to the main flow, by a slot or an array of holes inclined, or perpendicular, to the free stream, and it produces a thin layer which shields the area downstream of the slot from the hot gases. It can be used for most of the turbine components, but mainly it is used for the blades and vanes.

The cooling air mixes with the main flow in the boundary layer and it reduces the temperature downstream of the slot and at the same time it decreases the heat transfer along the wall of the blade. Owing to the considerable mixing of the main hot gases and the secondary flow, the method of film cooling does not apply for a long distance downstream from the slot. However, of all the above methods, film cooling is considered the most effective way to protect the turbine and its components and the least demanding method as far as airflow is concerned. More information on all the methods of cooling described above can be found in Barnard & Philpott (1989), Kerrebrock (1977), Oates (1985) and in the book published by the Rolls–Royce Co. (1966).

In the chapters to follow it may be seen that the research work discussed is based on film cooling and one of the main concerns has been to predict the injected mass flow needed to maintain an acceptable temperature in the area of the film and along the wall.

CHAPTER 4
FILM COOLING IN A SUPERSONIC MAIN FLOW

4.1. INTRODUCTION

The efficiency and the life expectancy of a jet engine depends greatly on its effective cooling. The higher the temperature of the gases entering the turbine the higher will be the efficiency for a given jet temperature. Nevertheless, these high operating temperatures cause problems to many parts of the turbine. In order to avoid these problems an efficient method of cooling the various parts of the turbine must be used.

Cooling the turbine by film cooling is found to be the most effective method. In this method cool air enters the turbine from the compressor and it cools the turbine disc and the nozzle vanes. This secondary flow of air, at lower temperature, is introduced into the boundary layer to produce an insulating film between the turbine and the main hot gas flow. The driven cool air, which is at a higher pressure than the hot gases that enter the turbine, prevents the exhaust gas flow from flowing inwards into the components of the engine and destroying them. The injected flow, due to its lower temperature, reduces the temperature in the region downstream of the injection. It is assumed that in the boundary layer there is a uniform temperature, due to the mixing of the main flow and the cooling air. As it has been said before, further down from the injection hole there is a considerable mixing of the secondary fluid and the main flow. Nevertheless, if the cooling of the turbine is efficient then higher operating temperatures and pressures can be used in order to increase the whole

engine performance and to optimize the fuel consumption.

Much study has been carried out on various aspects of using film cooling as a practical method for cooling a turbine and its components. As we already know, the mass of the injected flow is vital to the performance of the whole engine. Thus, if the optimum amount of mass flow needed to protect the turbine is used then the efficiency of the engine will increase.

In the next section we will discuss, briefly, the experimental and theoretical work of Fitt et al (1985) on the problem of finding this optimum amount of mass flow in the case where the main stream is subsonic, and in the section 4.3 we will discuss the problem where the main flow is supersonic.

The discussion of the subsonic problem is essential for the reader in order to understand fully the physics and the mathematics behind the process of film cooling. Also the author of this thesis, by studying and recalculating some of the results, had the opportunity to understand better the work of Fitt et al (1985) and to solve the supersonic case.

4.2. THE SUBSONIC FILM COOLING PROBLEM

Fitt et al (1985) have suggested a simple model for the injection of fluid from a slot into a main stream. The injected flow produces a thin layer which separates the secondary flow from the free stream, figure 4.1. The separation of the injected flow may occur at the end of the slot, but further down the flow will reattach.

The secondary flow and the main stream are both taken to be inviscid, incompressible and irrotational, so that both flows satisfy the condition for irrotational flow, i.e. $\nabla^2\Phi_o = 0$ and $\nabla^2\Phi_i = 0$, where Φ_o is the velocity potential of the main flow and Φ_i is the velocity potential of injected flow. We have also assumed that the injected flow is thick compared with any viscous layers, so justifying the assumption of inviscid flow. Furthermore, a small pressure difference, Δp, has been considered to exist between the free stream and the flow in the slot. Also the total outer pressure is taken to be slightly greater than the slot pressure and this pressure difference means that the injected flow separates tangentially from the front edge of the slot. This

phenomenon leads to the 'lid' effect over the upstream edge of the slot, which causes the injected fluid to come out of the slot only in small quantities from the downstream edge.

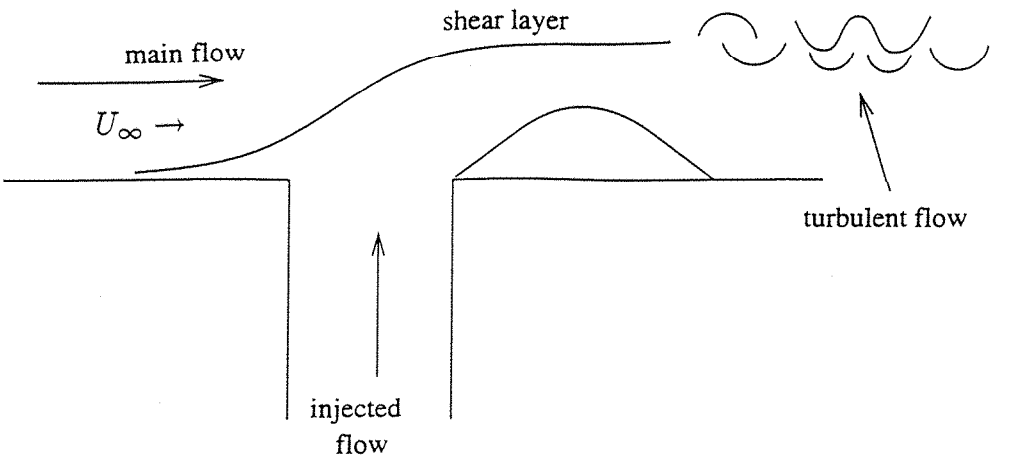

FIGURE 4.1. Diagram of the slot problem

The velocity of the main flow is taken to be U_∞, the main stream static pressure is p_∞, ρ_∞ is the density of the fluid of the main flow, the mass flow of the injected fluid is M, $\mathbf{q}$ is the fluid velocity and the slot has width L, figure 4.2.

The total outer pressure is given by $p_{t\infty} = p_\infty + \frac{1}{2}\rho_\infty U_\infty^2$ and the total pressure in the slot is slightly different: $p_{ti} = p_\infty + \frac{1}{2}\rho_\infty U_\infty^2 \epsilon^2$, thus defining a small parameter ϵ, where $\epsilon \ll 1$. This means that the parameter is defined in such a way to describe a small perturbation to the main flow. This perturbation affects the region of the slot and the film downstream of the slot.

Across the dividing streamline, $y = S(x)$, the pressure must be continuous, thus from the difference of the order of magnitude of the perturbations between p_∞ and the slot pressure we can deduce that the film has thickness of $O(\epsilon^2 L)$ (since we know that an obstacle of thickness of $O(\epsilon^2)$ produces a perturbation to p_∞ of $O(\epsilon^2)$). For the pressure of the slot and the film to be of the same order of magnitude, the film pressure must be within $O(\rho_\infty U_\infty^2 \epsilon^2)$ of p_∞, thus the horizontal velocity component,

u, in the film is of order $U_\infty \epsilon$, which is substantially different to the main horizontal velocity which is of order of U_∞. Thus a vortex sheet is created which separates the main flow and the injected flow.

In the film we have established that the tangential velocity is $O(U_\infty \epsilon)$, meaning that the mass flow must be of order $U_\infty \epsilon^3 L$ (since in general $M = U\delta$, where U is the velocity of the flow in the film, which has thickness δ). From the conservation of mass, the mass flow in the slot must be equal to the mass flow in the film, thus M in the slot is also of order $U_\infty \epsilon^3 L$, and thus the vertical velocity in the slot is $O(U_\infty \epsilon^3)$. We will make an assumption here that these orders of magnitude apply all the way to the top of the slot. In fact there will be a small region to the downstream edge of the slot where this will not apply, because the outer flow treats this region as a point source of the fluid. However, we can disregard this region to lowest order.

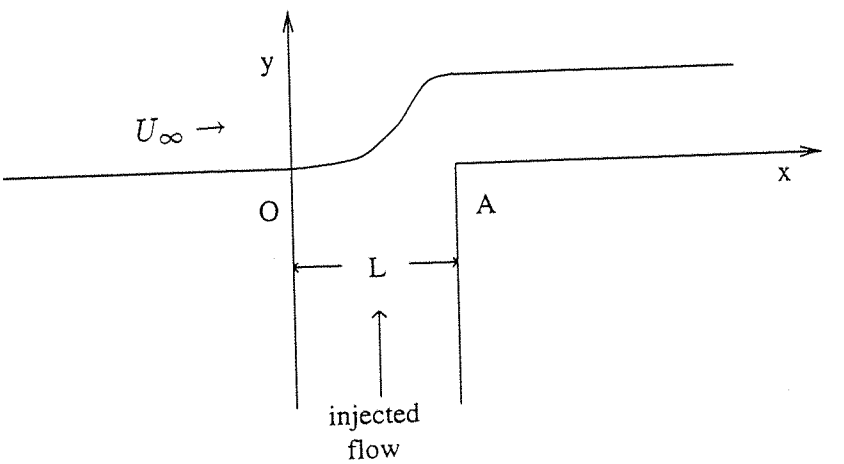

FIGURE 4.2. The simplified model

Now that we have established the orders of magnitude of all the variables we can calculate the pressure for each region separately.

In the outer flow , as it is been stated already, a perturbation of order ϵ^2 to the main flow exists, which affects the secondary flow downstream of the slot. This small disturbance allows us to approximate the flow problem by using thin airfoil theory.

According to the thin airfoil theory, (described by Van Dyke (1975)), we can treat the slot using a superposition of a uniform stream and a source distribution (also described previously). This means that the equation for the stream function in the outer flow has the form

$$\Psi(x,y) = U_\infty y + \epsilon^2 \frac{U_\infty}{\pi} \int_0^\infty g(t) \tan^{-1}\left(\frac{y}{x-t}\right) dt \tag{4.1}$$

from which

$$u = \Psi_y = U_\infty + \epsilon^2 \frac{U_\infty}{\pi} \int_0^\infty g(t) \frac{x-t}{(x-t)^2+y^2} dt$$

and

$$v = -\Psi_x = \epsilon^2 \frac{U_\infty}{\pi} \int_0^\infty g(t) \frac{y}{(x-t)^2+y^2} dt,$$

where the unknown function $g(t)$ is the source/sink distribution of the disturbance.

In order to find $g(t)$ we must employ the steady version of the kinematic condition of the streamline $y = S(x)$ as $y \to 0$. Therefore

$$(\mathbf{q}\cdot\nabla)(y - S(x)) = 0 \Rightarrow (u\frac{\partial}{\partial x} + v\frac{\partial}{\partial y})(y - S(x)) \Rightarrow$$

$$-uS'(x) + v = 0 \Rightarrow v = uS'(x). \tag{4.2}$$

By substituting the expressions for u and v to the leading order into the kinematic condition, we have

$$U_\infty S'(x) = \frac{U_\infty}{\pi} \int_0^\infty g(t) \frac{y}{(x-t)^2+y^2} dt, \Rightarrow$$

$$S'(x) = \frac{1}{\pi} \int_0^\infty g(t) \frac{y}{(x-t)^2+y^2} dt.$$

As $y \to 0$ it may be seen that the function $\frac{y}{(x-t)^2+y^2}$ has the properties of the delta function, since it is zero for $x \neq t$ and its value is infinity when $x = t$. Thus the integral of this function as $y \to 0$ between $-\infty$ to ∞ is 1.

Also we know that the integral of the above function is part of the stream function given in equation (4.1). Thus we obtain

$$\int_{-\infty}^\infty \frac{y}{(x-t)^2+y^2} dt = 2\left[\tan^{-1}\left(\frac{t-x}{y}\right)\right]_0^\infty = \pi.$$

Substituting these two results into the equation for the kinematic condition we obtain an expression for $g(t)$

$$S'(x) = \frac{g(x)}{\pi}\pi \Rightarrow S'(x) = g(t).$$

Thus it may be seen that the source/sink distribution is equal to the slope of the streamline.

Since the source distribution has been determined we can continue with the solution of the problem, but first it is sensible to normalize the problem in the outer flow, by introducing dimensionless variables (the non–dimensional variables are denoted with a bar). We set $\overline{x} = \frac{x}{L}$, and non–dimensinalize the fluid velocity using $\overline{\mathbf{q}} = \frac{\mathbf{q}}{U_\infty}$, the pressure by $\overline{p} = \frac{p_\infty}{\rho_\infty U_\infty^2}$, the dividing streamline by $\overline{S} = \frac{s}{\epsilon^2 L}$ and the stream function using $\overline{\Psi} = \frac{\Psi}{\epsilon^3 L U_\infty}$. Having established the non–dimensional variables equation (4.2) becomes $\overline{v} = \epsilon^2 \overline{u}\overline{S}'(\overline{x})$.

In order to find the pressure of the main stream we have to use Bernoulli's equation given by the expression: $p + \frac{1}{2}\rho_\infty \mathbf{q}^2 = p_\infty + \frac{1}{2}\rho_\infty U_\infty^2$. Thus the main flow has non–dimensional pressure

$$\overline{p}_o + \frac{1}{2}\overline{\mathbf{q}}^2 = \overline{p}_{t\infty} = \frac{p_\infty}{\rho_\infty U_\infty^2} + \frac{1}{2} \Rightarrow \overline{p}_o = \frac{p_\infty}{\rho_\infty U_\infty^2} + \frac{1}{2} - \frac{1}{2}(\overline{u}^2 + \overline{v}^2), \qquad (4.3)$$

since $\overline{\mathbf{q}} = \sqrt{\overline{u}^2 + \overline{v}^2}$. In order to obtain expressions for $\bar{u}$ and $\bar{v}$ we use their definitions from the stream function. Then the two integral expressions for the velocity components can be written on the line $\overline{y} = 0$ as

$$\overline{u} = 1 + \frac{\epsilon^2}{\pi} \mathcal{C} \int_0^\infty \frac{\overline{S}'(t)}{t - \overline{x}} dt \qquad \text{and} \qquad \overline{v} = 0, \qquad (4.4)$$

where $\mathcal{C}\int$ denotes a Cauchy principal value integral. Thus substituting the above expressions to equation (4.3) we obtain the pressure for the free stream

$$\overline{p}_o = \frac{p_\infty}{\rho_\infty U_\infty^2} + \frac{1}{2} - \frac{1}{2}\left(1 + \frac{2\epsilon^2}{\pi} \mathcal{C} \int_0^\infty \frac{\overline{S}'(t)}{t - \overline{x}} dt\right) \Rightarrow$$

$$\overline{p}_o = \frac{p_\infty}{\rho_\infty U_\infty^2} - \frac{\epsilon^2}{\pi} \mathcal{C} \int_0^\infty \frac{\overline{S}'(t)}{t - \overline{x}} dt \qquad (4.5)$$

In order to complete the model we must consider the flow in the slot and the film downstream of the slot. We also have to find the pressure in each one of the these regions.

In the film region we non–dimensionalize the variables. We set $\overline{x} = \frac{x}{L}$, $\overline{y} = \frac{y}{\epsilon^2 L}$, $\overline{\mathbf{q}} = \frac{\mathbf{q}}{U_\infty}$, and scale the pressure with $\overline{p} = \frac{p_\infty}{\rho_\infty U_\infty^2}$. The streamline is non–dimensionalized by $\overline{S} = \frac{s}{\epsilon^2 L}$, and the non–dimensional stream function is $\overline{\Psi} = \frac{\Psi}{\epsilon^3 L U_\infty}$ and finally the mass flow $\overline{M} = \frac{M}{\epsilon^3 L U_\infty}$. Also for the area of the film we have: $\overline{\Psi} = 0$ on $\overline{y} = 0$; on $\overline{y} = \overline{S}(\overline{x})$ $\overline{\Psi} = \overline{M}$ and on $0 < \overline{y} < \overline{S}(\overline{x})$ $\overline{\Psi}$ is a function of $\overline{x}$ and $\overline{y}$. However, we know that the injected flow is irrotational, meaning that $\nabla^2 \overline{\Phi}_i = 0$ and $\nabla^2 \overline{\Psi}_i = 0$, thus we find, to lowest order, that

$$\frac{\partial^2 \overline{\Psi}_i}{\partial \overline{y}^2} = 0,$$

with the above two boundary conditions ($\overline{\Psi} = 0$ on $\overline{y} = 0$ and on $\overline{y} = \overline{S}(\overline{x})$ $\overline{\Psi} = \overline{M}$) we obtain an expression for $\overline{\Psi}_i$

$$\overline{\Psi}_i = \overline{y} A(\overline{x}) + B(\overline{x})$$

where $A(\overline{x})$ and $B(\overline{x})$ are functions of $\overline{x}$. Now, from the boundary condition $\overline{\Psi} = 0$ on $\overline{y} = 0$ we deduce that $B(\overline{x})$ is zero and by setting $\overline{y} = \overline{S}(\overline{x})$ and $\overline{\Psi} = \overline{M}$ we find that $\overline{\Psi}_i = \overline{y} \frac{\overline{M}}{\overline{S}(\overline{x})}$. This means that $\overline{u} = \overline{\Psi}_{\overline{y}} = \frac{\overline{M}}{\overline{S}(\overline{x})}$ and $\overline{v} = -\overline{\Psi}_{\overline{x}} = \overline{y} \frac{\overline{M}\overline{S}_{\overline{x}}}{\overline{S}^2(\overline{x})}$.

Applying Bernoulli's equation in the film region to the correct order of magnitude we find that the pressure of the film, $\overline{p}_f$, must be equal to the total injection pressure, p_{ti}, thus $\overline{p}_f$ is given by

$$\overline{p}_f + \frac{1}{2}\overline{\mathbf{q}}^2 = \overline{p}_{ti}$$

and using the definition for the total injection pressure, $\overline{p}_{ti} = \frac{p_\infty}{\rho_\infty U_\infty^2} + \frac{1}{2}\epsilon^2$, the above equation becomes

$$\overline{p}_f = \frac{p_\infty}{\rho_\infty U_\infty^2} + \frac{1}{2}\epsilon^2 - \frac{1}{2}\overline{\mathbf{q}}^2, \tag{4.6}$$

but $\overline{\mathbf{q}} = \sqrt{\overline{u}^2 + \overline{v}^2}$ and in the film downstream of the slot we have $\overline{v} = 0$ and the tangential component of the velocity is $\overline{u}\epsilon$. Thus equation (4.6) becomes

$$\overline{p}_f = \frac{p_\infty}{\rho_\infty U_\infty^2} + \frac{1}{2}\epsilon^2 - \frac{1}{2}\epsilon^2 \overline{u}^2. \tag{4.7}$$

Also we know that $\overline{u} = \frac{\overline{M}}{\overline{S}}$, which means that equation (4.7) can be expressed as

$$\overline{p}_f = \frac{p_\infty}{\rho_\infty U_\infty^2} + \frac{1}{2}\epsilon^2 - \frac{1}{2}\epsilon^2 \frac{\overline{M}^2}{\overline{S}^2}. \tag{4.7a}$$

Finally, in the slot $\overline{u} = 0$ and the vertical non–dimensional velocity component is $O(\epsilon^3)$, thus the non–dimensional pressure $\overline{p}_i$ is obtained by using Bernoulli's equation to the right order of magnitude

$$\overline{p}_i + \frac{1}{2}\overline{\mathbf{q}}^2 = \overline{p}_{ti} \Rightarrow \overline{p}_i + \frac{1}{2}\overline{\mathbf{q}}^2 = \frac{p_\infty}{\rho_\infty U_\infty^2} + \frac{1}{2}\epsilon^2, \tag{4.8}$$

where $\overline{\mathbf{q}} = \overline{\Psi}_{\overline{y}}^2 + \overline{\Psi}_{\overline{x}}^2$, but $\overline{\Psi}_{\overline{y}} = 0$ and $\overline{\Psi}_{\overline{x}}$ is $O(\epsilon^3)$, thus $\overline{\Psi}_{\overline{x}}^2$ is $O(\epsilon^6)$. This means that equation (4.8) becomes

$$\overline{p}_i = \frac{p_\infty}{\rho_\infty U_\infty^2} + \frac{1}{2}\epsilon^2 + O(\epsilon^6). \tag{4.8a}$$

From the above equation it may be seen that the pressure in the slot is almost equal to the total injection slot pressure $\overline{p}_{ti}$, since the term $O(\epsilon^6)$ is very small and it does not have any effects on the slot pressure, thus it can be neglected.

In order to complete the model we have to match the pressures on the streamline. The assumption that the pressure is continuous across $\overline{y} = \overline{S}(\overline{x})$ is used. We can drop the bars, for reasons of convenience and use equations (4.8a), (4.7a) and (4.5) to get

$$\frac{1}{\pi}\mathcal{C}\int_0^\infty \frac{S'(t)}{t-x}dt = \begin{cases} -\frac{1}{2} & 0 < x < 1 \\ -\frac{1}{2} + \frac{1}{2}\frac{M^2}{S^2} & 1 < x < \infty \end{cases}, \tag{4.9}$$

as in Fitt et al (1985). The above integro–differential equation must be solved subject to the boundary conditions $S(0) = 0$, $S'(0) = 0$, $S'(\infty) = 0$. The first condition means that the flow separates at the upstream edge of the slot, whilst the second asserts that the flow exits the slot tangentially (zero slope) at the upstream edge of the slot due to the 'lid' effect described earlier. Finally, the third boundary condition means that $S(\infty)$ must be equal to M. In this way the right hand side of equation (4.9) for the interval $x > 1$ will hold and the condition $S'(\infty) = 0$ will be satisfied.

4.2.1. The Numerical Scheme

Equation (4.9) was solved numerically to give a unique solution for M. In order to achieve this first we had to invert the integral of the equation (4.9) and use the boundary condition $S'(0) = 0$. Thus we obtained

$$S'(x) = \frac{x^{\frac{1}{2}}}{2\pi}\mathcal{C}\int_1^\infty \frac{M^2 dt}{S^2(t)t^{\frac{1}{2}}(t-x)}, \tag{4.10}$$

and then M was eliminated from the above equation by a simple scaling $S = TM^{\frac{2}{3}}$, as in Fitt et al (1985). Then equation (4.10) yielded

$$T'(x) = \frac{x^{\frac{1}{2}}}{2\pi} C \int_1^{\infty} \frac{d\xi}{T^2(\xi)\xi^{\frac{1}{2}}(\xi - x)}, \tag{4.10a}$$

Fitt et al (1985). Equation (4.10a) was integrated with respect to x subject to the condition $T(0) = 0$ to obtain the following expression for $T(x)$

$$T(x) = \frac{1}{2\pi} \int_1^{\infty} T^{-2}(\xi) \left\{ -2 \left(\frac{x}{\xi} \right)^{\frac{1}{2}} + \log \frac{\xi^{\frac{1}{2}} + x^{\frac{1}{2}}}{|\xi^{\frac{1}{2}} - x^{\frac{1}{2}}|} \right\} d\xi \tag{4.11}$$

which was evaluated numerically, since the above equation did not include any singular integrals or derivatives. Discritizing $T(x)$ and assuming that it was piecewise constant on the interval (ξ_k, ξ_{k+1}), where $k = 1...N$, for each x then

$$2\pi T(x_i) \approx \sum_{k=1}^{N} T^{-2}(\xi_k) \int_{\xi_k}^{\xi_{k+1}} \left\{ -2 \left(\frac{x_i}{\xi} \right)^{\frac{1}{2}} + \log \frac{\xi^{\frac{1}{2}} + x_i^{\frac{1}{2}}}{|\xi^{\frac{1}{2}} - x_i^{\frac{1}{2}}|} \right\} d\xi + E_N \tag{4.12}$$

where $i = 1...N$ and E_N was the error term defined as

$$E_N = \int_{\xi_{N+1}}^{\infty} T^{-2}(\xi_k) \left\{ -2 \left(\frac{x_i}{\xi} \right)^{\frac{1}{2}} + \log \frac{\xi^{\frac{1}{2}} + x_i^{\frac{1}{2}}}{|\xi^{\frac{1}{2}} - x_i^{\frac{1}{2}}|} \right\} d\xi.$$

The error term was needed in order for equation (4.12) to give us good accuracy for $T(x)$ when $x \to \infty$, since the mesh could not practically be extended to infinity. The above expressions were then integrated with respect to ξ and the error term calculated for large ξ_{N+1} to give the following numerical relaxation scheme

$$\begin{aligned} 2\pi \overline{T}_{j+1}(x_i) &= \sum_{k=1}^{N} T_j^{-2}(\xi_k) A_{ik} + 2x_i T_j^{-2}(\xi_{N+1}) Q(\alpha) \\ T_{j+1}(x_i) &= T_j(x_i) + \theta(\overline{T}_{j+1}(x_i) - T_j(x_i)), \qquad (i = 1...N, j = 1...). \end{aligned} \tag{4.13}$$

where

$$\alpha = \left(\frac{\xi_{N+1}}{x_i} \right)^{\frac{1}{2}},$$

$$Q(\alpha) = \alpha + \frac{1}{2}(1 - \alpha^2) \log \frac{\alpha + 1}{\alpha - 1},$$

$$A_{ik} = 2x_i^{\frac{1}{2}}(\xi_k^{\frac{1}{2}} - \xi_{k+1}^{\frac{1}{2}}) + (\xi_{k+1} - x_i)\log\frac{\xi_{k+1}^{\frac{1}{2}} + x_i^{\frac{1}{2}}}{|\xi_{k+1}^{\frac{1}{2}} - x_i^{\frac{1}{2}}|} - (\xi_k - x_i)\log\frac{\xi_k^{\frac{1}{2}} + x_i^{\frac{1}{2}}}{|\xi_k^{\frac{1}{2}} - x_i^{\frac{1}{2}}|}$$

for the flow problem in the interval $[1, \infty)$. The solution for the region of the slot was then calculated by using equation (4.12).

The above method, equation (4.13), was used to calculate $T(x)$ for the interval $1 < x < \infty$ by using initial guessing values $T_0(x)$. The calculations for $T(x)$ would stop when the results of the previous $T(x)$ coincided with the values of the new $T(x)$ to 5 d.p. Finally, the value for the mass flow was obtained by using the expression $M = T(\infty)^3$.

The numerical scheme produced by Fitt et al (1985) was used by the author of this dissertation to recalculate the mass flow for the region of the film. This was achieved by writing a FORTRAN code which used this numerical method. In order to estimate $T(x)$ a positive initial guess value for $T(x)$ was needed together with a relaxation parameter $\theta < 0.1$. After several iterations the value of $T(\infty)$ was found to be 1.024 and the corresponding mass flow was calculated as $M = T^3(\infty) = 1.075$.

The reader is referred to Fitt et al (1985) for a more detailed discussion of the above analytical and numerical solution.

4.2.2. Results and Discussion

The computer code written for the numerical method described in the previous section, was tested for various meshes with different step sizes. For each run the user could decide the length of the grid by using different number of points. In each case the values of $T(1)$ and $T(\infty)$ were compared. Several different tests were performed which are described below; other cases can also be seen in Fitt et al (1985).

For the first set of tests the step length was kept constant, ($\Delta x = 0.2$), but each time the number of points in each mesh was increased, i.e. the mesh was extended along the x direction. It was found that the time needed for each iteration increased as the number of points was increased. On the other hand the values of $T(x)$ were found to converge faster, i.e. it was taking less time for the values of $T(x)$ to coincide with the results of the previous $T(x)$, in 5 d.p.

The table 4.1 includes results for a number of different meshes and also shows the values for $T(1)$ and $T(\infty)$ for these meshes. It may be seen that the value for $x = 1$ converged to $T(1) = 0.552$ (in 3 d.p.) and that the value of each $T(\infty)$ increased as the x values moved away from the origin.

Mesh length	Mesh points	$T(1)$ values	$T(\infty)$ values
$1 \leq x \leq 2$	6	0.561	0.889
$1 \leq x \leq 4$	16	0.531	0.956
$1 \leq x \leq 7$	31	0.552	0.983
$1 \leq x \leq 9$	41	0.552	0.991
$1 \leq x \leq 10$	46	0.552	0.993
$1 \leq x \leq 14$	66	0.552	0.999

TABLE 4.1. Values of T(1) and T(∞) for constant step

Another set of runs was performed to investigate the convergence of $T(1)$ and $T(\infty)$ when the mesh was taken to be fixed, it was extended up to $x = 2$, see table 4.2. This time the step length and the number of mesh points were changed with every test of the program. For each run the values of $T(x)$ at $x = 1$ and $x = 2$ were compared. It was found that the computational time taken for each iteration was increased when the step length decreased, but the numerical method converged to the correct values of $T(x)$ faster than in the previous case. Also from this table it may be seen that $T(x)$ for $x = 1$ converged to a value close to 0.527, whereas the values for $T(2)$ were found to converge to $T(2) = 0.892$. The results for $T(x)$ seemed to be in good agreement for most of the meshes, whereas the results for the downstream edge of the slot indicated that good agreement was achieved if many points were used in each mesh.

Δx	Mesh points	$T(1)$ values	$T(2)$ values
0.2000	6	0.561	0.889
0.1000	11	0.547	0.891
0.0500	21	0.538	0.891
0.0010	1001	0.527	0.892
0.0005	2001	0.527	0.892

TABLE 4.2. Values of T(1) and T(∞) for various step lengths

In order to estimate $T(\infty)$ downstream from the slot the mesh had to be extended. This was achieved by constructing an exponential grid in the x-direction.

The expression used in the code to represent this was

$$x_n = x_{n-1} + dx(sf)^{n-1},$$

where dx is the initial step length in the x-direction and sf the scaling factor used to produce the non–uniform mesh.

Various combinations of scaling factors and step sizes were used in order to compare the value of $T(\infty)$ with the numerical value for M obtained by Fitt et al (1985). The step size Δx was kept small and the scaling factor, sf, less than 1.10, in order to have a fairly fine mesh for the whole domain and accurate results to be produced. Also the relaxation parameter θ was taken to be less than 0.1, but not too small because a small value of θ meant that the numerical scheme tended to converge to the solution very slowly, i.e. it needed many iterations in order to obtain the correct result. When Δx was changed the number of points in the mesh changed too. Thus, although we had to use small x steps we kept the number of the mesh points more than 130 during all tests in order to obtain acceptable results, i.e. accuracy to 3 d.p. Finally, the length of the meshes was extended up to about 33 slot–widths.

In table 4.3 some of the different step lengths and scaling factors used may be seen, along with values of $T(1)$ and $T(\infty)$. From the table it may be seen that the value of $T(1)$ converged to 0.518 and the value of $T(x)$ for infinity approached 1.024. Also, the best results were produced for scaling factors in the range of 1.02 to 1.04 with step sizes between 0.001 and 0.008.

Δx	Scaling factor	Number of points	$T(1)$ values	$T(x)$ values
0.001	1.02	327	0.518	T(32.76)=1.024
0.001	1.04	183	0.518	T(32.45)=1.024
0.005	1.02	246	0.518	T(32.73)=1.024
0.005	1.04	142	0.518	T(32.40)=1.024
0.008	1.04	130	0.519	T(32.30)=1.024
0.008	1.07	83	0.520	T(32.30)=1.023

TABLE 4.3. Values of T(1) and T(∞) for non-constant meshes

4.2.3. Conclusions

Numerical tests were conducted in order to compare them with numerical results that Fitt et al (1985) produced for a two-dimensional, time-independent model for the

slot cooling problem. The fluid for both the main and the injected flows was taken to be incompressible and irrotational and the injected flow was assumed to be inviscid.

The most important results of the investigation can be summarized as follows:

(a) The numerical scheme discussed provided a quick and economical way to solve the flow problem.

(b) A scaling factor (exponential mesh) had to be used in order to produce a solution of the problem for meshes that extended for a long distance downstream from the slot.

(c) The model was a good approximation to the viscous problem, but in cases where there was viscous interaction a different approach would possibly have to be used.

(d) The small pressure difference that existed between the main flow and the injected flow affected a great deal the amount of the gas that was coming out of the slot by creating a 'lid' over the slot.

(e) Finally, the model did not take into account the separation of the injected flow that seems likely to occur downstream of the slot.

4.3. INTRODUCTION TO THE SUPERSONIC PROBLEM

The problem of film cooling in a supersonic environment has been of great interest to many researchers over the years and many investigations have been conducted, as we have seen in chapter 2.

The main difference between a supersonic flow and a subsonic flow is the possible formation of shock waves in the former case generated on the leading edge of a body as the main stream passes over its surface with supersonic velocity. The formation of shock waves affects the velocity of the main flow (speed reduction) and gives rise to rapid pressure rises. This means that the thickness of the boundary layer formed by the main flow increases causing earlier separation. These aerodynamic effects show how important it is to design and use correctly the technique of film cooling, since an incorrect use of the method could lead to heat and efficiency problems in the engine.

Before we start analyzing the supersonic problem, it is essential to give the definition of the free stream Mach number M_∞ and to write down the governing equation for supersonic flow. The Mach number is defined as

$$M_\infty = \frac{U_\infty}{a_\infty}$$

where U_∞ is the velocity of the free stream and a_∞ is the speed of sound in the free stream.

The governing equation for a supersonic flow has the general form

$$-B^2\Phi_{xx} + \Phi_{yy} = 0 \tag{4.14}$$

where $B = \sqrt{M_\infty^2 - 1}$ and Φ is the velocity potential. For a derivation of the above linear partial differential equation the reader is referred to Carafoli (1969), chapter 1. In the case where $M_\infty < 1$, we obtain a differential equation of elliptic type (Laplace's equation) and the flow is subsonic. When M_∞ is greater than unity the flow is supersonic and the differential equation that we obtain is hyperbolic.

Finally, we have denoted U_∞ the velocity of the main stream; suppose that the main flow encounters a small disturbance then the flow is slightly deflected, resulting in a velocity U'_∞. Then the main velocity has its two components u and v be written as

$$u = U_\infty + u', \qquad v = v', \tag{4.15}$$

where u' and v' are the components of the disturbance velocity U'_∞. Now we know that for irrotational flow

$$\nabla^2\Phi = 0 \qquad \text{or} \qquad \frac{\partial u}{\partial y} - \frac{\partial v}{\partial x} = 0,$$

but $u = U_\infty + u'$ and $v = v'$ and since U_∞ is a constant, the irrotationallity condition becomes

$$\frac{\partial u'}{\partial y} - \frac{\partial v'}{\partial x} = 0.$$

This means that the potential velocity flow for the resultant main stream may be written as

$$\Phi = xU_\infty + \Phi' \tag{4.16}$$

where Φ' is the perturbation velocity potential and $\Phi'_x = u'$ and $\Phi'_y = v'$. The above equation is also the general solution of the equation (4.14).

After the introduction of the Mach number, the governing hyperbolic equation and the equation of the potential flow, we can move on to the supersonic problem.

4.3.1. The Supersonic Case

We shall consider the problem when $M_\infty > 1$ in the same domain as the subsonic case, namely figure 4.2.

In the main stream the velocity U_∞ is supersonic, whilst under the film the secondary flow has subsonic velocity. The pressure across the streamline is continuous and the total pressures in the film and in the slot are defined as before (section 4.2), together with the small parameter ϵ.

Thus as the flow passes a small disturbance of height $O(\epsilon^2)$ equation (4.16) for our problem becomes

$$\Phi = xU_\infty + \epsilon^2 U_\infty F(x - By) \tag{4.17}$$

where F is unknown and $x > By$. Referring back to equation (4.16) we may note that F represents the perturbation velocity potential of the main stream, also described in Carafoli (1969). In equation (4.17) the function $F(x - By)$ allows constant values of Φ along the lines $x = By + c$ and $x = -By + c$ with an angle $\tan^{-1}(\pm\frac{1}{B})$ to the x-axis; these lines are known as Mach lines. All disturbances created at the surface propagate unchanged away from the wall along the Mach lines. Since disturbances cannot be propagated forwards into supersonic flow the lines are inclined downstream. In addition, the effect of the disturbance is felt only in the region between the first and last Mach lines.

Using the steady version of the kinematic condition, $y = S(x)$, as $y \to 0$ we obtain, as before,

$$(\mathbf{q}\cdot\nabla)(y - S(x)) = 0 \Rightarrow (u\frac{\partial}{\partial x} + v\frac{\partial}{\partial y})(y - S(x)) \Rightarrow$$

$$-uS'(x) + v = 0 \Rightarrow v = uS'(x). \tag{4.18}$$

At this point we must non–dimensionalize the variables again. The normalization is the same as in section 4.2. Thus we non–dimensionalize x with L, y by $\epsilon^2 L$, $\mathbf{q}$ by U_∞, the pressure p is scaled with $\rho_\infty {U_\infty}^2$, S by $\epsilon^2 L$ and finally the mass flow M by $\epsilon^3 L U_\infty$ (all the no–dimensional variables will be denoted by an overbar). Thus equation (4.18) becomes

$$\overline{v} = \epsilon^2 \overline{u} \overline{S}'(\overline{x}). \tag{4.18a}$$

Now, using (4.17) and (4.18a), we obtain for the two non–dimensional velocity components $\overline{u}$ and $\overline{v}$

$$\overline{u} = 1 + \epsilon^2 F'(\overline{x} - B\overline{y}), \qquad \overline{v} = -B\epsilon^2 F'(\overline{x} - B\overline{y}),$$

and using the above equations together with (4.18a) we get an expression for the unknown function F

$$\frac{\overline{v}}{\overline{u}} = -B\epsilon^2 F'(\overline{x} - B\overline{y}) = \epsilon^2 \overline{S}'(\overline{x}) \Rightarrow F'(\overline{x} - B\overline{y}) = -\frac{\overline{S}'(\overline{x})}{B}. \tag{4.19}$$

In order to calculate the pressures in the various regions we have to use Bernoulli's equation: $p + \frac{1}{2}\rho_\infty \mathbf{q}^2 = p_\infty + \frac{1}{2}\rho_\infty U_\infty^2$. The expression for $\overline{\mathbf{q}}$ using the equations for $\overline{u}$ and $\overline{v}$ becomes

$$\overline{\mathbf{q}}^2 = \overline{u}^2 + \overline{v}^2 \Rightarrow \overline{\mathbf{q}}^2 = 1 + 2\epsilon^2 F'(\overline{x} - B\overline{y}) = 1 - 2\epsilon^2 \frac{\overline{S}'(\overline{x})}{B}.$$

Thus, for the non–dimensional pressure in the main stream, $\overline{p}_o$, we have

$$\overline{p}_o + \frac{1}{2}\overline{\mathbf{q}}^2 = \overline{p}_{t\infty} = \frac{p_\infty}{\rho_\infty U_\infty^2} + \frac{1}{2} \Rightarrow$$

$$\overline{p}_o = \frac{p_\infty}{\rho_\infty U_\infty^2} + \frac{1}{2} - \frac{1}{2}\overline{\mathbf{q}}^2 \Rightarrow \overline{p}_o = \frac{p_\infty}{\rho_\infty U_\infty^2} + \epsilon^2 \frac{\overline{S}'(\overline{x})}{B}, \tag{4.20}$$

In order to complete the model we have to obtain expressions for the pressures in the slot and the film region downstream of the slot. Thus, using Bernoulli's equation again, the non–dimensional pressure in the slot, $\overline{p}_i$, must be equal to the total non–dimensional injection pressure, thus we obtain

$$\overline{p}_i + \frac{1}{2}\overline{\mathbf{q}}^2 = \overline{p}_{ti} = \frac{p_\infty}{\rho_\infty U_\infty^2} + \frac{1}{2}\epsilon^2 \Rightarrow$$

$$\overline{p}_i = \frac{p_\infty}{\rho_\infty U_\infty^2} + \frac{1}{2}\epsilon^2, \tag{4.21}$$

since $\overline{\mathbf{q}} = \overline{u} + \overline{v}$, where $\overline{u} = 0$ and $\overline{v}$ is $O(\epsilon^3)$.

For the film region the non–dimensional tangential velocity component is $O(\epsilon)$, thus the film pressure, $\overline{p}_f$, is

$$\overline{p}_f = \frac{p_\infty}{\rho_\infty U_\infty^2} + \frac{1}{2}\epsilon^2 - \frac{1}{2}\epsilon^2 \frac{\overline{M}^2}{\overline{S}^2}. \tag{4.22}$$

The pressure across the streamline is taken to be continuous thus we can equate the pressure in the film and in the slot, equations (4.22) and (4.21) respectively, with the outer pressure equation (4.20) to give

$$\frac{S'(x)}{B} = \begin{cases} \frac{1}{2} & 0 \leq x \leq 1 \\ \frac{1}{2} - \frac{1}{2}\frac{M^2}{S^2} & 1 \leq x < \infty \end{cases}, \tag{4.23}$$

(again we have dropped the bars for reasons of convenience). Equation (4.23) must be solved subject to the boundary conditions $S(0) = S'(0) = 0$, since the streamline comes out of the upstream edge of the slot and it separates tangentially at $x = 0$. Also downstream from the slot the boundary condition $S'(\infty) = 0$ must be used in order for $M = S(x)$ as soon as x becomes greater than 1 and the slope of the streamline to be zero at infinity.

However, if we take a closer look at equation (4.23) it may be seen that the slope of the streamline $S'(x)$ at $x = 0$ is $S'(0) = \frac{1}{2}$. It seems that in the interval between $x = 0$ to $x = 1$ the boundary condition holds, but in the region very close to $x = 0$ the condition cannot be satisfied, since from equation (4.23) we have proved that $S'(0) = \frac{1}{2}$. This means that the fluid does not exit at the front edge of the slot tangentially to the slot (as we have assumed), but with slope equal to $\frac{1}{2}$. The same may be said for the region very close to $x = 1$. We expected $S'(x) = 0$, but we obtained $\frac{1}{2}$. This contradicts what we have said that the streamline at $x = 0$ is parallel to the wall surface.

Downstream from the slot we expected the streamline to be flat, which means that as the flow leaves $x = 1$ the slope of the streamline must be positive or negative as it approaches the flat region of the streamline as x increases. If $S'(x)$ is positive

then from the right hand side of the equation (4.23) may be seen that $S(x)$ will always be greater than M, but then $S'(\infty) \neq 0$. On the other hand, if $S'(x)$ is negative then $S(x) < M$, which means that again $S'(\infty)$ cannot be zero. Either way, the boundary condition cannot be satisfied. The only possible case is that $S(x)$ becomes M as soon as $x = 1$ and the slope of the streamline is zero from the beginning of the rear edge of the slot.

These inconsistencies cannot be ignored, because as we just showed the boundary conditions for equation (4.23) cannot be satisfied. Thus a different approach should be used to solve the flow problem subject to these boundary conditions

4.4. NUMERICAL SOLUTION

One method to solve the problem numerically is to compare the pressures at selected points across the streamline for the interval $0 \leq x \leq 1$ by calculating the outer and the film pressures. First the outer pressure of a selected number of points was calculated on $y = S(x)$ by using equation (4.20) and then the average pressure of the points was obtained. Also the film pressure along the streamline was estimated for the same points as above by using equation (4.22) and then the average pressure of the points for the film region was calculated. Then the two averaged pressures were compared and a value for a pressure difference, Δp was obtained. This process was repeated several times using different number of points for each test. Eventually the smallest Δp gave the optimum value of mass flow. The absolute difference between equations (4.20) and (4.22), defined as Δp, was given by

$$\Delta p = |p_{ao} - p_{af}| = |\frac{1}{2}\epsilon^2(1 - u^2) - \epsilon^2 \frac{S'(x)}{B}|,$$

where p_{ao} and p_{af} were the average pressures of the outer flow and the film for the interval 0 to 1 respectively and $u = \frac{M}{S(x)}$ and $B = \sqrt{M_\infty^2 - 1}$. A typical value for $M_\infty = 2$ was used to give $B = \sqrt{3}$. The equation for $S(x)$, the shape of the streamline for the region of the slot, was modelled by using straight lines and splines.

The mass flow, M, was treated as an unknown variable, which had to be calculated. The value of M that would give the minimum pressure difference would be the optimum mass flow coming out of the slot. Consequently, that was considered to be

the solution to the flow problem.

One factor that we had to take under consideration, since we were dealing with supersonic flow, was the continuity of the pressure on the dividing streamline. Due to the velocity difference between the main flow and the injected stream (see section 4.3.1), it was possible that shocks form upstream from the slot. This meant that the pressure would rise rapidly at that point and the thickness of the boundary layer would increase. However, as it was shown at the formulation of the problem, the pressure in the region of the film was $O(\rho_\infty U_\infty^2 \epsilon^2)$ of p_∞. This meant that the pressure difference between the main and the injected flows was very small, so the formation of shock waves was not possible. Thus the pressure across $y = S(x)$ was taken to be continuous.

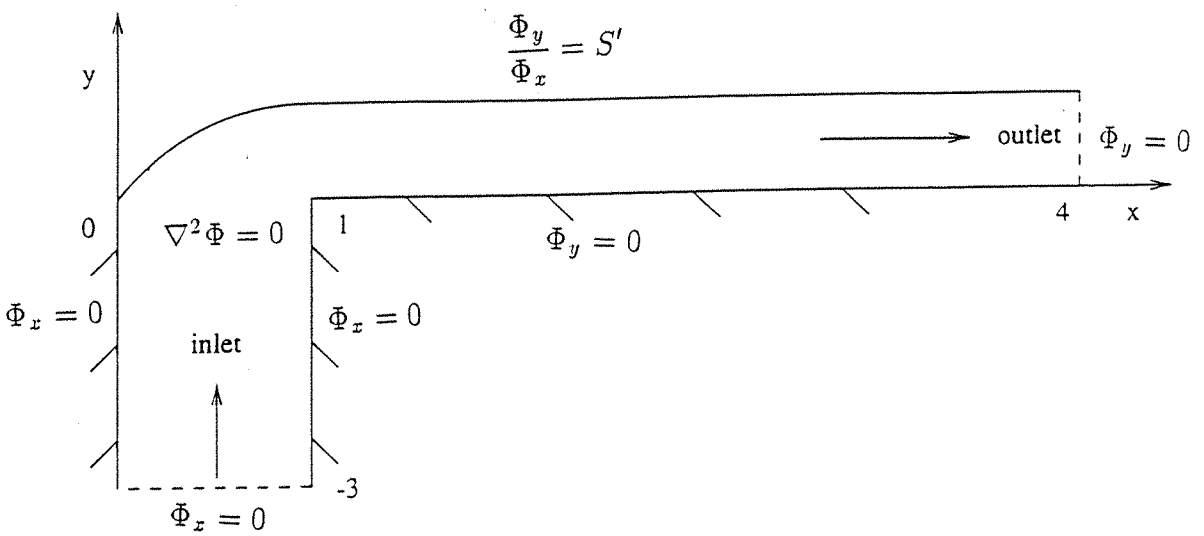

FIGURE 4.3.Diagram of the computational domain

Since the flow was taken to be irrotational we could use the condition $\nabla^2\Phi = 0$, where Φ is the velocity potential. Thus the numerical problem that we had to solve was the Laplace equation for the domain bounded by the streamline and the wall and subject to the boundary conditions given in figure 4.3.

When $y = 0$ $v = 0$, thus Φ_y was set to zero on the wall. Also on the walls inside the slot, where $y < 0$, $\Phi_x = 0$. From the equation of the streamline, $y = S(x)$,

and the kinematic condition we deduced that $\frac{\Phi_y}{\Phi_x} = S'(x)$ on the streamline and finally on the inlet we imposed the condition $\Phi_x = 0$ and $\Phi_y = 0$ on the outlet. However, as it may be seen from the boundary condition on the streamline Φ_y was unknown. Thus it was decided to solve the problem for the same geometry but for the stream function Ψ instead, since the values of Ψ and Ψ_x and Ψ_y were all known on the boundary. Hence, the Laplace equation took the form $\nabla^2\Psi = 0$, subject to the boundary conditions shown in figure 4.4. As it may be seen from figure 4.4 the value of Ψ on the streamline was known and set to M, described in section 4.2.

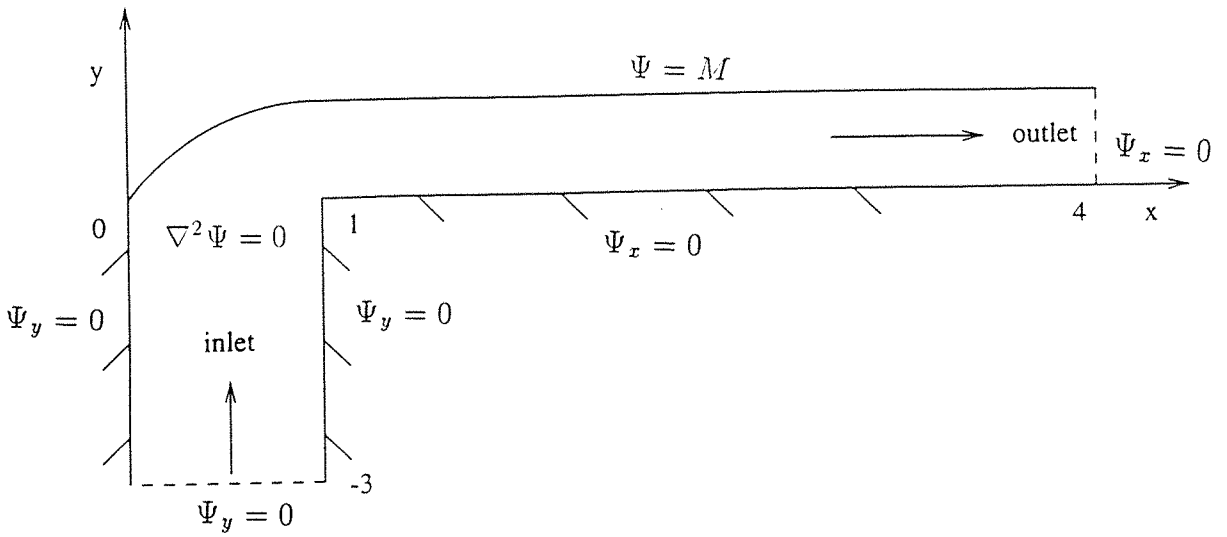

FIGURE 4.4.Diagram of the Laplace domain, using the stream function $\Psi(x, y)$

A FORTRAN program for the Unix operating system was written, to solve the Laplace equation by using a NAG routine. The NAG subroutine D03EAF, Fox and Wilkinson (1993), was utilized, which solves the Laplace equation for any geometry prescribed by the user. In order for this subroutine to work effectively the domain of the model has to be in 2–dimensions and bounded by a closed contour. Also values of the derivatives or of the unknown function must be given for all the points of the boundary. The subroutine calculates the unknown function Ψ by using an integral equation method, based upon Green's formula, Fox and Wilkinson (1993).

The FORTRAN code, written to solve the flow problem, before using the NAG routine created a mesh bounded by the streamline and the wall and on the boundary

the values of Ψ and Ψ_x and Ψ_y were imposed. The interval $0 \leq x \leq 1$ on $y = S(x)$ and the unknown shape of the streamline were modelled by using various functions such as straight lines or splines. Then the subroutine D03EAF was utilized.

4.4.1. Generating the Mesh

The first task was to determine the shape of the streamline in the region $x = 0$ to $x = 1$, i.e. over the slot, since the streamline after 1 and for a long distance downstream from the cavity was known to be flat and parallel to the wall.

The first approach to model this part of the streamline was to use straight lines. It was decided to join two straight lines with different slopes at the midpoint of the interval, $x = 0.5$, figure 4.5. Then we had to determine their slope and the number of points on the boundary.

It was decided to use three different domains, each one with more points than the previous one: D_0, D_1 and D_2. Thus D_0 had 61 points from which 33 were used as nodal points (the values of Ψ and Ψ_x and Ψ_y were prescribed on them). The second mesh, D_1 had 85 points and the nodes this time were 42. Finally, the third domain, D_2 was created by using 119 points from which 59 were nodes. Then, a fourth one, D_3, was created, which combined some features from the previous three: on the sharp corners of the mesh more points were added, whilst at the intervals where the variations of Ψ and its derivatives were small, some points were omitted. The new mesh had 127 points from which 63 were nodal points.

Each domain was tested for the same mass flow, $M = 2$, but for different number of points on the boundary and the streamline. This was done in order to determine which mesh was the best to use in order to proceed with the solution of the problem. Measurements of the mass flow coming out of the slot ($0 \leq x \leq 1$) were also recorded and points on the outlet and inlet of the model were also monitored.

The results from D_0, D_1 and D_2 were compared with the ones produced by D_3, case 4. Table 4.4 shows the results that each mesh produced when the mass flow was taken to be 2. From this table it may be seen that on the streamline the value obtained for Ψ is 2, as it was expected since it was set to this value. On the walls

the program estimated the Ψ values to be zero, or very close to zero. Finally, the Ψ values for some points on inlet and outlet were also recorded. Table 4.5 illustrates better the differences between each of the domains D_0, D_1, D_2 and D_3 for a given set of points. The absolute difference of the mass flow between each domain and D_3 was measured for many points on the boundary. From this table it may be seen that the difference between D_3 and the other domains decreased as the points on the boundary increased. There was also good agreement between D_2 and D_3 for many of the points on the domain. As it can be seen from both tables the number of points on the boundary influenced the final outcome.

The most coarse domain produced results which are accurate for some of the tested points, those which were not sensitive to changes of Ψ and Ψ_x and Ψ_y on the boundary, along the flat part of the streamline and on the wall. However, for the case of the coarse mesh, where there were very few points, only 33 nodes, or 67 points, it is clear that the difference between D_0 and D_3 was quite high at the points where there was a sharp corner, or where the stream function changed value, or when the streamline changed shape ($x = 1$ and $x = 0$).

When more points were added to the domain (D_1 and D_2) the results in general were improved. Thus the absolute differences of D_1 and D_2 with D_3 were very small. With more points added on the mesh (D_1 had 42 nodes and for D_2 59) the results and the difference in the values of the mass flow were in general improved, since the grid had more points at the regions where the shape of the boundary was not smooth, near $x = 0$ and $x = 1$.

4.4.2. Using Straight Lines

After determining the number of points on the boundary we continued with the next stage which was to use two straight lines, joined at a point, to model the shape of the streamline and to calculate the pressure difference along the boundary.

In order to find the slopes of the lines where Δp was minimum, we decided to keep the mass flow and the x-coordinate constant and change the y-coordinate of the point, i.e. the slope of both lines would change each time the y value was changing, figure 4.5. The mass flow was taken to be 2 and $x = 0.5$ and we tested the

program for various values of y. The meshes had the same number of points on the boundary, except in the interval $0 < x < 1$, where different number of points were used: $n = 4, 6, 9$ and 11. The table 4.6a shows some pressure differences, Δp, for various y-coordinates, for $x = 0.5$ and different slopes of the two lines for the case where $n = 6$. When more points were added on the interval it was found that the outcome was not affected significantly.

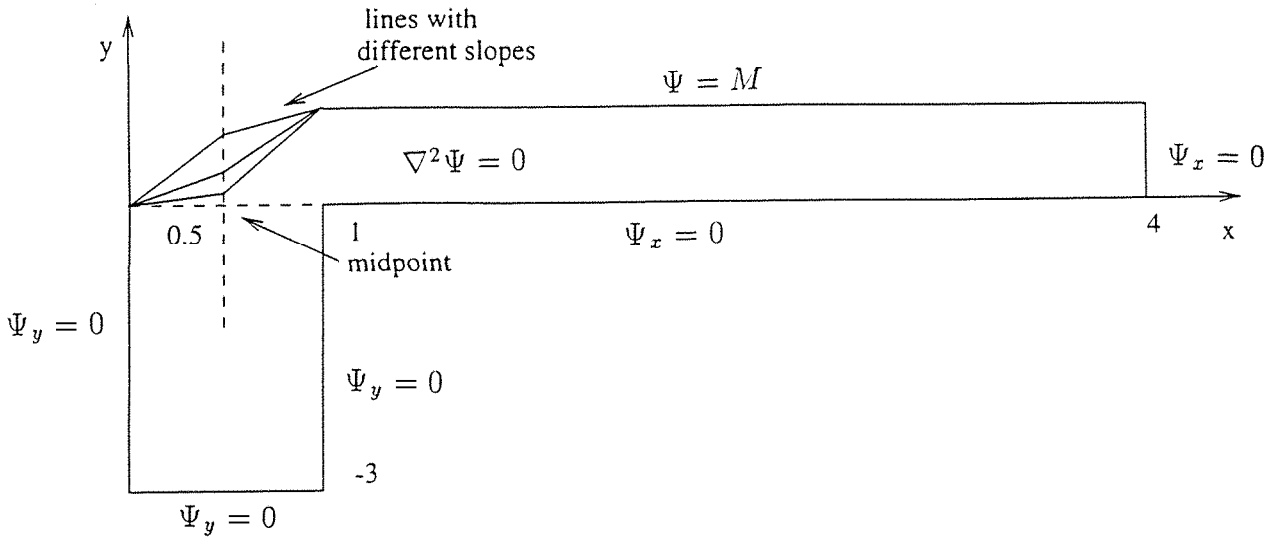

FIGURE 4.5. Diagram of the model, using lines

From the table 4.6a it may be seen that the minimum pressure difference was in the region $0.20 \leq y \leq 0.35$, where the value of $y = 0.22$ acted like a lower limit and $y = 0.35$ the upper bound. It can also be seen that the y-coordinate of the point should have been closer to 0.22 than to 0.35, since the pressure difference at $y = 0.22$ was less. Thus we investigated this region in more detail, by testing some more points which were around 0.22. The results obtained from some of the tested points can be seen in table 4.6b.

From the table 4.6b, it may be seen that the y-coordinate of the point with the minimum pressure difference was $y = 0.25$, since Δp was found to be very small. Thus this point was used as the joining one for the two lines, x =0 to 0.5 and x =0.5 to 1.

Having established the slopes of the two lines, it was then decided to continue the

investigation by testing various mass flows. In this way we would be able to deduce the optimum value of M, which would give the minimum pressure difference.

We tested five more different values of mass flow and various y-coordinates of the point x =0.5. The results can be seen at the tables 4.7a–4.7e.

From the tables 4.7a–4.7e it may be seen that the point (0.5,0.25) produced the lowest value for the pressure difference: $\Delta p \approx 0$, for any value of mass flow. However, it seems that the minimum pressure difference was zero. This cannot be right, since we had assumed that there was only one non–zero mass flow which would give the lowest Δp. The graphical representation of the above results (Δp vs mass flow) can be seen in figure 4.6. The graphical solution that we obtained had the form of a line touching the x–axis, instead of a curve which would have a minimum, positive point (the unique value of the mass flow and the minimum Δp).

Thus the approach that we had followed to solve the problem, by using two straight lines, was proven to be not the right one. Then another method was used: to solve the problem by using smooth curves in the interval 0 to 1. These curves should also satisfy the boundary conditions $S'(0) = S'(1) = 0$.

4.4.3. Using Polynomials of High Order

The fitting of a polynomial curve to a set of data points has applications in the area of computer graphics and mathematics, when a smooth curve must be drawn through data points. Also in cases where continuity of function derivatives is essential, a spline can be utilized. A spline function $P(x)$ is a polynomial between each pair of data points, but one whose coefficients are determined nonlocally. This property is intended to ensure global smoothness in the finite interval $[x_0, x_N]$ where the spline is defined. Splines are more stable than polynomials because they tend to oscillate less between the data points. Mathematically, it is possible to construct a spline, $P_k(x)$, on each strictly increasing interval $[x_k, x_{k+1}]$ so that the resulting curve $y = P(x)$ and its first derivatives are all continuous on the larger interval $[x_0, x_N]$. The continuity of $P'(x)$ means that the graph $y = P(x)$ will not have sharp corners.

The function $P(x)$ defined in the interval $[x_0, x_N]$ is called a spline of degree N

if it has the following properties:

(i) in each local interval $[x_k, x_{k+1}]$ $P(x)$ is given by a spline of degree N, denoted as $P_k(x)$,

(ii) at each point x_k the function $P(x) = f_k$, where f_k is the function value of the point x_k,

(iii) at the common point x_k of the two subintervals $[x_{k-1}, x_k]$ and $[x_k, x_{k+1}]$ P satisfies

(1) $P_{k-1}(x_k) = P_k(x_k)$ and

(2) $P'_{k-1}(x_k) = P'_k(x_k)$ and finally,

(iv) the function $P(x)$ and its derivatives up to order $N-1$ are all continuous in the global interval $[x_0, x_N]$, given in Conte and de Boor (1965).

Splines of high order were constructed for the interval $0 \leq x \leq 1$ and they were found to produce a very smooth streamline, similar to the one in figure 4.2.

The same process as before was followed in order to determine the optimum value of the mass flow: the pressure difference was calculated across the streamline for different values of M and then the results from each case were compared with each other. The mass flow which would produce the minimum Δp would be the desired M. It was also decided to use different methods to represent the interval from 0 to 1. Thus various tests were performed with one curve passing through all the points of the interval, two curves joined at the middle point, $x = 0.5$ and having the y-coordinate moving up and down and finally, having two 'moving' points, i.e. three curves joined at equally spaced intervals. For all these cases a FORTRAN code was written to construct the splines in the interval 0 to 1 and then to solve Laplace's equation using the NAG routine mentioned in section 4.4. Since it was decided to use three ways (three different interpolating functions) to estimate the streamline for the interval 0 to 1, the numerical code had to change slightly each time a different case was used. Nevertheless, the process to determine the shape of $y = S(x)$ in the area above the slot was similar as in section 4.4.2. The interpolating curve(s) was constructed and then the pressure of the film and the outer flow on the streamline were compared.

The smallest pressure difference obtained by a given mass flow would produce the solution to the flow problem.

During the process of constructing the splines we guaranteed that the derivative conditions were satisfied and also that the curves were continuous at the joining points of the interval 0 to 1. Also the number of points in the rest of the mesh was remained constant, i.e. only the number of the points in the interval was changed.

For the first case one spline was constructed to connect the interval 0 to 1 with an intermediate point at $x = 0.5$. The y-coordinate of this point could change to produce a different spline each time. The spline curve had to pass through these 3 points and create some more, which would be placed in equally spaced positions, in the smaller intervals 0 to 0.5 and 0.5 to 1. The number of these data points varied from $n = 2$ to $n = 21$. For each case various values of mass flow were used in order to determine which M would give the minimum Δp. This value of mass flow was then compared with the results obtained from the other cases. The mass flow which would give the minimum pressure difference when the results from all cases were compared would be the optimum M and the solution to our flow problem. However, the results produced from this method proved to be inconclusive. The tables 4.8a–4.8f show the results of Δp obtained for various mass flows and y-coordinates for $x = 0.5$. From the graphs of figures 4.7a–4.7f, where the pressure difference is plotted against the mass flow, it may be seen that it is very difficult to draw any conclusions for the optimum value of mass flow.

Since the method of using one curve did not work, it was decided to use two curves for the interval 0 to 1, by joining them at $x = 0.5$. In the middle of each of the two smaller intervals created (0 to 0.5 and 0.5 to 1) one point was placed, estimated by the interpolating curve. The y-coordinate of the point could move up, or down depending on the input data. We were careful to keep both functions continuous at the joining point. The total number of points for each curve varied from $n = 5$ to $n = 21$ for the whole interval. The tables 4.9a–4.9e show various pressure differences for different values of M. Also the graphs of figures 4.8a–4.8e show Δp plotted against the mass flow M. For this set of results, again, the optimum mass flow was different for different numbers of points in the interval. Thus, once again we were not able to

obtain any useful results.

Thus it was decided to use two 'moving' points at $x = 0.333$ and $x = 0.667$. For the three intervals created one point was added at an equal spaced position, whose y-coordinate was calculated by the spline. In this way three splines were used. Again, all three functions were kept continuous at the joining points and at the same time the boundary conditions for $S'(x)$ at $x = 0$ and $x = 1$ were satisfied. During each test one of the two 'moving points' was kept constant and the y-coordinate of the other point, together with the mass flow were changing, i.e. the same method that was used before was also followed this time. Then the reverse process was used: the former was taken as the 'moving point' and the latter as the stationary point. In the tables 4.10a–4.10b we present some representative results for two sets of points: $n = 5$ and $n = 17$. As it may be seen the results obtained were once again not satisfactory, and hence it was decided to try a completely different method.

4.4.4. Using a Optimization Technique

Since the above approaches to find a minimum pressure difference did not work it was decided to use a optimization method. The process of optimization was very similar to the method described above.

The streamline was approximated by using spline interpolation and having two 'moving' points in the interval 0 to 1. One more point equally placed in each of the subintervals was created by the splines. Then an initial guessing value for the mass flow together with two guessing values for the y-coordinates of the 'moving' points were supplied. Then the pressure difference was estimated by following the same process as in section 4.4.3. The optimizing NAG routine E04CCF treated the above parameters as initial data in order to start the iterations for M and the two y-coordinates. The routine used the Simplex method, Fox and Wilkinson (1993), to produce the new values of the mass flow and the two y-coordinates. These parameters produced a new Δp, which was compared with the previous pressure difference. The smallest pressure difference together with the entries produced this particular Δp were stored in order to repeat the above process and comparisons. Eventually, the value of M and the values of the two y-coordinates for the points $x = 0.333$ and $x = 0.667$

which produced the overall minimum pressure difference, were found.

The minimization process was initiated by testing the program for different numbers of points in the interval 0 to 1. The first test was performed by having 7 overall points in the interval above the slot and then the number of points was increased to 9 and 11. However, with more points added to the mesh the results were inconclusive. That was due to the fact that each time the number of points was changed the results for the optimum mass flow changed too. Thus we could not verify the initial results produced for the case $n = 7$, shown in table 4.11. This table shows various values of the mass flows together with the value of Δp for two moving points: $p_1 = 0.333$ and $p_2 = 0.667$, with variable y-coordinates. Figure 4.9 shows a typical curve of the pressure difference vs the mass flow.

4.5. DISCUSSION OF RESULTS

A numerical investigation was conducted for the problem of film cooling in a supersonic main stream. The main and the injected flows were taken to be inviscid, incompressible and time independent.

The first stage in solving the problem was to determine the shape of the streamline for the interval $x = 0$ to $x = 1$. Three methods were used to find the optimum shape of the boundary: by joining two straight lines and two/three splines at the middle point and by using a minimization technique. For each method the pressure difference across the boundary was calculated, by obtaining the pressure in the film and the main flow and then comparing them. The mass flow which would produce the minimum Δp was the solution to our problem. However, all methods produced inconclusive results due to the fact that the mass flow calculated from all three techniques did not converge to a specific value, thus we could not be confident about it.

In the sections to follow we comment on the results obtained from each method.

4.5.1. Discussion of Results for the Method of Straight Lines

The first approach was to use straight lines to join the interval above $x = 0$ and $x = 1$. The results produced are summarized in the tables 4.7a–4.7e. From these

tables it can be seen that the mass flow did not converge to a specific value. The pressure difference declined as M decreased and for two cases (table 4.7a and 4.7c) Δp was found to be very close to zero, this means that that there were two different mass flows for which the same minimum pressure difference was obtained. The graph of figure 4.6 illustrates clearly our conclusion. We obtained a broken line, with no minimum point, instead of a curve with a lowest minimum, which would have been the appropriate mass flow for a specific non–zero Δp.

From the shape of the first graph (figure 4.7a) it was obvious that a minimum mass flow existed. This mass flow was found to be 0.487 and it produced a $\Delta p = 0.1173e - 3$ (table 4.8a). The above results were obtained by running a program for 5 points in the interval.

The second test was performed with n (number of points in the interval) equal to 7. The numerical results can be seen in table 4.8b. Their graphical representation, figure 4.7b, another $\Delta p = 0.1262e - 2$ for another optimum mass flow ($M = 0.554$). This graph produced a minimum point but we could not be sure that this mass flow was the right one, since it was not close to the value of M calculated by the previous case.

From the third run, it may be seen that the increase at the number of points $n = 9$ influenced, once again, the final outcome. This is evident from the table 4.8c and the graph of Δp vs M of figure 4.7c. The pressure difference went up ($\Delta p = 0.1518e - 2$) whilst the mass flow decreased, $M = 0.234$. The shape of the graph has the same form as the previous ones, i.e. a minimum point was established, but the results were nowhere near to the previous ones.

Another test was performed, with the number of points been increased to 11. The results from this run can be seen in figure 4.7d and the table 4.8d. The behaviour of the model was similar to the previous ones. It seems that it was very sensitive to mesh changes. This time M was found to be 0.340 with a minimum $\Delta p = 0.1406e - 2$. The graph of figure 4.7d produced a minimum point, but it was not close to any previous points that we obtained from the last runs.

This time n was taken to be 17 and from the graph of figure 4.7e and the table

4.8e, we can see that the pressure difference was found to be less than the ones obtained in the case where $n = 9$, 11. Thus $\Delta p = 0.1334e - 2$ with a mass flow of 0.231. Furthermore, the mass flow was less than the previous case, but very close to M for $n = 9$. Nevertheless, it was not very wise to say that the optimum mass flow was found to be somewhere in the region of 0.231 and 0.234 since the two values of Δp (for $n = 9$ and $n = 17$) did not coincide.

The last set of tests was performed with $n = 21$. The graph of figure 4.7f has all the characteristics of all the previous ones: a minimum point with a value of $M = 0.100$ and $\Delta p = 0.1267e - 2$. All the above results showed us that the optimum value of mass flow was greatly affected by the number of points.

4.5.2. Discussion of Results for the Method of Splines

The second method used, was to model the unknown streamline (from $x = 0$ to 1) by using splines, which could satisfy the boundary conditions: $S'(0) = S'(1) = 0$. With this method we were able to produce a smooth curve to join the interval. Different number of points were used for the section $x = 0$ to 1 in order to test the dependency of the solution on the mesh.

This method involved the construction of two curves joined together at a point, the middle of the interval $x = 0.5$. Both curves were continuous at the connecting point and satisfied the boundary conditions.

The first test performed for $n = 5$ and the results can be seen in table 4.9a and graphically in the figure 4.8a, where a plot of the mass flow against Δp is shown. The optimum mass flow was found to be $M = 0.585$ with $\Delta p = 0.1487e - 2$. This graph is very similar to previous ones: a minimum point was found, but its value was not close to any other one from the previous tests.

The second run was performed for $n = 9$. The graph of figure 4.8b shows a similar pattern with the previous graph. From the table 4.9b we can see that $\Delta p = 0.1464e-2$ was very close to the previous value, but this time the mass flow changed: $M = 0.350$.

Another test, with $n = 9$, shows (table 4.9c) a pressure difference of $0.1412e - 2$, but for a mass flow of 0.280. We can say that this result was close to the previous one,

but we still could not be confident about the actual mass flow. Finally, the graph of figure 4.8c has all the properties of the previous ones, a minimum point which gave the minimum Δp for an optimum mass flow.

When the number of points in the interval was increased, $n = 17$, the pressure difference dropped to $0.1265e-2$ (table 4.9d) for a mass flow of 0.152. The shape of the graph, figure 4.8d, was found to be very similar to the ones produced by all the previous runs, with fewer points in the interval.

For the last run, $n = 21$ (figure 4.8e) good agreement existed between the above results and the results from this test, since $M = 0.170$ and $\Delta p = 0.1269e-2$, table 4.9e. However, these results were still inconclusive, since we could not say with great confidence the actual value of the mass flow.

Another way to solve the problem was then employed: two moving points were used, with three curves joined at two equally spaced points, i.e. $x = 0.333$ and $x = 0.667$. A lot of runs were performed at this stage and the general approach was to keep stationary one of the points and move the y-coordinate of the second point up, or down. At the same time we changed the value of the mass flow. Then the same process was repeated for the other moving point. The tests conducted involved a various number of points, from $n = 5$ to $n = 21$. However, most of the produced combinations of the two moving points and the mass flow were unsuccessful, i.e. the pressure difference was too high.

The tables 4.10a and 4.10b show the two most successful combinations for $n = 5$ and $n = 17$. As may be seen the two tests gave different values for M and Δp. Table 4.10a shows a minimum $\Delta p = 0.2004e-1$ for a range of mass flows: 0.237–0.239, and for two points with coordinates: (0.333,0.10) and (0.667,0.45). On the other hand, from table 4.10b we obtained a lower $\Delta p = 0.8307e-3$ for $M = 0.235 - -0.240$ and points (0.333,0.10) and (0.667,0.35). Clearly, it may be seen that for the same values of mass flow we obtained entirely different pressure differences. Thus we could not say with confidence which test produced the optimum pressure difference and correct mass flow.

4.5.3. Discussion of Results for the Minimization Method

Since the above method did not work, it was decided to use a minimization technique. In this way we would specify the mass flow and we would guess two initial values for the y-coordinates of the moving points. A NAG routine that was utilized attempted to find two suitable y-coordinates, which would give a minimum Δp for a given value of M. This process was repeated several times, until an optimum value of M was found.

The table 4.11 shows tabulated values of mass flow and Δp, for optimized y-coordinates. The graph of Δp vs M, figure 4.9, is very similar to all the previous ones, only in this case the minimum $\Delta p = 0.1538e - 1$ for $M = 0.610$. As we can see this value of mass flow was not close to any of the previous ones. Thus it was decided to use again, more points in the interval 0 to 1. However, all the tests proved inconclusive, the mass flow did not converge to a specific value and in many cases the algorithm did not converge to a specific pressure difference value.

4.6. CONCLUSIONS

A lot of different methods were used in order to obtain the optimum mass flow for the problem of film cooling in supersonic main flow. Unfortunately, all of the techniques failed to produce trustworthy results. It seems that all the solutions were mesh dependent, since changing the number of points in the interval 0 to 1 the mass flow and subsequently the pressure difference also changed. Thus we could never be sure about the results produced. It is possible that the numerical solution of the problem was affected by possible singularities in the region very close to the slot edges. As has been discussed earlier there are inner regions in the slot that the boundary conditions do not apply. This phenomenon did not influence the results of the subsonic case, but it is possible that it affected the solution for the supersonic flow problem.

If some experiments were conducted it would have been possible to compare these results with the numerical ones which were obtained from the above methods. Another approach would possibly be to use CFD methods, since fluid dynamics packages could

give us some information about the flow in the film and the pressure on the streamline.

Physically, we know, that there is only one value of mass flow that gives the minimum pressure difference with the above scaling. It is, however, possible that for other scalings the mass flow, and maybe the pressure difference will vary.

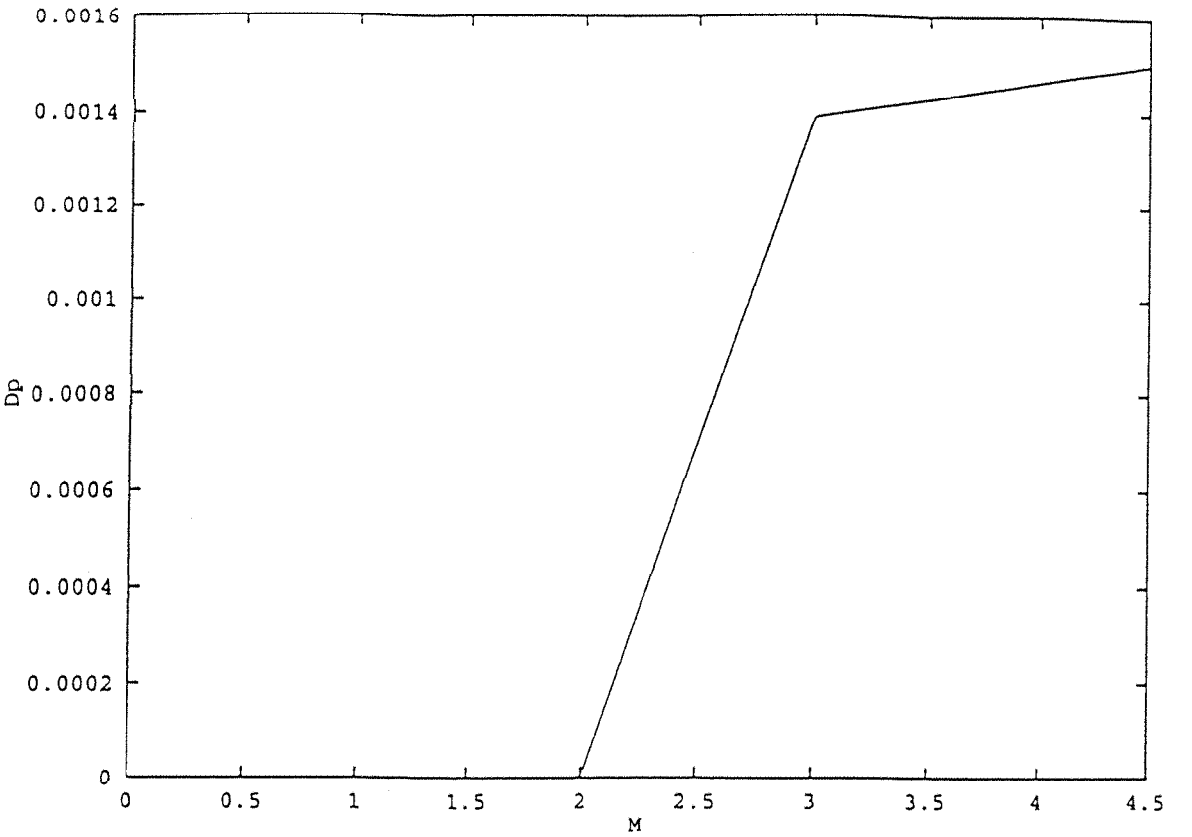

FIGURE 4.6. Graph of pressure difference against M

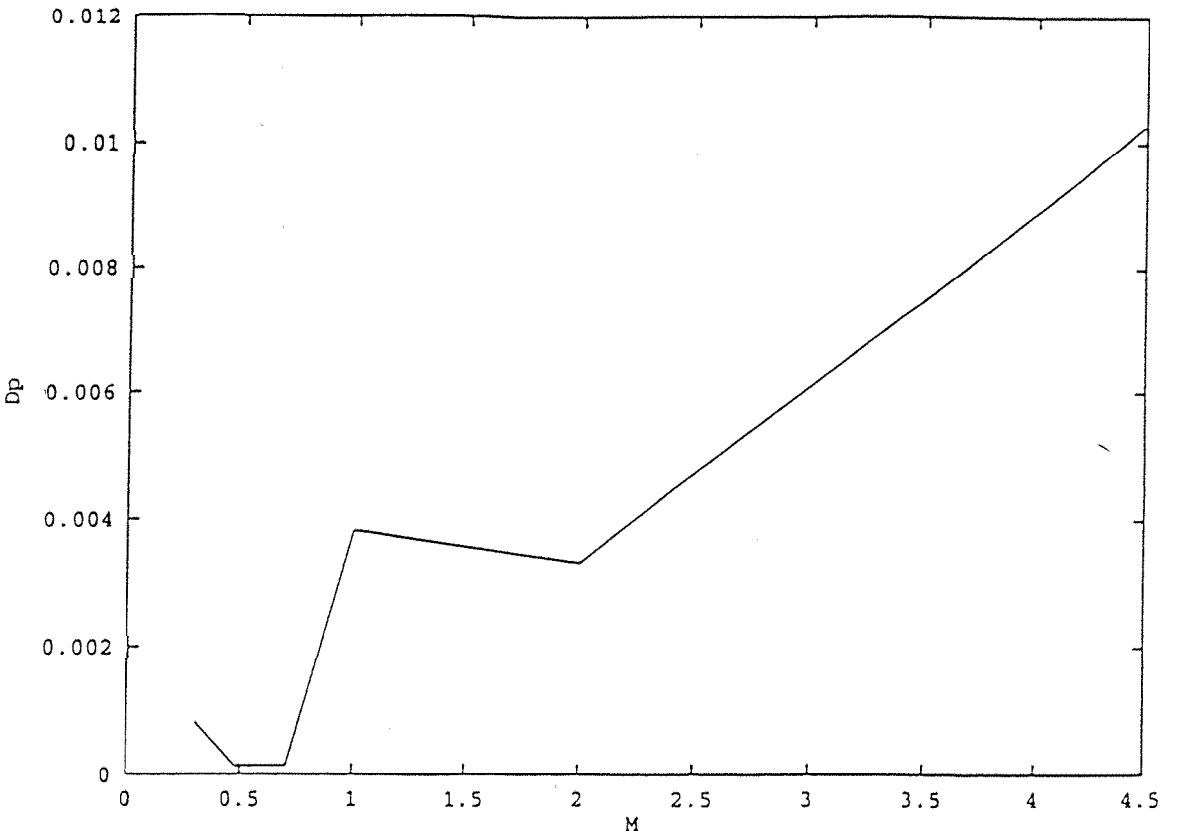

FIGURE 4.7a. Graph of pressure difference against M for n=5

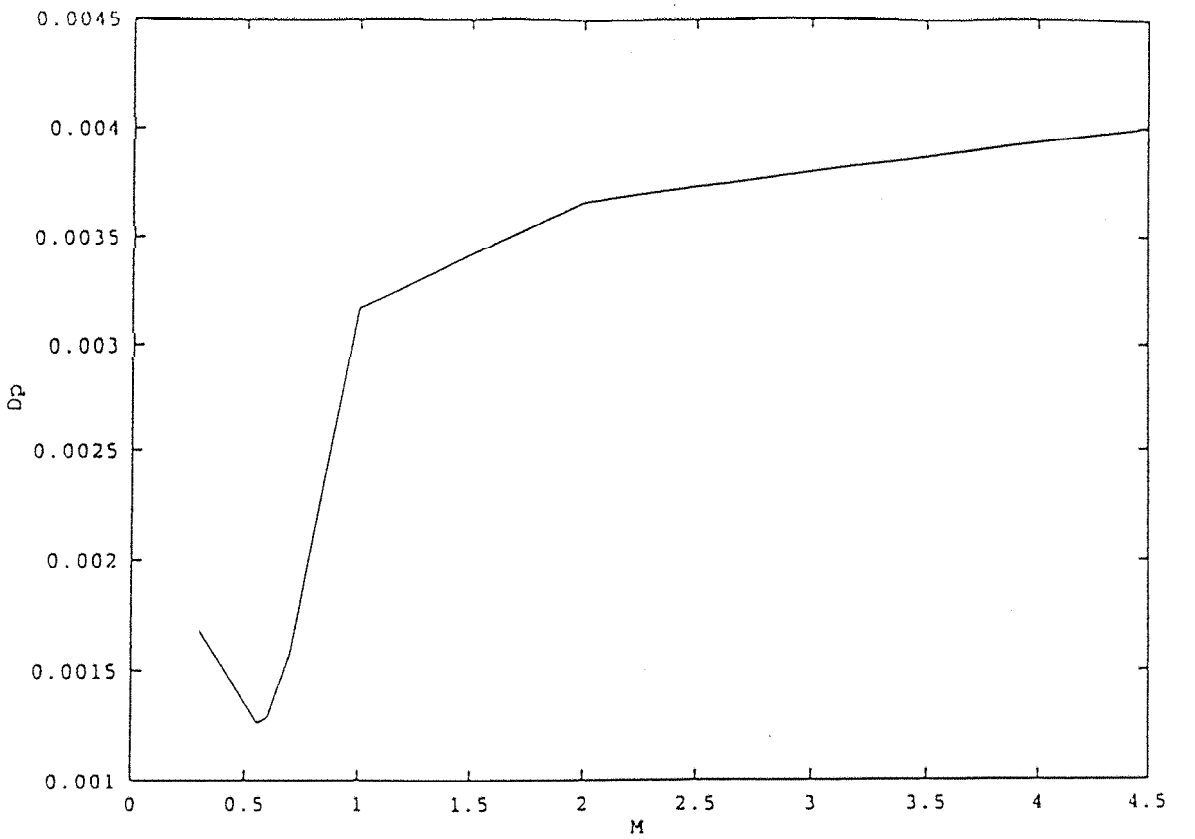

FIGURE 4.7b. Graph of pressure difference against M for n=7

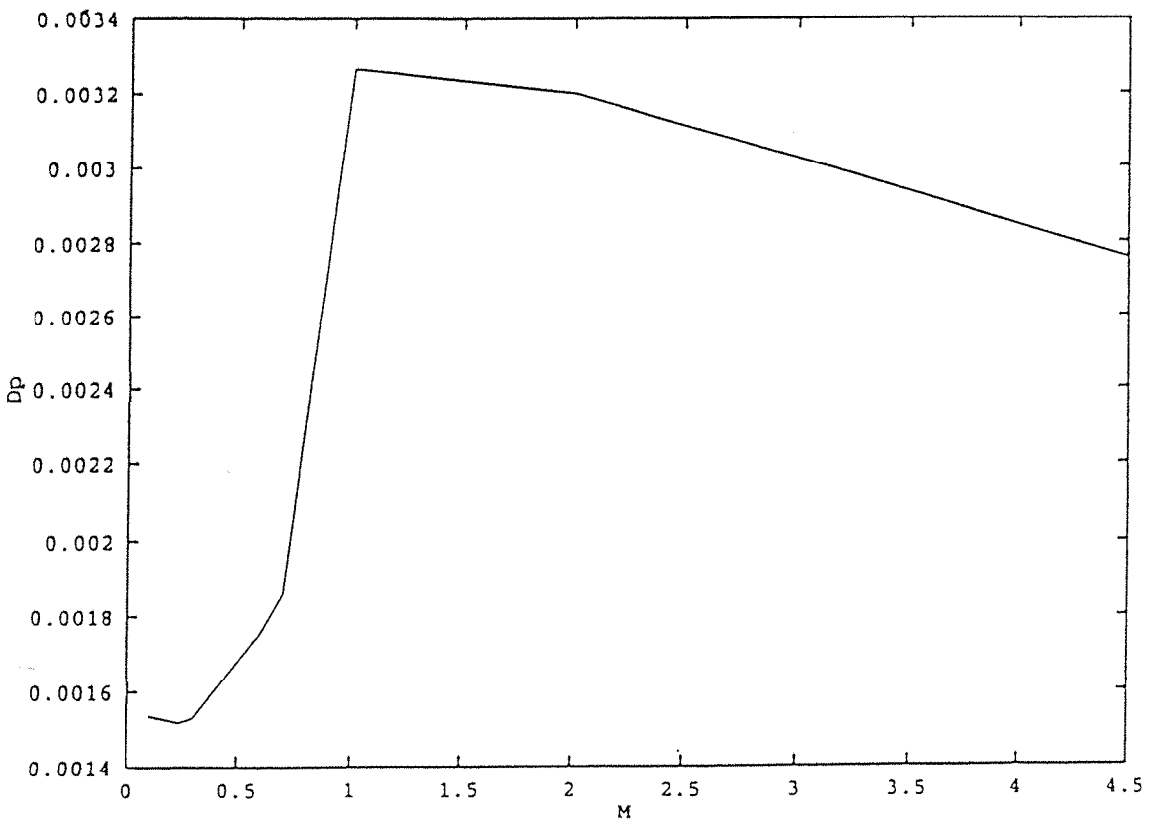

FIGURE 4.7c. Graph of pressure difference against M for n=9

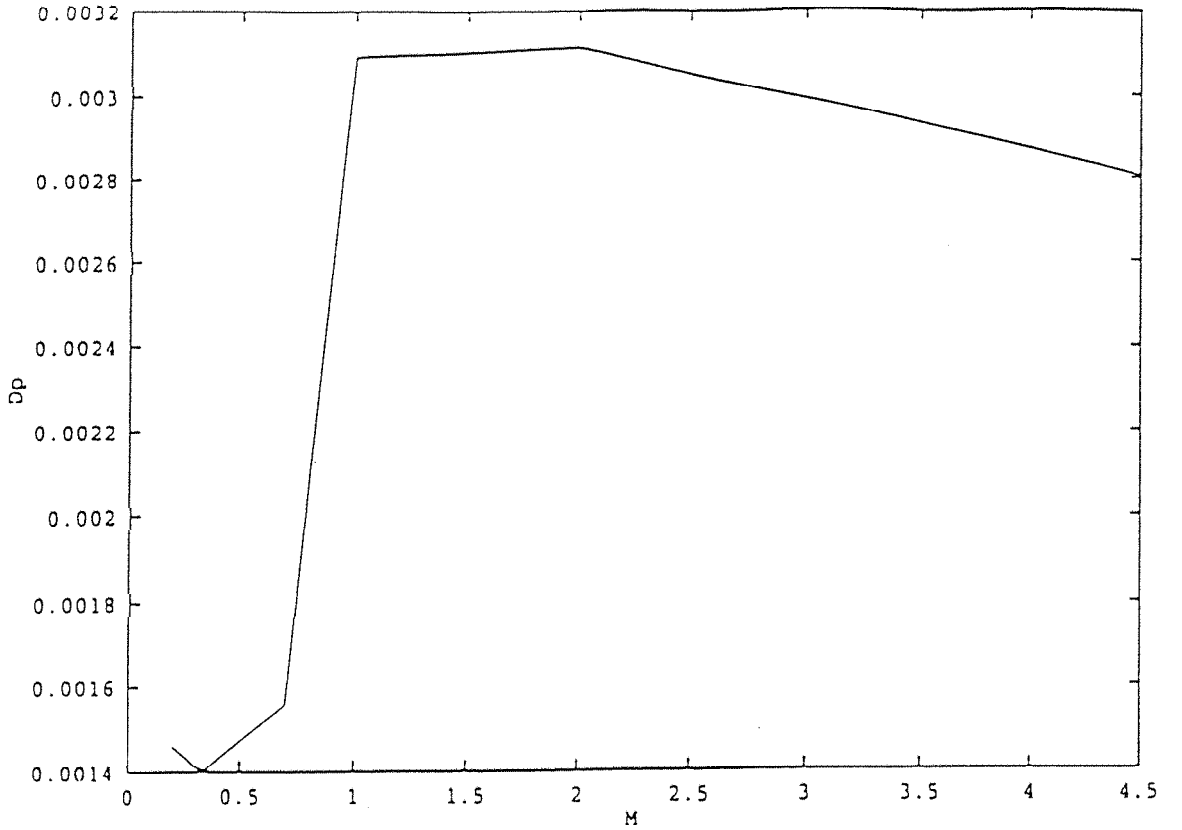

FIGURE 4.7d. Graph of pressure difference against M for n=11

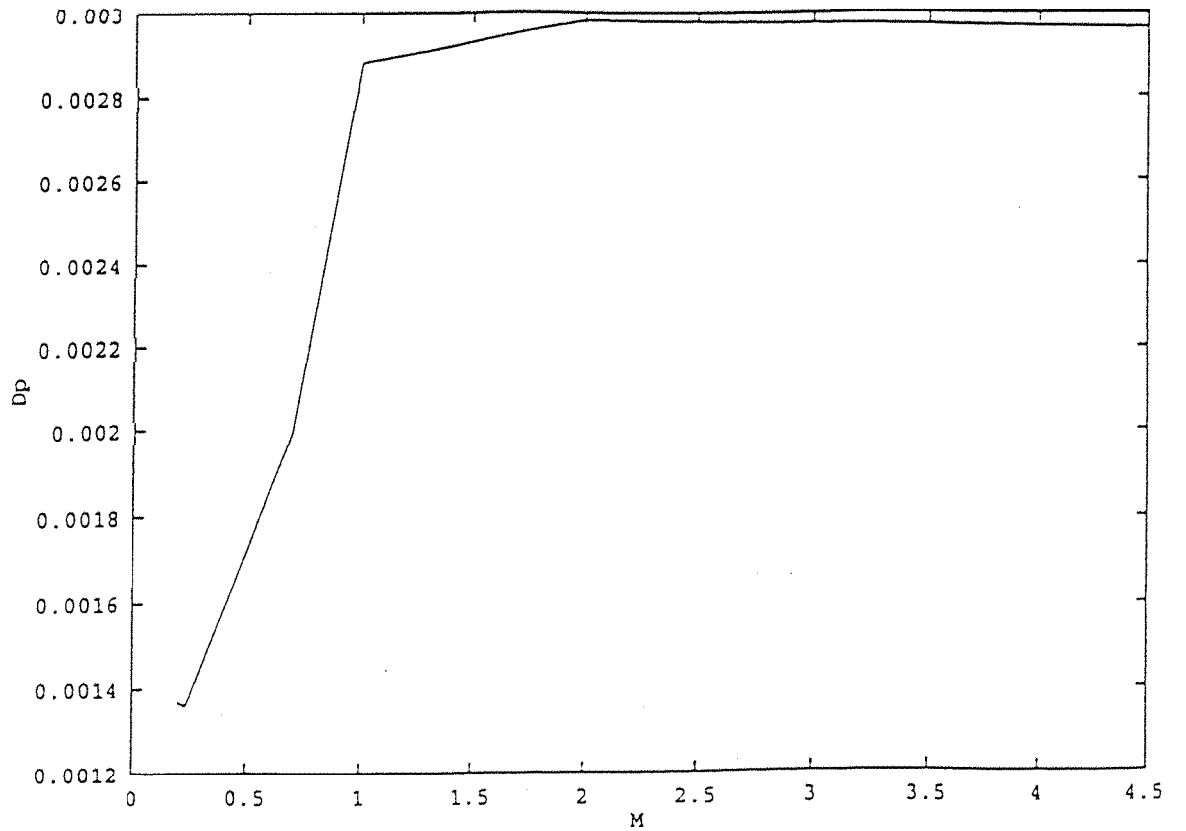

FIGURE 4.7e. Graph of pressure difference against M for n=17

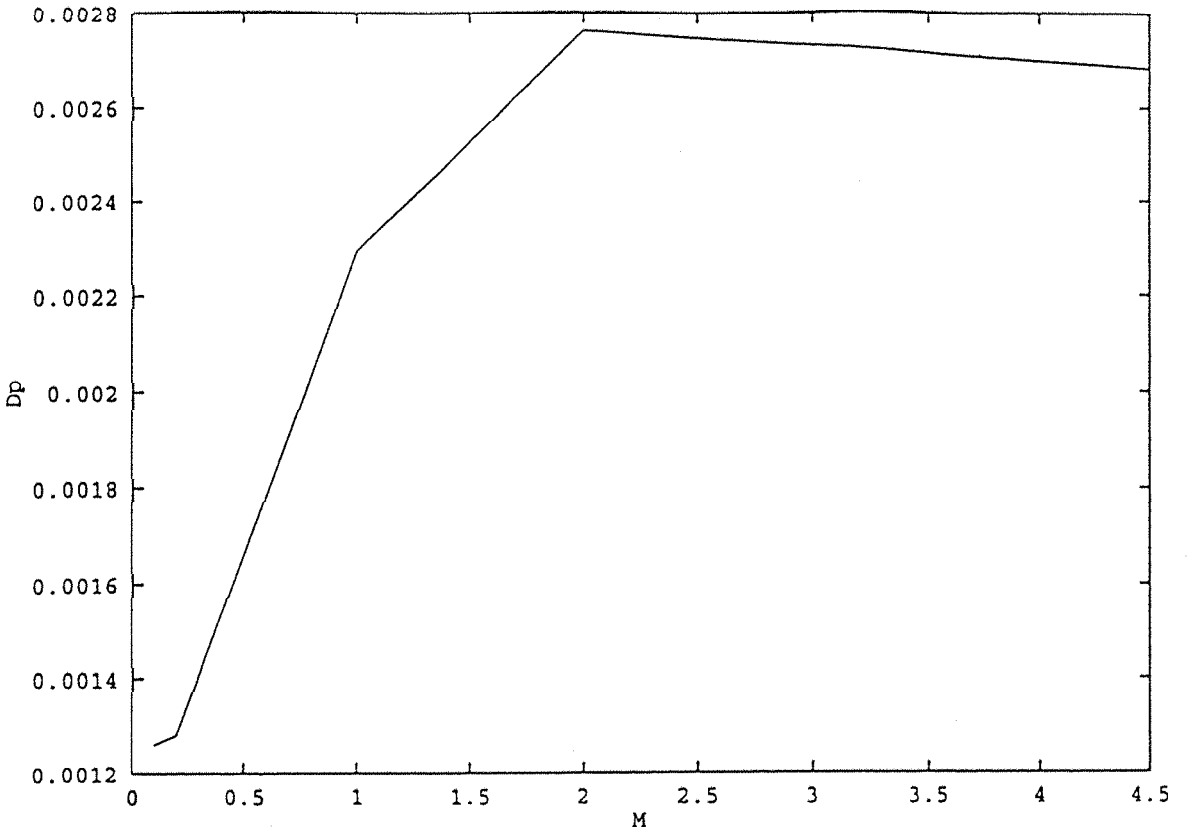

FIGURE 4.7f. Graph of pressure difference against M for n=21

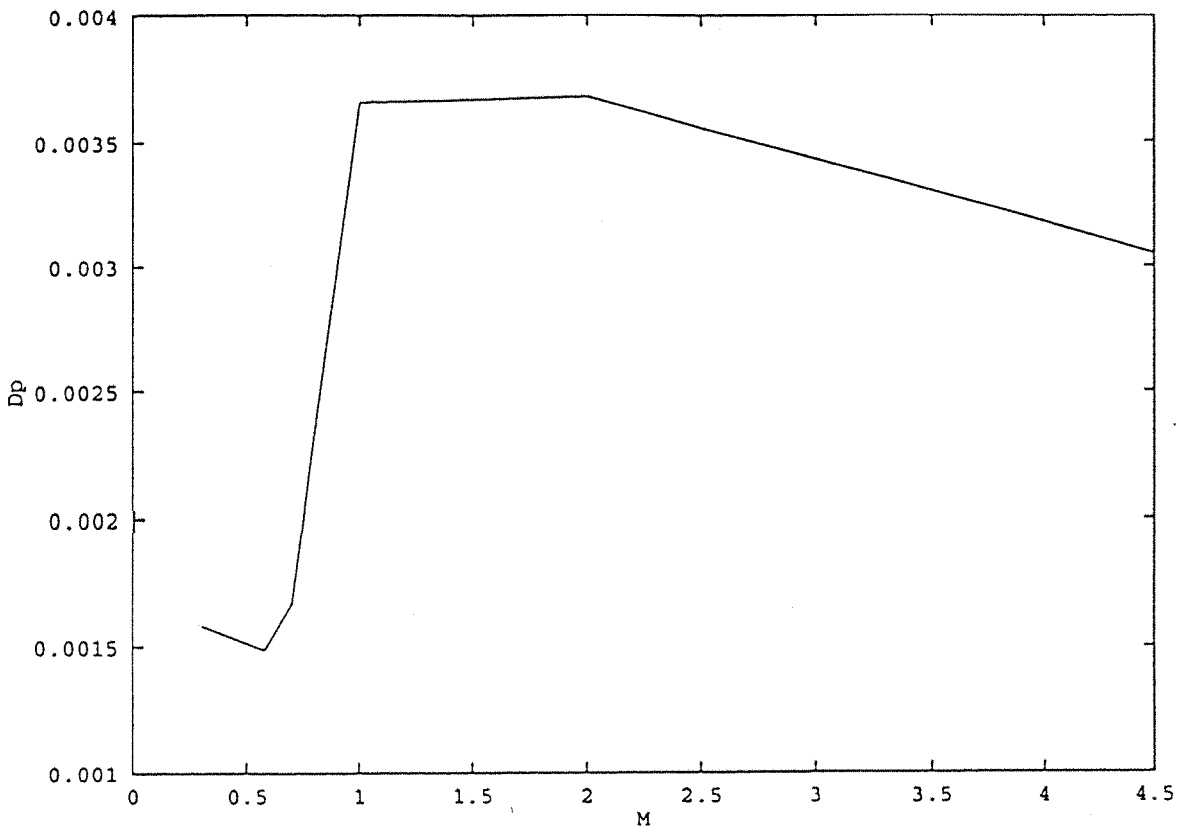

FIGURE 4.8a. Graph of pressure difference against M for n=5, using two curves

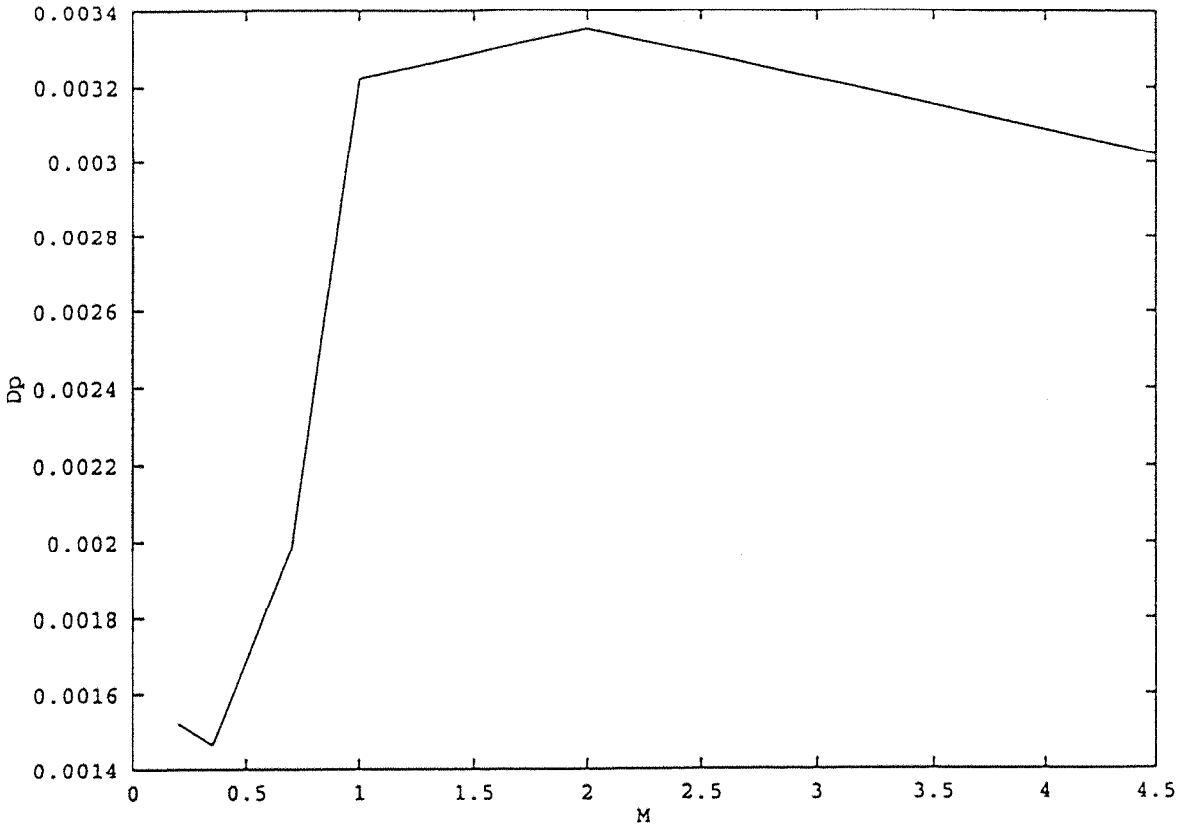

FIGURE 4.8b. Graph of pressure difference against M for n=7, using two curves

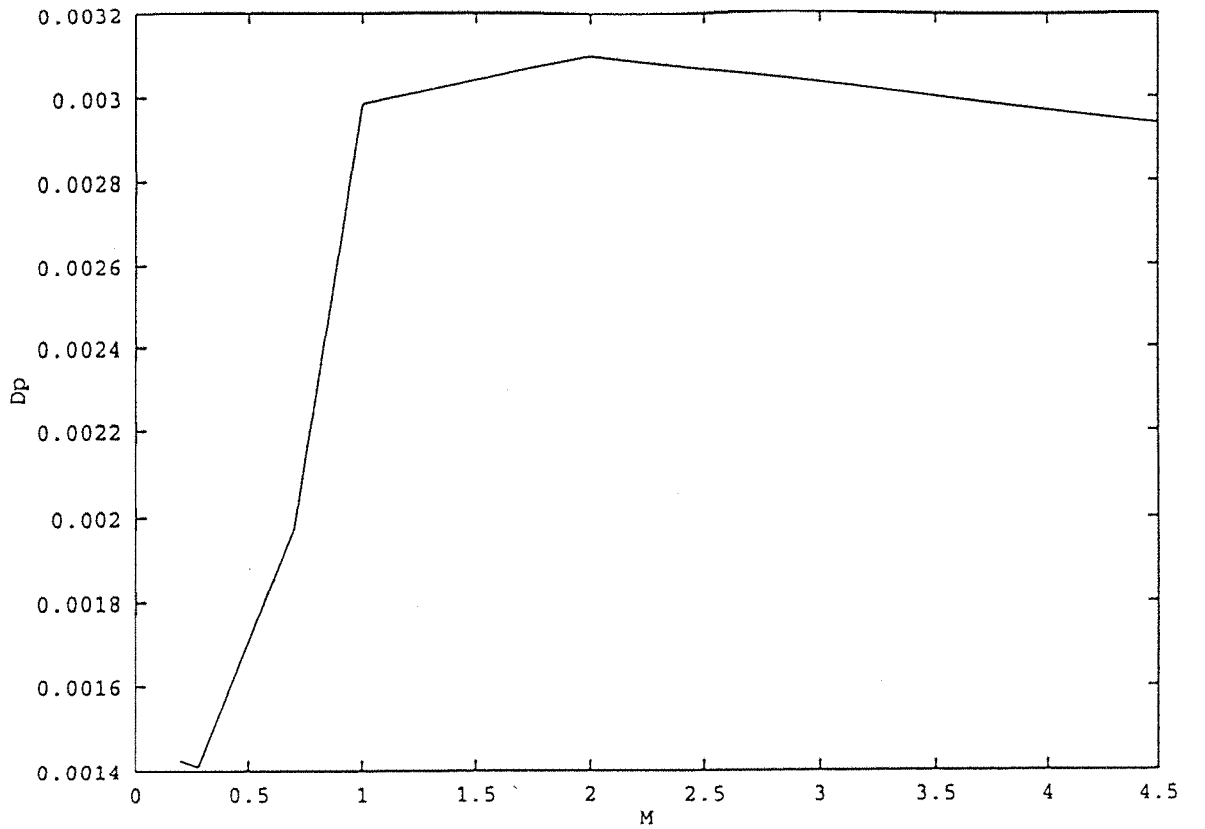

FIGURE 4.8c. Graph of pressure difference against M for n=9, using two curves

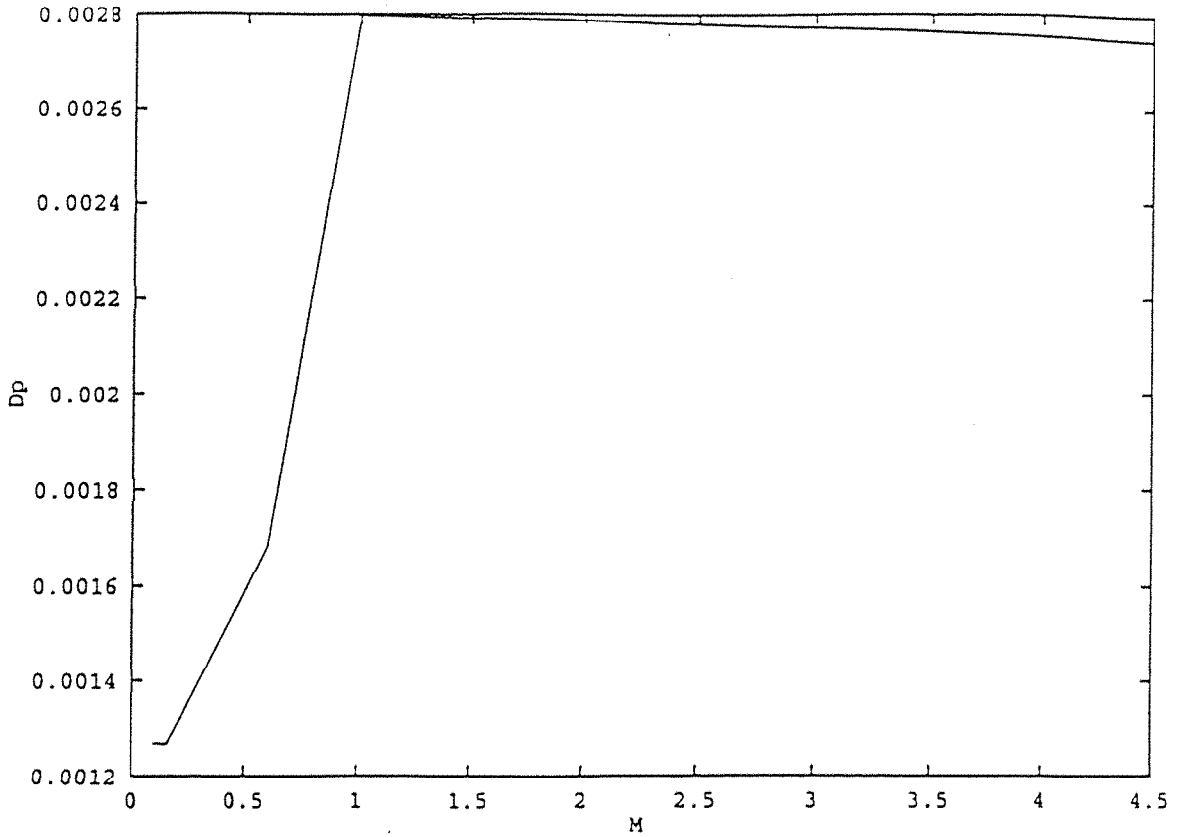

FIGURE 4.8d. Graph of pressure difference against M for n=17, using two curves

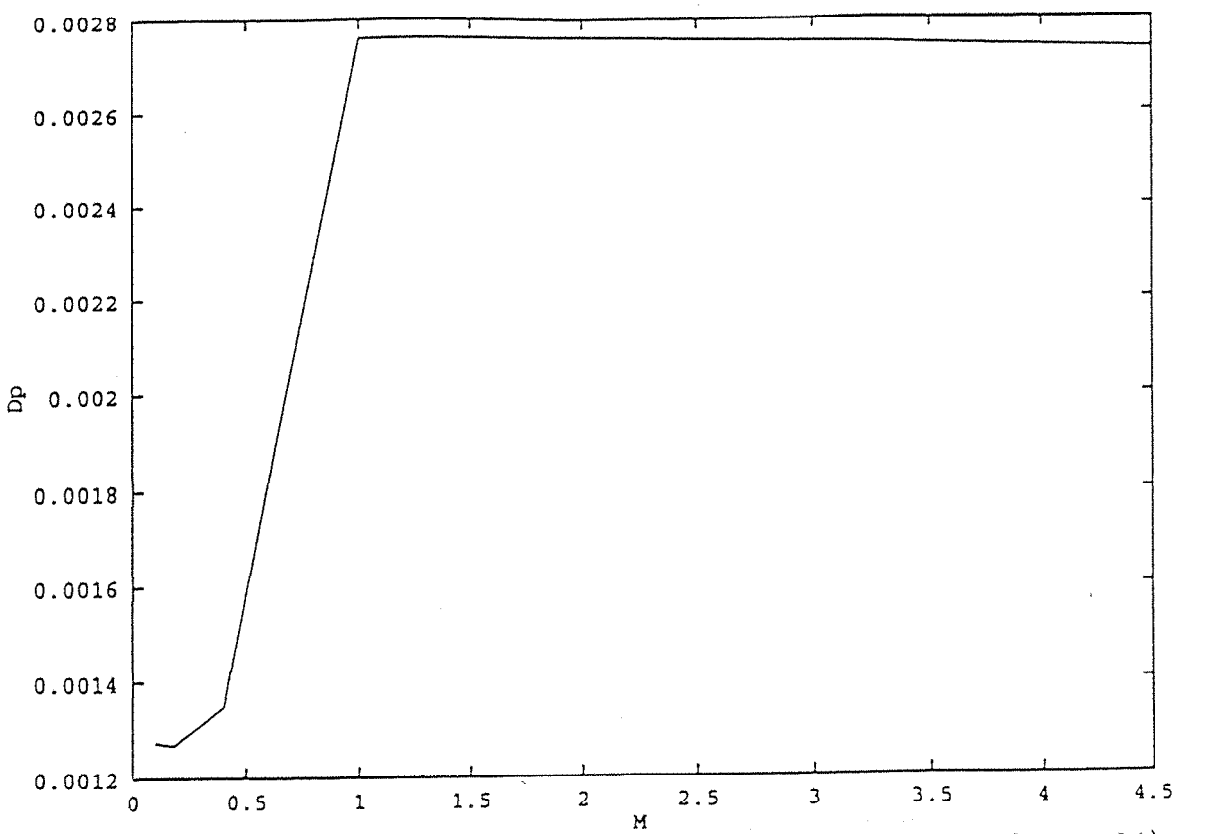

FIGURE 4.8e. Graph of pressure difference against M for n=21, using two curves

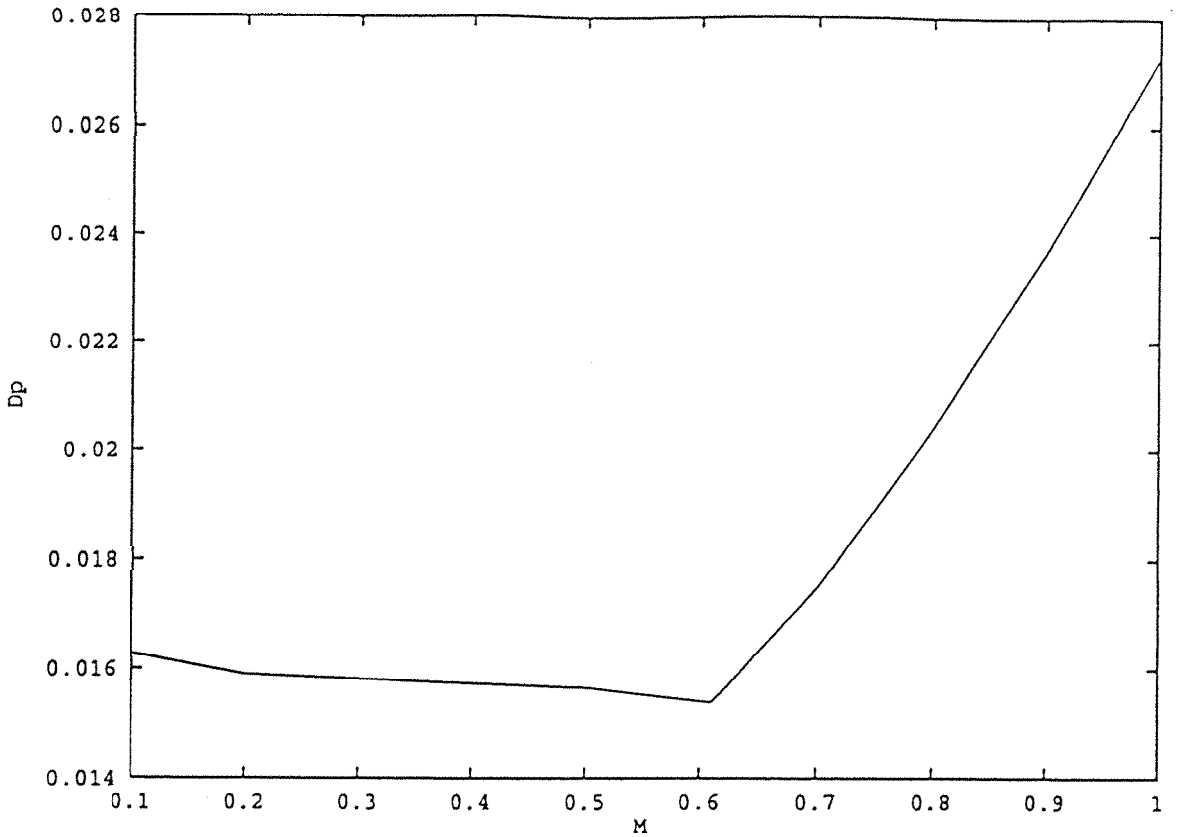

FIGURE 4.9. Graph of pressure difference against M for the minimization method

x	y	D_0	D_1	D_2	D_3
4.00	0.30	0.6012	0.6047	0.6000	0.6175
3.50	1.00	2.0044	1.9992	2.0011	2.0000
1.75	1.00	2.0000	2.0006	1.9978	1.9992
1.00	1.00	2.0896	2.0000	2.0066	2.0063
0.89	0.89	1.9952	1.9999	2.0016	2.0016
0.40	0.40	1.9973	2.0000	1.9996	1.9996
0.00	0.00	0.0004	0.0000	0.0000	0.0000
0.00	-1.10	0.0005	0.0001	0.0000	0.0000
0.00	-2.75	0.0000	0.0000	0.0000	0.0000
0.25	-3.00	1.5083	1.5047	1.5019	1.5069
0.50	-3.00	1.0013	0.9995	0.9991	1.0057
0.50	0.00	1.4067	1.3243	1.3689	1.3681
1.00	-2.50	0.0066	0.0006	0.0005	0.0003
1.00	-0.75	0.0124	0.0124	0.0007	-0.0028
2.00	0.00	0.0009	0.0000	0.0015	0.0015
3.80	0.00	0.0005	0.0000	0.0063	0.0000

TABLE 4.4. Values of M at different points for various domains

x	y	$\lvert D_3 - D_0 \rvert$	$\lvert D_3 - D_1 \rvert$	$\lvert D_3 - D_2 \rvert$
4.00	0.30	$1.63e{-2}$	$1.30e{-2}$	$1.75e{-2}$
3.50	1.00	$4.40e{-3}$	$8.00e{-4}$	$1.10e{-3}$
1.75	1.00	$7.00e{-4}$	$1.30e{-3}$	$1.50e{-3}$
1.00	1.00	$8.30e{-2}$	$6.30e{-3}$	$3.00e{-4}$
0.89	0.89	$6.40e{-3}$	$1.80e{-3}$	$0.00e{-0}$
0.40	0.40	$2.30e{-3}$	$4.00e{-4}$	$0.00e{-0}$
0.00	0.00	$4.00e{-4}$	$0.00e{-0}$	$0.00e{-0}$
0.00	-1.10	$5.00e{-4}$	$0.00e{-0}$	$0.00e{-0}$
0.00	-2.75	$0.00e{-0}$	$6.00e{-4}$	$0.00e{-0}$
0.25	-3.00	$1.40e{-3}$	$2.20e{-3}$	$5.00e{-3}$
0.50	-3.00	$4.40e{-3}$	$6.23e{-3}$	$6.58e{-3}$
0.50	0.00	$3.76e{-2}$	$4.48e{-2}$	$2.00e{-4}$
1.00	-2.50	$6.59e{-3}$	$5.94e{-3}$	$4.51e{-4}$
1.00	-0.75	$9.54e{-3}$	$9.55e{-3}$	$2.15e{-3}$
2.00	0.00	$6.49e{-4}$	$1.51e{-3}$	$2.18e{-5}$
3.80	0.00	$1.08e{-2}$	$2.64e{-3}$	$3.69e{-3}$

TABLE 4.5. Absolute differences of M for different domains

y	S_1'	S_2'	Δp
0.65	1.30	-0.30	$0.233e{-}1$
0.45	0.90	0.10	$0.483e{-}1$
0.35	0.70	0.30	$0.654e{-}2$
0.20	0.40	0.60	$0.312e{-}2$
0.15	0.30	0.70	$0.656e{-}2$
0.10	0.20	0.80	$0.980e{-}2$
0.21	0.42	0.58	$0.261e{-}2$
0.22	0.44	0.56	$0.197e{-}2$

TABLE 4.6a. Pressure differences for various points, M=2

y	S_1'	S_2'	Δp
0.26	0.52	0.48	$0.65e{-}3$
0.25	0.50	0.50	$O(10^{-6})$
0.24	0.48	0.52	$0.65e{-}3$

TABLE 4.6b. Pressure differences for some specific points, M=2

y	Δp
0.35	$0.6532e{-}2$
0.24	$0.6528e{-}3$
0.25	$0.0000e{-}0$
0.26	$0.6529e{-}3$
0.22	$0.1959e{-}2$
0.20	$0.3261e{-}2$
0.10	$0.9798e{-}2$

TABLE 4.7a. Pressure differences for M=0.1, using lines

y	Δp
0.35	$0.6528e{-}2$
0.24	$0.6531e{-}3$
0.25	$0.4452e{-}6$
0.26	$0.1961e{-}2$
0.22	$0.6527e{-}3$
0.20	$0.3252e{-}2$
0.10	$0.9798e{-}2$

TABLE 4.7b. Pressure differences for M=0.3, using lines

y	Δp
0.35	$0.6534e{-2}$
0.24	$0.6593e{-3}$
0.25	$0.0000e{-0}$
0.26	$0.6723e{-3}$
0.22	$0.1965e{-2}$
0.20	$0.3212e{-2}$
0.10	$0.9760e{-2}$

TABLE 4.7c. Pressure differences for M=1, using lines

y	Δp
0.24	$0.1394e{-2}$
0.25	$0.1702e{-2}$
0.26	$0.2205e{-2}$
0.22	$0.1745e{-2}$
0.20	$0.3362e{-2}$
0.10	$0.9620e{-2}$

TABLE 4.7d. Pressure differences for M=3, using lines

y	Δp
0.24	$0.1503e{-2}$
0.25	$0.1790e{-2}$
0.26	$0.2276e{-2}$
0.22	$0.1810e{-2}$
0.20	$0.2864e{-2}$
0.10	$0.9564e{-2}$

TABLE 4.7e. Pressure differences for M=4.5, using lines

M	y	Δp
0.200	0.25	$0.1395e{-}2$
0.300	0.25	$0.8336e{-}3$
0.487	0.25	$0.1173e{-}3$
0.500	0.25	$0.1318e{-}3$
0.700	0.25	$0.1395e{-}2$
1.000	0.24	$0.3843e{-}2$
2.000	0.26	$0.3342e{-}2$
4.500	0.26	$0.1029e{-}1$

TABLE 4.8a. Pressure differences obtained by using one curve, n=5

M	y	Δp
0.300	0.25	$0.1678e{-}2$
0.554	0.25	$0.1262e{-}2$
0.600	0.25	$0.1293e{-}2$
0.700	0.25	$0.1578e{-}2$
1.000	0.26	$0.3170e{-}2$
2.000	0.24	$0.3663e{-}2$
4.500	0.24	$0.4000e{-}2$

TABLE 4.8b. Pressure differences obtained by using one curve, n=7

M	y	Δp
0.100	0.25	$0.1535e{-}2$
0.200	0.25	$0.1595e{-}2$
0.234	0.25	$0.1518e{-}2$
0.300	0.25	$0.1529e{-}2$
0.600	0.25	$0.1752e{-}2$
0.700	0.25	$0.1859e{-}2$
1.000	0.24	$0.3265e{-}2$
2.000	0.25	$0.3204e{-}2$
4.500	0.24	$0.2755e{-}2$

TABLE 4.8c. Pressure differences obtained by using one curve, n=9

M	y	Δp
0.20	0.25	$0.1459e{-2}$
0.30	0.25	$0.1412e{-2}$
0.34	0.25	$0.1406e{-2}$
0.50	0.25	$0.1558e{-2}$
0.70	0.25	$0.1989e{-2}$
1.00	0.26	$0.3091e{-2}$
2.00	0.25	$0.3112e{-2}$
4.50	0.25	$0.2805e{-2}$

TABLE 4.8d. Pressure differences obtained by using one curve, n=11

M	y	Δp
0.200	0.25	$0.1335e{-2}$
0.231	0.25	$0.1334e{-2}$
0.700	0.25	$0.1993e{-2}$
1.000	0.22	$0.2795e{-2}$
2.000	0.25	$0.2941e{-2}$
4.500	0.25	$0.2926e{-2}$

TABLE 4.8e. Pressure differences obtained by using one curve, n=17

M	y	Δp
0.1	0.25	$0.1267e{-2}$
0.2	0.25	$0.1276e{-2}$
0.3	0.25	$0.1280e{-2}$
1.0	0.26	$0.2294e{-2}$
2.0	0.25	$0.2761e{-2}$
4.5	0.25	$0.2684e{-2}$

TABLE 4.8f. Pressure differences obtained by using one curve, n=21

M	y	Δp
0.300	0.20	$0.1583e{-2}$
0.585	0.25	$0.1487e{-2}$
0.700	0.25	$0.1671e{-2}$
1.000	0.25	$0.3659e{-2}$
2.000	0.24	$0.3679e{-2}$
4.500	0.20	$0.2951e{-2}$

TABLE 4.9a. Pressure differences obtained by using two curves, n=5

M	y	Δp
0.20	0.25	$0.1523e{-2}$
0.35	0.25	$0.1464e{-2}$
0.70	0.20	$0.1982e{-2}$
1.00	0.25	$0.3221e{-2}$
2.00	0.24	$0.3348e{-2}$
4.50	0.24	$0.3020e{-2}$

TABLE 4.9b. Pressure differences obtained by using two curves, n=7

M	y	Δp
0.20	0.25	$0.1425e{-2}$
0.28	0.25	$0.1412e{-2}$
0.70	0.26	$0.1973e{-2}$
1.00	0.25	$0.2983e{-2}$
2.00	0.24	$0.3098e{-2}$
4.50	0.24	$0.2937e{-2}$

TABLE 4.9c. Pressure differences obtained by using two curves, n=9

M	y	Δp
0.100	0.25	$0.1268e{-2}$
0.152	0.25	$0.1265e{-2}$
0.600	0.25	$0.1682e{-2}$
1.000	0.27	$0.2795e{-2}$
2.000	0.27	$0.2787e{-2}$
4.500	0.27	$0.2747e{-2}$

TABLE 4.9d. Pressure differences obtained by using two curves, n=17

M	y	Δp
0.10	0.24	$0.1273e{-2}$
0.17	0.24	$0.1269e{-2}$
0.40	0.26	$0.1349e{-2}$
1.00	0.26	$0.2759e{-2}$
2.00	0.27	$0.2761e{-2}$
4.50	0.27	$0.2734e{-2}$

TABLE 4.9e. Pressure differences obtained by using two curves, n=21

y_1	y_2	M	Δp
0.10	0.45	0.237–0.239	$0.2004e{-1}$
0.15	0.45	0.685–0.699	$0.2014e{-1}$
0.24	0.45	0.732	$0.2571e{-1}$
0.25	0.45	0.718	$0.2637e{-1}$
0.26	0.45	0.701	$0.2698e{-1}$
0.22	0.45	0.760	$0.2445e{-1}$
0.20	0.45	0.785–0.789	$0.2320e{-1}$
0.27	0.45	0.685	$0.2762e{-1}$

TABLE 4.10a. Pressure differences for various M and y-coordinates using three curves, n=5

y_1	y_2	M	Δp
0.10	0.35	0.235–0.240	$0.8308e{-3}$
0.22	0.10	0.370–0.380	$0.3894e{-2}$
0.24	0.10	0.580	$0.3939e{-2}$
0.25	0.10	0.594–0.599	$0.3950e{-2}$
0.26	0.65	0.392–0.401	$0.3956e{-2}$
0.30	0.22	0.568–0.577	$0.3531e{-2}$

TABLE 4.10b. Pressure differences for various M and y-coordinates using three curves, n=17

y_1	y_2	M	Δp
0.2370	0.7591	0.10	$0.1628e{-1}$
0.2162	0.8143	0.40	$0.1594e{-1}$
0.2041	0.7953	0.50	$0.1566e{-1}$
0.1874	0.8140	0.61	$0.1538e{-1}$
0.1630	0.7673	0.70	$0.1748e{-1}$
0.1891	0.7515	0.80	$0.2044e{-1}$
0.1975	0.7265	0.90	$0.2368e{-1}$
0.2053	0.6893	1.00	$0.2731e{-1}$

TABLE 4.11. Pressure differences for various M and y-coordinates, n=7

CHAPTER 5
THE HEAT TRANSFER PROBLEM

5.1. INTRODUCTION TO THE PROBLEM

High temperatures in a turbine cause thermal stresses which can affect its life expectancy. In order to limit these effects it is essential to determine the temperature profiles in the area of the turbine and its components. In this chapter we will examine the phenomenon of heat transfer in a subsonic main stream on the surface of a turbine blade when film cooling takes place. The thin layer of fluid is created when a secondary flow is injected from a slot. This injected flow covers the slot and the area downstream of the cavity. The temperature of the main stream is much higher than the temperature of the injected fluid. Both fluids are assumed to be inviscid and incompressible.

5.2. THE ENERGY EQUATION

The partial differential equation governing heat transfer is the energy equation. For a constant property viscous fluid with heat convection, heat conduction and viscous dissipation the equation has the general form

$$\rho c\left(\frac{\partial T}{\partial t}+(\mathbf{q}\cdot\nabla)T\right)=k\nabla^2 T+\mu\sum_{i=1}^{3}\sum_{j=1}^{3}\left(\frac{\partial q_i}{\partial x_j}\right)^2 \tag{5.1}$$

where $T(x,y)$ is the temperature of the fluid, ρ is the density of the fluid, c the specific heat capacity, k the thermal conductivity, μ the viscosity coefficient, Özişik (1977), and $\mathbf{q}$ the velocity vector. When the fluid is incompressible and the viscous

dissipation effects are negligible (as in our case), equation (5.1) becomes

$$\rho c\left(\frac{\partial T}{\partial t}+(\mathbf{q}\cdot\nabla)T\right)=k\nabla^2 T. \tag{5.2}$$

Since the flow is considered to be steady, equation (5.2) can be simplified further by omitting from the left hand side of the equation the time derivative term. Thus the equation becomes

$$\rho c(\mathbf{q}\cdot\nabla T)=k\nabla^2 T, \tag{5.3a}$$

which in 2 dimensions can be written

$$\rho c\left(u\frac{\partial T}{\partial x}+v\frac{\partial T}{\partial y}\right)=k\left(\frac{\partial^2 T}{\partial x^2}+\frac{\partial^2 T}{\partial y^2}\right). \tag{5.3b}$$

The first boundary condition for equation (5.3a) is that the temperature on the boundary between the free stream and the film is taken to be equal to the main stream temperature, T_1. Thus

$$T=T_1 \qquad \text{at} \qquad y=S(x),$$

where $S(x)$ is the streamline. At the wall there will be a second condition which prescribes the heat transfer there. For an insulated wall

$$\frac{\partial T}{\partial y}=0 \qquad \text{at} \qquad y=0,$$

or more generally,

$$\frac{\partial T}{\partial y}=h'(T_w-T_f),$$

where h' is the heat transfer coefficient, T_w the wall temperature and T_f the fluid temperature. Another possible condition is

$$T_w=\text{constant} \qquad \text{at} \qquad y=0,$$

which means that the wall temperature is constant. Away from the slot the temperature T tends to the main stream temperature T_1: $T\to T_1$ as $x\to\infty$. Finally, the temperature in the slot is taken to be equal to T_0, where $T_0<T_1$, thus

$$T=T_0 \qquad \text{when} \qquad 0\le x\le 1 \qquad \text{and} \qquad 0\le y\le S(x).$$

This means that we can approximate the solution of the problem by calculating the temperature profiles starting from $x = 1$, because we assume that the main stream temperature does not affect the slot temperature, since the 'lid' effect (described in chapter 4, section 4.2) keeps the slot temperature at T_0. Figure 5.1 shows the geometry of the heat transfer problem. Equation (5.3b) must be solved subjected to the boundary conditions shown in figure 5.1, in order to obtain the temperature profiles in the film and to determine the temperature of the wall downstream of the slot.

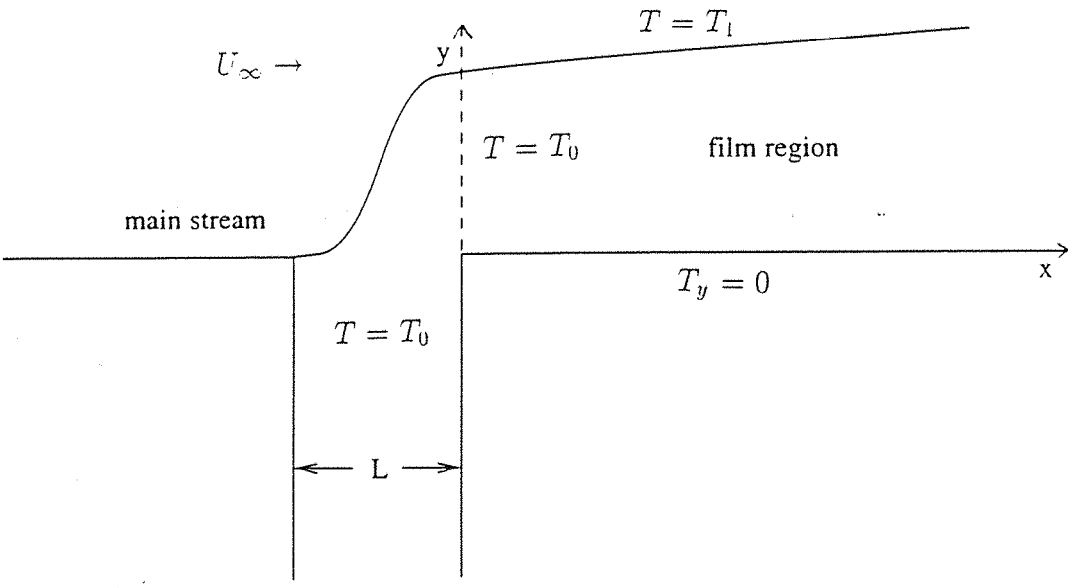

FIGURE 5.1. The domain for the heat transfer problem

Before proceeding with the solution of the problem, it is sensible to scale and non–dimensionalize the variables of the model to see if any simplifications are possible.

5.3. DEFINING THE PROBLEM

We will use the same dimensionless variables as in chapter 4 and section 4.2. Thus U_∞ is the velocity of the main stream, ρ_∞ the density of the fluid of the free stream, L is the slot width and ϵ is a small parameter, defined by equation (4.1), which describes a small disturbance to the main flow. Also we introduce the following

non–dimensional parameters $\overline{x} = \frac{x}{L}$, $\overline{y} = \frac{y}{L\epsilon^2}$, $\overline{u} = \frac{u}{U_\infty \epsilon}$, $\overline{v} = \frac{v}{U_\infty \epsilon^3}$ and $\overline{T} = \frac{T-T_0}{T_1-T_0}$, where T is the temperature of the film, T_1 the main stream temperature and T_0 the temperature of the injected secondary fluid, with $T_0 < T_1$ for film cooling. The above non–dimensionalization reduces equation (5.3b) to the following form

$$\begin{aligned}
&\alpha[\overline{u}U_\infty \epsilon \overline{T}_{\bar{x}}(T_1 - T_0) + \overline{v}U_\infty \epsilon \overline{T}_{\bar{y}}(T_1 - T_0)] = \\
&\frac{1}{L}\overline{T}_{\bar{x}\bar{x}}(T_1 - T_0) + \frac{1}{L\epsilon^4}\overline{T}_{\bar{y}\bar{y}}(T_1 - T_0) \Rightarrow \\
&\alpha L U_\infty \epsilon[(\overline{u}\overline{T}_{\bar{x}}(T_1 - T_0) + \overline{v}\overline{T}_{\bar{y}}(T_1 - T_0)] = \\
&\overline{T}_{\bar{x}\bar{x}}(T_1 - T_0) + \frac{1}{\epsilon^4}\overline{T}_{\bar{y}\bar{y}}(T_1 - T_0) \qquad (5.4)
\end{aligned}$$

where $\alpha = \frac{\rho_\infty c}{k}$ and is the thermal diffusivity. If we look closely at equation (5.4) we will see that the $\overline{T}_{\bar{y}\bar{y}}$ term is orders of magnitude greater than $\overline{T}_{\bar{x}\bar{x}}$, since $\epsilon \ll 1$. This means that $\overline{T}_{\bar{y}\bar{y}}$ is the dominant term of the right hand side, and thus we can omit the term $\overline{T}_{\bar{x}\bar{x}}$. Equation (5.4) becomes, therefore

$$\alpha L U_\infty \epsilon^5 (uT_x + vT_y)(T_1 - T_0) = T_{yy}(T_1 - T_0), \qquad (5.5)$$

(we have also dropped the bars over the variables for simplicity). If we examine equation (5.5) more carefully, we can see that the left hand side of the equation represents the convective heat transfer term and the right hand side is the conduction–(diffusion) term. Now, we can define $\delta = \alpha L U_\infty \epsilon^5$, a parameter that determines which terms dominate equation (5.5).

When $\delta \gg 1$, the flow has negligible effect on the temperature distribution and the temperature is considered constant in the area of the film. This means that the convective term is the dominant term of equation (5.5) and film cooling occurs, with the region downstream of the slot well protected from the main stream temperature. In fact, film cooling will not be effective at a long distance downstream of the slot due to the considerable mixing of the main stream and secondary flows.

In the case when $\delta \ll 1$, diffusion dominates the area downstream of the cavity and the main stream temperature is spread in the area of the film. Thus, to lowest order equation (5.5) gives

$$T_{yy} = 0,$$

with boundary conditions $T_y = 0$ on $y = 0$ and $T = 1$ on $y = S(x)$. The solution of the above equation is

$$T = yA(x) + B(x),$$

where $A(x)$ and $B(x)$ are function of x, determined by the boundary conditions. Thus when $T = 1$ on $y = S(x)$ we obtain $1 = S(x)A(x) + B(x)$ and for $T_y = 0$ on $y = 0$, we get $A(x) = 0$. Thus the temperature in the film is simply $T = 1$. However, this case is beyond our present aim and we will ignore it.

The most interesting case is when δ is $O(1)$ and the terms in equation (5.5) balance each other (as seems likely in our case, where $\delta = 1$) and both sides of the energy equation must be retained. This means that $\frac{1}{LU_\infty \alpha}$ must be $O(\epsilon^5)$. Then film cooling occurs for a distance downstream of the slot and at the same time the main stream temperature affects the temperature in the film region, i.e. heat transfer occurs.

As has been said before we can approximate the solution of the temperature domain by starting the calculations from x =1. We have assumed that the secondary flow comes out of the slot tangentially at the upstream edge of the cavity, meaning that the outer flow forms a 'lid' over the slot, which affects a great deal the amount of mass flow coming out of the cavity. Nevertheless, due to this phenomenon, the area of the slot is well protected from the hot gases of the outer flow and the slot temperature is not influenced by the main stream temperature.

Thus the mesh for the heat transfer problem starts from x =1 and extends downstream from the slot. The grid is also bounded by the streamline on top, and the wall at the bottom. The boundary conditions may be seen on diagram of figure 5.1 and are very similar to those given in section 5.2. Thus, on the wall we assume there is no heat exchange between the surface and the fluid (the wall is perfectly insulated), i.e.

$$\frac{\partial T}{\partial y} = 0 \qquad \text{at} \qquad y = 0.$$

On the streamline we have prescribed the main stream non–dimensional temperature

$$T = 1 \qquad \text{at} \qquad y = S(x)$$

and at the beginning of the mesh, on the downstream edge of the slot, we use the non–dimensional slot temperature

$$T = 0 \qquad \text{at} \qquad x = 1.$$

5.4. NUMERICAL SOLUTION, FINITE DIFFERENCE SCHEME

Equation (5.5) can be solved numerically by using a finite difference method. If we denote the value of T at a point, p, on the grid by t_p and the step length in the x and y directions by h and l respectively, then the mesh point p will have coordinates $x = 1 + (n-1)h$ and $y = (j-1)l$, where $n = 1...nx$ (where nx is the number of points in the x direction) and $j = 1...ny$, (where ny is the number of points in the y direction). Thus the value t_p at the point can also be written in the form

$$t_p = t(nh, jl) = t_{n,j}.$$

Now using Taylor's theorem we can write the first derivatives on the left hand side of (5.5) by using forward–difference expressions and for the second derivative of the right hand side we can use central–differences. Thus the derivatives in equation (5.5) become

$$T_x \simeq \frac{t_{n+1,j} - t_{n,j}}{h}$$

$$T_y \simeq \frac{t_{n,j+1} - t_{n,j}}{l}$$

$$T_{yy} \simeq \frac{t_{n,j+1} - 2t_{n,j} + t_{n,j-1}}{l^2}.$$

For the derivative condition, $T_y = 0$, on the wall ($j = 1$), we use

$$T_y = \frac{t_{n,2} - t_{n,0}}{2l} = 0,$$

which implies

$$t_{n,2} = t_{n,0},$$

where $t_{n,0}$ is a fictional point that has been introduced only for reasons of convenience. From the above expression it may be seen that we can substitute $t_{n,2}$ for $t_{n,0}$ each time it appears. The above expressions for the derivatives can be used in equation

(5.5) to produce a finite difference approximation to the energy equation. The finite difference scheme is

$$\frac{\delta u}{h}t_{n+1,j} - \frac{\delta u}{h}t_{n,j} + \frac{\delta v}{l}t_{n,j+1} - \frac{\delta v}{l}t_{n,j} = \frac{1}{l^2}t_{n,j+1} - \frac{2}{l^2}t_{n,j} + \frac{1}{l^2}t_{n,j-1}$$

and on multiplying by h and defining $r = \frac{h}{l^2}$ we obtain

$$\delta u t_{n+1,j} - \delta u t_{n,j} + \delta v l r t_{n,j+1} - \delta v l r t_{n,j} = r t_{n,j+1} - 2r t_{n,j} + r t_{n,j-1}.$$

Rearranging the equation to have all the known values of t on the right hand side we obtain

$$\delta u t_{n+1,j} = r t_{n,j-1} - t_{n,j}(2r - \delta v l r - \delta u) + r t_{n,j+1}(1 - \delta v l) \Rightarrow$$

$$t_{n+1,j} = \frac{1}{\delta u}(r t_{n,j-1} - t_{n,j}(2r - \delta v l r - \delta u) + r t_{n,j+1}(1 - \delta v l)) \qquad (5.6)$$

where δ is defined previously (and set equal to 1) and u cannot be equal to zero (the values for both velocity components are given in the following section). The above formula is called a *simple explicit* method, Smith (1965), since it has one unknown value ($t_{n+1,j}$) directly expressed in terms of known ones.

5.4.1. Defining the Three Regions of the Problem

The numerical scheme given in equation (5.6) must be used together with some results obtained for the subsonic flow problem in Fitt et al (1985). Defining $\Psi(x,y) = y\frac{M}{S(x)}$, where M is the mass flow at infinity and $S(x)$ the streamline, we can obtain expressions for u and v. We know that $u = \Psi_y$ and $v = -\Psi_x$ which means that $u = \frac{M}{S(x)}$ and $v = yS_x\frac{M}{S(x)^2}$. Since the mass flow and the streamline are known, u and v can easily be calculated. However we have three regions where v changes according to y. These regions are

region (i) when $y = 0$, $\Psi(x,0) = 0$ and $v = 0$,

region (ii) when $0 < y < S(x)$, $\Psi(x,y) = y\frac{M}{S(x)}$ and $v = yS_x\frac{M}{S(x)^2}$ and

region (iii) when $y = S(x)$, $\Psi(x,y) = M$ and $v = S_x\frac{M}{S(x)}$.

The mass flow is defined as $M = H^3(\infty)$ and the streamline $S(x) = M^{\frac{2}{3}}H(x)$, section 4.2.1 and Fitt et al (1985). Thus by substituting these equations into the above three expressions we get

region (i) $u = \frac{M^{\frac{1}{3}}}{H(x)}$, $v = 0$,

region (ii) $u = \frac{M^{\frac{1}{3}}}{H(x)}$, $v = yS_x \frac{1}{H^2(x)M^{\frac{1}{3}}}$ and

region (iii) $u = \frac{M^{\frac{1}{3}}}{H(x)}$, $v = S_x \frac{M^{\frac{1}{3}}}{H(x)}$.

Before we solve equation (5.6) described at the section 5.4 it is essential to check the stability of the simple explicit method.

5.4.2. Stability Analysis of the Numerical Scheme

We consider the solution t of the finite difference equation approximating the exact solution T of the energy equation. Now, due to truncation errors of the numerical solution, we will obtain a solution t^*. The difference $(t - t^*)$ is defined as the error E and it can be expressed as a Fourier series $E_n^j = \sum_{k=0}^{\infty} A_k e^{i\beta_k n}$, where $i = \sqrt{(-1)}$. We will consider only the propagation of one component of the error, which can be written as $e^{i\beta j}$. In order to determine this error we assume a solution of the difference equation of the form

$$E_n^j = G^n e^{i\beta j}.$$

The quantity G is called the amplification factor of the method since

$$|E_n^j| = |G^n||e^{i\beta j}| = |G|^n.$$

In order for the method to be stable we need $|G| < 1$, Smith (1965). By the term stability we mean that the values of $t_{n,j}$ and any local error must be bounded as n increases since numerical operations are applied to both values as the solution propagates forward in space. Thus, in order for the solution of the finite difference equation to converge to the exact solution, the error should not be magnified as the solution of the problem continues.

It may be seen that the tangential velocity component is a function of x, i.e. $u = u(x)$ and the y velocity component is a function of y, i.e. $v = v(y)$ (see also section 5.4.1). Thus for simplicity reasons we can set $v = 0$ and check the stability for the following equation

$$uT_x = T_{yy},$$

since u is considered to be constant along the y direction. Substituting $t_{n,j}$ with $G^n e^{i\beta j}$ into the difference equation (5.6) we obtain the following expression

$$G^{n+1}e^{i\beta j} = \frac{1}{\delta u}(rG^n e^{i\beta(j-1)} - G^n e^{i\beta j}(2r - \delta u) + rG^n e^{i\beta(j+1)}).$$

Dividing by $G^n e^{i\beta j}$

$$G = \frac{1}{\delta u}(re^{-i\beta} - 2r + \delta u + re^{i\beta}) \Rightarrow$$

$$\delta u G = (re^{-i\beta} - 2r + \delta u + re^{i\beta}).$$

Rearranging and replacing $e^{-i\beta} = \cos\beta - i\sin\beta$ and $e^{i\beta} = \cos\beta + i\sin\beta$, we obtain

$$\delta u G = 2r(\cos\beta - 1) + \delta u.$$

For stability we require $|G| < 1$, therefore we have

$$|\frac{2r(\cos\beta - 1)}{\delta u} + 1| < 1.$$

The left hand side of this inequality gives

$$-1 < \frac{2r(\cos\beta - 1)}{\delta u} + 1 \Rightarrow -2 < \frac{2r(\cos\beta - 1)}{\delta u} \Rightarrow$$

$$1 > \frac{r}{\delta u}(1 - \cos\beta).$$

Thus we want $\frac{\delta u}{1-\cos\beta} > r$. The main term in this inequality is $1 - \cos\beta$. Thus we want

$$|1 - \cos\beta| \leq 2.$$

The left hand side of this inequality gives $3 \geq \cos\beta$ which is true and the right hand side gives $-1 \leq \cos\beta$ which is also true. Thus $1 - \cos\beta \leq 2$ is true and we can say now that the inequality $\frac{\delta u}{1-\cos\beta} > r$ becomes $\frac{\delta u}{2} > r$. The constant δ is taken to be 1, thus we obtain

$$\frac{u}{2} > r.$$

Now we have to check the value of u. We know that $u = \frac{M^{\frac{1}{3}}}{H(x)}$ (from section 5.4.1) and also that $M = H^3(\infty)$. From here it may be seen that $M^{\frac{1}{3}} \geq H(x)$, thus setting $M^{\frac{1}{3}} = H(\infty)$ (from section 4.4.2) we obtain that $1.024 \geq H(x)$. Thus the value of u

will always have a lower limit, meaning that always $u \geq 1$ and the ratio will have an upper bound,

$$\frac{1}{2} > r.$$

Thus it may be seen that r must be marginally less than $\frac{1}{2}$ in order for the left hand side of the original inequality to stand.

Now, the right hand side of the inequality gives

$$\frac{2r(\cos\beta - 1)}{\delta u} + 1 < 1 \Rightarrow \frac{2r(\cos\beta - 1)}{\delta u} < 0.$$

From here it is obvious that $\cos\beta \leq 1$ for the above expression to be satisfied, since δ and u can only be non–zero positive numbers. Thus for the right hand side we also obtain $r < \frac{1}{2}$.

Since an analytical solution of equation (5.5) does not exist we can also solve the heat problem by using a different numerical scheme. In this way we will be able to compare the results produced from both methods to show that the solution obtained for the energy equation is correct.

5.4.3. The Crank–Nicolson Scheme

This method is based on using central difference approximations at the intermediate mesh point $(n + \frac{1}{2}, j)$ for the second derivative in equation (5.5). Thus for the first derivatives T_x and T_y the finite difference equations remain the same as before, but now T_{yy} becomes

$$T_{yy} \simeq \frac{1}{2l^2}(t_{n+1,j+1} - 2t_{n+1,j} + t_{n+1,j-1} + t_{n,j+1} - 2t_{n,j} + t_{n,j-1}),$$

and the difference approximation to equation (5.5) is

$$\frac{\delta u}{h}t_{n+1,j} - \frac{\delta u}{h}t_{n,j} + \frac{\delta v}{l}t_{n,j+1} - \frac{\delta v}{l}t_{n,j} = \frac{1}{2l^2}(t_{n+1,j+1} -$$

$$2t_{n+1,j} + t_{n+1,j-1} + t_{n,j+1} - 2t_{n,j} + t_{n,j-1}).$$

Multiplying by h and defining $r = \frac{h}{l^2}$ leads to

$$\delta u t_{n+1,j} - \delta u t_{n,j} + \delta v r l t_{n,j+1} - \delta v r l t_{n,j} = \frac{r}{2}t_{n+1,j+1} -$$

$$rt_{n+1,j} + \frac{r}{2}t_{n+1,j-1} + \frac{r}{2}t_{n,j+1} - rt_{n,j} + \frac{r}{2}t_{n,j-1}$$

and rearranging the equation to have all the unknowns on the left hand side we obtain the following result

$$(r + \delta u)t_{n+1,j} - \frac{r}{2}t_{n+1,j+1} - \frac{r}{2}t_{n+1,j-1} = \frac{r}{2}t_{n,j-1} +$$

$$(\delta u - r + \delta vrl)t_{n,j} + (\frac{r}{2} - \delta vrl)t_{n,j+1}. \tag{5.7}$$

This is the Crank–Nicolson finite difference method. The terms on the left hand side of equation (5.7) are the unknown values of t, whereas on the right hand side the values of t are all known. This numerical scheme is *implicit*, Smith (1965), meaning that the unknown values of t can be found only by the solution of simultaneous equations generated when the expressions for the values of the unknown t are derived.

5.4.4. Stability Analysis of the Crank–Nicolson Scheme

Now, before we progress any further we consider the stability of the above method. The same process will be followed as before. Thus if we introduce the quantity $G^n e^{i\beta j}$ and substitute it for $t_{n,j}$ and set $v = 0$, equation (5.7) becomes

$$(\delta u + r)G^{n+1}e^{i\beta j} - \frac{r}{2}G^{n+1}e^{i\beta(j-1)} - \frac{r}{2}G^{n+1}e^{i\beta(j+1)} = \frac{r}{2}G^n e^{i\beta(j-1)} +$$

$$(\delta u - r)G^n e^{i\beta j} + \frac{r}{2}G^n e^{i\beta(j+1)}.$$

Dividing by $G^n e^{i\beta j}$ we obtain

$$(\delta u + r)G - \frac{r}{2}Ge^{-i\beta} - \frac{r}{2}Ge^{i\beta} = \frac{r}{2}e^{-i\beta} + \delta u - r + \frac{r}{2}e^{i\beta}.$$

Now using Euler's formula again, $e^{i\beta} = \cos\beta + i\sin\beta$, and rearranging the above equation to have G on the left hand side, we obtain

$$G(r + \delta u - r\cos\beta) = r\cos\beta + \delta u - r.$$

For stability we require $|G| < 1$, thus the above expression becomes

$$|G| = |\frac{r(\cos\beta - 1) + \delta u}{r(1 - \cos\beta) + \delta u}| < 1 \Rightarrow$$

$$-1 < \frac{r(\cos\beta - 1) + \delta u}{r(1 - \cos\beta) + \delta u} < 1.$$

We examine first the left hand side

$$-1 < \frac{r(\cos\beta - 1) + \delta u}{r(1 - \cos\beta) + \delta u} \Rightarrow$$

$$-\delta u - r(1 - \cos\beta) < r(\cos\beta - 1) + \delta u \Rightarrow -2\delta u < 0,$$

which is true, since $\delta = 1$ and u cannot be negative. Now the right hand side will give

$$r(\cos\beta - 1) + \delta u < r(1 - \cos\beta) + \delta u \Rightarrow \cos\beta < 1,$$

which is also true as long as $\beta \neq 0$ (for the case $\beta = 0$ the method is unstable). From the above analysis it is obvious that r in unconditionally stable and can take any positive non–zero values. Thus the Crank–Nicolson scheme is proven to be stable for any values of r.

5.4.5. The Crank-Nicolson Equations

The scheme developed above, equation (5.7), leads to a system of equations which can be solved numerically by writing it in the matrix form

$$\mathbf{Ax} = \mathbf{b}$$

where $\mathbf{A}$ is the coefficient matrix, $\mathbf{x}$ the unknown vector and $\mathbf{b}$ the vector of the known values. If the system of equations is written down for all the unknowns, then the coefficient matrix will be

$$\mathbf{A} = \begin{pmatrix} \delta u + r & r & 0 & \dots & \dots & 0 \\ -\frac{r}{2} & \delta u + r & -\frac{r}{2} & 0 & \dots & 0 \\ \vdots & \vdots & \vdots & \vdots & \vdots & \vdots \\ 0 & 0 & 0 & \dots & -\frac{r}{2} & \delta u + r \end{pmatrix}$$

and the general form of the vector $\mathbf{b}$ will be

$$\mathbf{b} = \frac{r}{2} t_{n,j-1} + (\delta u - r + \delta v r l) t_{n,j} + (\frac{r}{2} - \delta v r l) t_{n,j+1}.$$

Note here that for the first row, $j = 1$, $t_{n,j-1} = t_{n,j+1}$ and in the last row we add to the vector the known value of the boundary point, $t_{n+1,j+1}$. The above matrix has a

tri–diagonal structure which makes the system ideally suited for solution by iterative methods, such as Jacobi or Gauss–Seidel. The latter was used to solve the system of equations and produce the temperatures of the wall surface for the region of the film as discussed below.

5.5. THE TEST PROBLEM

Before we proceed any further in the solution of the energy equation in the film it is essential to check the validity of the model and the two numerical schemes (simple explicit and Crank–Nicolson methods), by solving a test problem for which the analytical solution can be found.

The simplest equation related to our problem is the heat equation in a rectangular region with the same boundary conditions as above, except now the upper boundary of the mesh is $y = 1$ and not $y = S(x)$ as it is for the actual heat problem. Thus the two–dimensional heat equation considered is

$$c\frac{\partial T}{\partial x} = \frac{\partial^2 T}{\partial y^2}, \tag{5.8}$$

where c =constant, and the boundary conditions are

$T_y = 0$ on $y = 0$

$T = 1$ on $y = 1$ and

$T = 0$ on $x = 1$.

For simplicity we define a new variable Θ such that $\Theta(x, y) = 1 - T(x, y)$. Figure 5.2 shows the domain in which the parabolic equation must be solved together with the boundary conditions in terms of Θ, which are

$\Theta_y = 0$ on $y = 0$,

$\Theta = 0$ on $y = 1$ and

$\Theta = 1$ on $x = 1$.

Thus equation (5.8) becomes

$$c\frac{\partial \Theta}{\partial x} = \frac{\partial^2 \Theta}{\partial y^2}. \tag{5.9}$$

The analytical solution of equation (5.9) with the above boundary conditions is easy to determine and will be used to compare the results obtained by the two numerical schemes described in sections 5.4 and 5.4.3. The two numerical methods will be used to solve equation (5.9) in order to produce a solution for the temperature Θ on the wall at a distance x downstream from a slot for the rectangular mesh shown in figure 5.2. By comparing the results of the two solutions (analytical and numerical) we will be able to examine the validity of the two numerical methods and also check if the numerical schemes have been implemented correctly into computer codes.

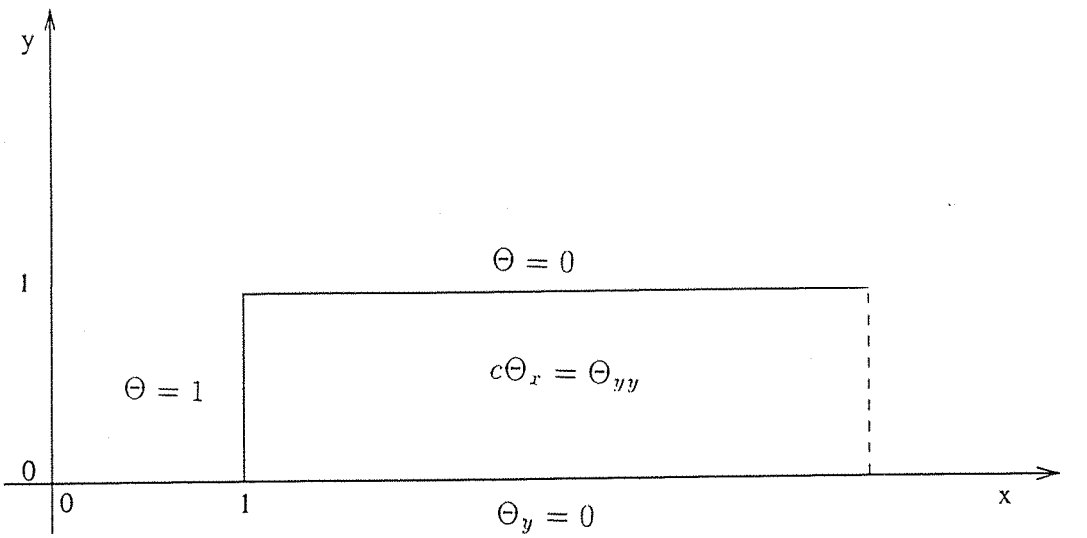

FIGURE 5.2. The domain for the test problem

5.5.1. The Analytical Solution of the Test Problem

In order to solve equation (5.9) analytically we assume a solution of the form $\Theta(x, y) = X(x)Y(y)$, where X is a function of x only and Y is a function of y only. Thus, starting with $\Theta = XY$ we can write (5.9) in terms of X and Y and separating variables, we obtain

$$c\frac{X'}{X} = \frac{Y''}{Y}. \tag{5.10}$$

We now make the assumption that since the left hand side is a function of x only and the right hand side a function of y only, for these to be equal each side must be equal

to the same constant. Let this constant be $-\lambda^2$. Thus the left hand side of equation (5.10) becomes

$$c\frac{X'}{X} = -\lambda^2 \Rightarrow cX' + \lambda^2 X = 0$$

which gives a solution of the form

$$X(x) = Ae^{-\frac{\lambda^2}{c}x}$$

where A is a constant, to be determined by the boundary conditions. The right hand side gives

$$\frac{Y''}{Y} = -\lambda^2 \Rightarrow Y'' + \lambda^2 Y = 0$$

which has a general solution of the form

$$Y(y) = B\cos(\lambda y) + D\sin(\lambda y),$$

where B and D are constants. Thus the general separable solution of the heat equation is

$$\Theta(x,y) = XY = [B\cos(\lambda y) + D\sin(\lambda y)]Ae^{-\frac{\lambda^2}{c}x}. \tag{5.11}$$

Now, in order to find the three unknown constants AB, AD and λ we will have to use the boundary conditions. Thus

$$\Theta_y = [-B\lambda\sin(\lambda y) + D\lambda\cos(\lambda y)]Ae^{-\frac{\lambda^2}{c}x} \tag{5.12}$$

and when $\Theta_y = 0$ at $y = 0$ equation (5.12) becomes

$$D\lambda Ae^{-\frac{\lambda^2}{c}x} \Rightarrow D = 0.$$

Thus equation (5.11) now becomes

$$\Theta(x,y) = A'e^{-\frac{\lambda^2}{c}x}\cos(\lambda y). \tag{5.13}$$

When $\Theta = 0$ at $y = 1$ equation (5.13) is

$$A'e^{-\frac{\lambda^2}{c}x}\cos(\lambda y) = 0 \Rightarrow \cos\lambda = 0 \Rightarrow \lambda_n = \frac{\pi}{2} + n\pi$$

where $n = 0,...,\infty$. The above results mean that (5.13) takes the new form

$$\Theta(x,y) = \sum_{n=0}^{\infty} A_n e^{-\frac{\lambda_n^2}{c}x}\cos(\lambda_n y). \tag{5.14}$$

To satisfy the boundary condition $\Theta(x, y) = 1$ at x =1, we obtain

$$\sum_{n=0}^{\infty} A_n e^{-\frac{\lambda_n^2}{c}} \cos(\lambda_n y) = 1,$$

and we find the coefficient A_n by using a Fourier series. Thus we get

$$A_n = 2e^{\frac{\lambda_n^2}{c}} \int_0^1 \cos(\lambda_n y) dy \Rightarrow A_n = \frac{2}{\lambda_n} e^{\frac{\lambda_n^2}{c}} \sin \lambda_n.$$

Thus equation (5.14) now becomes

$$\Theta(x, y) = 2 \sum_{n=0}^{\infty} \frac{1}{\lambda_n} \sin(\lambda_n) e^{-\frac{\lambda_n^2}{c}(x-1)} \cos(\lambda_n y). \tag{5.15}$$

This is the analytical solution of the heat equation for the prescribed boundary conditions. We can now use the simple explicit method and the Crank–Nicolson scheme, to numerically solve the equation (5.9) and then compare both sets of results with the results produced from the analytical solution (5.15).

5.5.2. Numerical Calculations for the Test Problem

Two FORTRAN codes were written to calculate the temperature Θ in the domain for any x downstream from the slot. One program solved the heat equation by using the simple explicit method, which for equation (5.9) is

$$c \frac{t_{n+1,j} - t_{n,j}}{h} = \frac{t_{n,j+1} - 2t_{n,j} + t_{n,j-1}}{l^2}.$$

Defining the ratio $r = \frac{h}{l^2}$ and rearranging the above finite difference equation, we obtain

$$t_{n+1,j} = t_{n,j} + \frac{r}{c}(t_{n,j+1} - 2t_{n,j} + t_{n,j-1}).$$

The other program used the Crank–Nicolson method, which for this case takes the following form

$$c \frac{t_{n+1,j} - t_{n,j}}{h} = \frac{1}{2l^2}(t_{n+1,j+1} - 2t_{n+1,j} + t_{n+1,j-1} + t_{n,j+1} - 2t_{n,j} + t_{n,j-1}) \Rightarrow$$

$$-\frac{r}{2c} t_{n+1,j-1} + (\frac{r}{c} + 1) t_{n+1,j} - \frac{r}{2c} t_{n+1,j+1} = \frac{r}{2c} t_{n,j-1} + (1 - \frac{r}{c}) t_{n,j} + \frac{r}{2c} t_{n,j+1}.$$

This expression produces a system of equations which can be solved with the same method described in section 5.4.5.

During the entire process of running the programs we kept the ratio, r, less than $\frac{1}{2}$ for the explicit method, since the stability analysis suggested that a stable scheme could be produced only if $r < \frac{1}{2}$. The Crank–NIcolson method was able to handle a wide range of values of r from 0.1 to even 3.33.

Since the solution would propagate along the x–axis, the step in this direction, Δx was taken to be small, so that a more accurate solution would be found. The x–step was in the range of 0.001 to 0.01. The y–step, Δy, was also taken to be relatively small between 0.02 to 0.08. The boundary conditions imposed on the mesh of figure 5.2. where also used in order to start the calculation of the temperature.

5.5.3. Results and Discussion of the Test Model

Many runs were performed to check that the results of the two numerical methods were reliable and close to the analytical solution.

Many different combinations of x and y discretisations were investigated to prove that the two methods were mesh–independent. As it is mentioned above Δx took any values from 0.001 to 0.01 and the y–step was also relatively small. However, for the explicit method we had to be sure that the ratio would always be less than $\frac{1}{2}$, in order to obtain an accurate solution. On the other hand when the Crank–Nicolson method was utilized Δy was taken to be even smaller than 0.05, (values for $\Delta y = 0.04$ to 0.01 were also used). The constant of the heat equation, c, was taken to be 1. In table 5.1 we show tabulated values of the temperature along the surface of the wall for a distance of up to one slot-width downstream from the cavity.

It may be seen that for the first few steps the temperature values are not that close to each other, but as we move away from the slot the temperature values produced by the Crank–Nicolson scheme seem to converge to the analytic results quicker than the results produced from the explicit method. Nevertheless, both methods have given results which are quite acceptable and trustworthy. This may also be seen from the graph of figure 5.3, where the temperature on the wall is plotted against x, the

distance from the slot. In figure 5.3 it is visible that the results from the explicit method, (expl), and the results from the Crank–Nicolson method, (cns), are very close to the analytic solution, (analyt).

x	Implicit Method	Analytic solution	Explicit Method
1.0	0.000000	0.000000	0.000000
1.1	0.000174	0.000032	0.000061
1.2	0.006705	0.000176	0.005714
1.3	0.030142	0.026281	0.028478
1.4	0.069781	0.064333	0.066643
1.5	0.119496	0.109967	0.113321
1.6	0.166398	0.159006	0.164859
1.7	0.217988	0.209954	0.215133
1.8	0.266672	0.258172	0.264043
1.9	0.313221	0.304373	0.312194
2.0	0.358601	0.349495	0.356404

TABLE 5.1. Comparison of the two numerical methods and the analytic solution for the test problem

Finally, we conclude that both numerical methods are reliable, produce very accurate results and can be used to solve the energy equation for the actual problem.

5.6. NUMERICAL CALCULATIONS FOR THE ACTUAL PROBLEM

In order to calculate the temperature profiles for the region of the wall it was necessary to estimate the shape of the streamline (which was considered to be one of the boundaries of the domain, seen in figure 5.1 and section 5.3) and the value of the mass flow at infinity. The results for the values of M and $S(x)$, obtained by using the FORTRAN code described in sections 4.2.1 and 4.2.2 and then were utilized in order to evaluate u and v (as they were given in section 5.4.1). These results were implemented in two numerical codes which solved the heat transfer problem by using the simple explicit and the Crank–Nicolson methods. Then the temperature readings obtained by the two programs were compared with each other.

The boundary condition $T = T_1$, where $T_1 = 1$, was implemented on the streamline and above it, whilst the boundary condition $T = T_0$, $T_0 = 0$, was imposed on the

line x =1. Finally, on the wall the boundary condition T_y =0 was used. It was thus assumed that the wall was insulated.

In order to accurately obtain the temperature downstream from the slot, it was decided to use an exponential mesh (employing a scaling factor, described in section 4.2.2) and a great number of points in the x–direction, in order to have the x–step relatively small. Δy was also chosen to be small in the region 0.02 to 0.08.

Both numerical schemes were tested many times for different Δx and Δy and the results were recorded. The ratios for the explicit method, as before, were taken to be less than $\frac{1}{2}$, whereas the Crank–Nicolson scheme was able to handle larger values of r. Tables 5.2. and 5.3 show some combinations for Δx, Δy and r used and the temperatures recorded on the surface of the wall downstream from the slot.

Δx	r	$T(x)$	x distance	Curve name
0.001	0.277	0.6185	1.345	t_{11}
0.002	0.408	0.6318	1.352	t_{12}
0.003	0.415	0.6403	1.365	t_{13}
0.004	0.458	0.6445	1.365	t_{14}

TABLE 5.2. Wall temperatures obtained by the explicit method, case $T_y = 0$

Δx	r	$T(x)$	x distance	Curve name
0.003	0.833	0.6365	1.365	t_{23}
0.003	1.200	0.6379	1.365	t_{24}
0.002	2.222	0.6211	1.352	t_{22}
0.001	2.500	0.6127	1.345	t_{21}
0.004	4.444	0.6381	1.360	t_{25}

TABLE 5.3. Wall temperatures obtained by the implicit method, case $T_y = 0$

5.7. RESULTS AND DISCUSSION

The results for the simple explicit method may be seen in table 5.2, where different ratios and different Δx and Δy (and hence r) were used and the values of the

temperature at a point $x \approx 1.360$, downstream from the slot have been recorded. (The decision to take $x \approx 1.360$ was based purely on the fact that Δx was relatively small and in order to extent the mesh at a long distance downstream from the slot more points had to be added, thus it would have taken longer for the computer codes to estimate the temperature values. Since the results obtained by the different combinations of Δx and Δy, (seen in tables 5.2 and 5.3), were in a good agreement with each other for each case, there was no need to extend the grid. However, we note here that for the comparison of the two methods the mesh was extended a long distance further down from the slot in order to check the difference in the results produced by the two methods.) It is obvious that the temperature values are all very close together. Thus for values of r less than $\frac{1}{2}$ the method seemed to work well and produced acceptable results. However, when r got close to $\frac{1}{2}$, or exceeded it, the solution deteriorated due to instability as indicated in section 5.4.2, i.e. the ratio must always be less than $\frac{1}{2}$ in order for the simple explicit method to work.

The graphical representation of the results obtained by the ratio combinations given in table 5.2. can be seen in figure 5.4, (curves t_{11} to t_{14}). The temperature on the wall surface against distance downstream from the slot were plotted for some of the different values of r for the explicit method. We see that the temperature profiles were all very similar, and all the curves had similar shapes. Thus, when r was kept small we were able to produce accurate results by using the simple explicit method. This meant that there was no mesh dependence for this method.

When the Crank-Nicolson scheme was utilized we were able to use ratio values greater than $\frac{1}{2}$, since the stability analysis had proved that the method was stable for any ratio values. Thus r was taken to be in the range of 0.833 to 4.444, table 5.3.

It may be seen that the temperature values on the wall were very similar for all the different discretisations. The temperature results seemed to converge to values in the range 0.627 to 0.635 for x around 1.360. As can be seen the differences between the temperature values for the sets of results for the various combinations of Δx and Δy were very small. This result is also illustrated, clearly, by the graphical representation of the figure 5.5, where all curves, (t_{21} to t_{25}), seemed to follow the same shape.

Two cases, one using each method, were plotted against each other, in figure

5.6. The curve of (expl) represented the results produced from the explicit case where Δx =0.003 and r =0.415. The graph of (cns) represented one case from the Crank–Nicolson method, with Δx =0.003 and r =1.2. Although the number of points differed in both situations the results were quite acceptable, since both curves had similar shapes and gave very similar temperatures for a long distance downstream from the slot. Finally, from figure 5.5 it can be seen that the explicit method reached the main stream temperature quicker than the Crank–Nicolson scheme. Thus a small difference existed between the two numerical schemes for temperature values at a long distances downstream of the slot. Nevertheless, this difference was only between 1 and 2%, as it may be seen in table 5.4.

5.8. CONCLUSIONS FOR THE CASE T_y=0

A numerical study was performed on the problem of heat transfer in subsonic main flow, when a secondary fluid is injected from a slot. The latter was at lower temperature than the former and as it came out of the cavity formed a thin film downstream from the slot. Both flows were taken to be irrotational and time independent and the fluids incompressible. Our aim was to calculate the temperature downstream from the slot in the area of the film and on the wall and find the distance away from the cavity at which the temperature would get significantly high. It was assumed that there was no heat transfer between the wall and the fluid, the wall was perfectly insulated, (T_y=0), although in most realistic cases the blade surface is not perfectly insulated due to internal blade cooling, see section 3.4.

Two methods were used, in order to be able to compare results and be sure that the results produced were trustworthy and accurate. The two methods were an explicit method and an implicit scheme. The results of both methods seemed to be in good agreement with each other and both models have predicted quite accurately the distance downstream from the slot at which the temperature rose to a critical value.

It may be seen that the above numerical schemes were very economical methods of solving heat transfer problems quickly and quite accurately. From the various tests that were performed it was obvious that there was no mesh dependence for any of the methods, since the various combinations of Δx and Δy used, seemed to produce

similar results all the time. However, when the results of the schemes were plotted against each other there was a small difference, around 1 to 2%. Nevertheless, they both produced curves with similar shapes and similar behaviour.

x	Explicit Method	Implicit Method
1.000	0.0000	0.0000
1.155	0.2675	0.2667
1.340	0.5374	0.5255
1.400	0.5887	0.5768
1.710	0.7524	0.7376
2.130	0.8553	0.8456
2.460	0.9101	0.8961
2.650	0.9306	0.9202
2.897	0.9606	0.9434

TABLE 5.4. Comparison of the two numerical methods for the case $T_y = 0$

In cases where we wanted to determine the temperature profiles a long distance downstream from the slot we had to use a scaling factor, which produced an exponential mesh. This enabled us to calculate $T(x)$ far downstream of the rear edge of the slot. Also Δx had to remain small during the whole process in order for both methods to produce accurate results.

From all the plots it may be seen that the temperature in the film would eventually reach the main stream temperature, but this would happen a long distance from the rear end of the slot. For both methods it seemed likely that the film temperature would reach the main stream temperature at distance of about 3.10 slot–widths.

By using the simple explicit method, or the Crank–Nicolson scheme, it would be very easy to find the distance downstream of the slot over which the film temperature rose significantly. It may be seen that for a distance of about 1.28 to 1.30 slot–widths the temperature of the film was close to 0.5 of T_1, and it reached 99% of T_1 at a distance of about 3.00 slot–widths. Thus the engineer can determine quite accurately the wall surface temperature and decide whether or not to use another slot arrangement downstream of the first hole, in order to keep the film temperature of acceptable levels and hence improve the life expectancy of the turbine blade.

Finally, it has to be said that, if a different value for the constant δ was used it would be possible that the film cooling process would be affected, due to the different properties that the fluids would possess. Removing this dependence would however amount to nothing more than a scaling in x.

5.9. THE HEAT TRANSFER CASE WITH $T_y \neq 0$

Another problem that was examined was the case where there was heat flow across the surface of the wall, i.e. the wall was not insulated. In this case heat transfer between the wall and the fluid was modelled by using the boundary condition

$$T_y = h'(T_w - T_f),$$

where h' is a constant called the heat transfer coefficient, T_w the temperature of the wall (usually the unknown quantity) and T_f the temperature of the fluid. This problem represented a more realistic case of the actual phenomenon of heat transfer met in the turbine engines and their components.

This problem approached in a similar way to the case when T_y =0. The only difference this time was the boundary condition at y =0. Thus both computer codes (for the explicit and the Crank–Nicolson schemes) were slightly modified in order to include the new boundary condition. The only problem that arose was the calculation of the heat transfer coefficient. However, after a literature search an empirical expression for h' was found and used in both programs. The equation for the coefficient is given by Jacob (1959) and is

$$h' = 0.057 \left(\frac{k}{d}\right)^{0.22} (\rho c_p U_\infty)^{0.78},$$

where k is the thermal conductivity, d the distance downstream of the slot, which varies according to x, ρ is the density of the fluid, c_p is the specific heat capacity and U_∞ is the velocity of the main flow. Some typical values for the above parameter were found by referring to Janna (1986). Thus we obtained: $\rho = 0.352$ kg/m^3, $c_p = 1141.7$ J/(kgK), $k = 0.06752$ W/(mK) at a temperature of $K = 1000$. The calculations for the temperature profiles were now carried out using the expression for h'.

5.9.1. Numerical Calculations

In order to implement the new boundary condition into the computer codes we first had to express it into a finite difference form in a similar way as before, section 5.3. Thus the expression $T_y = h'(T_w - T_f)$ became

$$T_y = \frac{t_{n,2} - t_{n,0}}{2l} = h'(t_{n,1} - T_f), \tag{5.16}$$

but $T_f = T_1$, where T_1 is the temperature of the main flow and $T_1 = 1$, thus equation (5.16) was solved for the unknown grid point $t_{n,0}$ and became

$$t_{n,0} = t_{n,2} - 2lh'(t_{n,1} - 1).$$

In this way we eliminated the fictional point $t_{n,0}$ and we used the two finite difference methods (simple explicit and Crank–Nicolson) to solve the problem.

Apart from this change in the FORTRAN programs the same process as before was followed. Thus the step in the x–direction was kept relatively small, the mesh was extended at a long distance downstream of the slot by using a scaling factor and Δy was allowed to take values up to 0.085. In this way the accuracy of the solution was kept at acceptable levels. Different combinations of Δx and Δy were used in order to check that the solution was independent of the mesh points for both the numerical methods. Finally, the ratio for the explicit method was kept less than $\frac{1}{2}$ in order to have a stable numerical scheme.

5.9.2. Results and Discussion

Both methods were tested for many different combinations of Δx and Δy, which meant that we used a wide range of ratios. The methods seemed to produced very accurate results of the temperature profiles on the wall surface.

The graph of figure 5.7 shows the four different cases for the explicit method. Each graph was produced with different values of r, and for some cases the number of grid points differed too. Table 5.5 shows the estimated temperature values for the

wall surface for four combinations.

Δx	r	$T(x)$	x distance	Curve name
0.001	0.400	0.4466	1.358	t_{41}
0.003	0.415	0.4567	1.365	t_{43}
0.002	0.421	0.4424	1.351	t_{42}
0.003	0.467	0.4505	1.365	t_{44}

TABLE 5.5. Wall temperatures obtained by the explicit method, case $T_y \neq 0$

It may be seen that the values were slightly lower than the ones produced in the previous case. This was due to the fact that the wall was not insulated this time and heat was allowed to pass across its surface. This meant that for the region downstream of the slot the wall and the film would be at a lower temperature than before, due to internal cooling of the turbine. Thus the blade surface and the film would reach the main stream temperature later than before.

The Crank–Nicolson method handled ratios r which exceeded the value of $\frac{1}{2}$. As may be seen from table 5.6, where only some combinations are tabulated, the ratio reached values up to 3.333.

Δx	r	$T(x)$	x distance	Curve name
0.002	0.420	0.4431	1.351	t_{52}
0.001	1.479	0.4465	1.358	t_{51}
0.003	3.333	0.4517	1.365	t_{53}

TABLE 5.6. Wall temperatures obtained by the implicit method, case $T_y \neq 0$

The temperature values produced from the explicit method were very close to the results calculated by the Crank–Nicolson scheme. The difference between the cases was very small, which allowed us to believe that the Crank–Nicolson scheme produced more accurate results, since it is a method which can use any given values for r and can achieve convergence faster. From the graph of figure 5.8 we can see that the curves of most of the cases were very close together, thus we can conclude that there was no mesh dependence.

Finally, a comparison was made between two of the most representative cases, one from each method, in order to investigate the behaviour of each numerical scheme at a long distance downstream from the slot. It was chosen to use Δx =0.001, and r =0.400 for the explicit method (expl) and for the Crank–Nicolson scheme (cns): Δx =0.002 and r =2.45. The two cases were extended to a distance of about 4.00 slot–widths downstream of the slot. The graph of figure 5.9 shows the explicit method (expl) together with the curve of the Crank–Nicolson scheme, (cns). It may be seen that both methods produced very similar results. Nevertheless, there was a difference between the numerical values of the temperature profiles produced by the two methods, but it was very small, around 1 to 2%, or in some cases even less, table 5.7.

x	Explicit Method	Implicit Method
1.000	0.0000	0.0000
1.101	0.1312	0.1348
1.305	0.3948	0.3871
1.816	0.6801	0.6767
2.070	0.7523	0.7452
2.428	0.8320	0.8211
2.681	0.8739	0.8699
2.939	0.9096	0.9007
3.280	0.9497	0.9358
3.514	0.9757	0.9664
3.735	0.9951	0.9829

TABLE 5.7. Comparison of the two numerical methods for the case $T_y \neq 0$

Since ΔT, where $\Delta T = T_w - T_f$, was not constant and the wall was not insulated the temperature rose very quickly on the surface of the wall near the trailing edge of the slot, where the thickness of the film was small. However, it took longer for T_w to reach T_1, since the wall surface absorbed an amount of the heat supplied by the main flow. The surface was subject to internal cooling thus its temperature was also affected by the temperature of the inner region of the turbine blade (lower than the free stream temperature). Thus conduction between the film fluid and the coolant of the turbine component took place and slowed down the process of heat transfer and

heating up the wall surface, i.e. convection was slower than before.

We have to mention here that the results obtained could have been different, if a different expression for h' had been used. The value of the coefficient h' was found experimentally and it is possible that this heat transfer coefficient is valid only for a few heat transfer problems, or only for a given distance downstream of the slot.

Another factor which also needs attention is the form of the boundary condition. It can be seen that the derivative on the wall surface depended also on the fluid temperature, in our case the main flow temperature T_1; if a different scaling was used for T_1 the derivative condition would change and the final outcome would change too. So it is possible to have different results depending on the normalization that we used at the formulation of the problem.

Nevertheless, we knew from the test problem and the previous case that the two numerical methods were implemented correctly. Thus the results they produced were trustworthy and reliable.

5.9.3. Conclusions for the Case $T_y \neq 0$

This numerical study involved the investigation of secondary flow injected across a free stream flow. The main stream flow temperature was T_1 and the secondary flow had temperature T_0, where $T_0 < T_1$. Our aim was to calculate the temperature profiles on the wall surface downstream from the injection, formed in the region of the film, where heat flux existed across the wall, i.e. the wall was not insulated.

Two methods, which were used for the previous two heat transfer problems, were utilized again. The two methods were a simple explicit method and the Crank–Nicolson method. Many tests were performed to examine the mesh dependence of the methods. It was shown that the two methods gave accurate results independently of the various combinations of the ratio r used.

However, it would have been possible to obtain different results if a different expression for the heat transfer coefficient was used, or if a different equation for the boundary condition was used, i.e. the scaling of the fluid temperature was taken to be different from $T_1 = 1$ and $T_0 = 0$ for the outer flow and the slot respectively.

Finally, the results produced from both numerical methods were very close to each other. A difference of about 1.5% suggests that the numerical schemes were used correctly, there was no mistake in their implementation into computer codes and the results produced could be believed to be accurate.

5.10. HEAT TRANSFER WITH CONSTANT WALL TEMPERATURE

This problem involved the calculation of the heat flux across the surface of the turbine blade when the wall temperature, T_w, was known and taken to be constant. Thus T_w was set equal to T_0 on $y = 0$ (internal cooling of the turbine blade was assumed to have kept the blade surface at a constant temperature) and by keeping the other boundary conditions the same as before ($T = T_0$ at $x = 1$ and $T = T_1$ at $y = S(x)$, where $S(x)$ is the streamline) we tried to obtain T_y at $y = 0$. In this way we were able to calculate the thermal stresses across the surface of the blade.

The two computer codes, used for the case $T_y = 0$, were utilized, only this time we prescribed the condition T_w =0 at y =0. This meant that the temperature along the wall surface was known and we would be examining the rate of heat transfer across the wall some distance downstream from the slot, when the temperature of the film region was increasing.

Many tests were performed for both numerical schemes, simple explicit and Crank–Nicolson methods, and the results for most of the runs were recorded and shown in the tables 5.8–5.10 and figures 5.10–5.13. We used a range of different combinations of Δx (from 0.001 to 0.004) and Δy (from 0.05 to 0.085) for both methods, but the ratio r was kept less than $\frac{1}{2}$ for the explicit method.

5.10.1. Results and Discussion

The results of the simple explicit method in figure 5.10, show the heat transfer across the wall against the distance x downstream from the slot. It may be seen that the heat flux increased rapidly for a short distance downstream of the slot, but as x was increasing T_y started to fall. The values of T_y were very similar for all the combinations, table 5.8, which meant that the scheme for $r < \frac{1}{2}$ was not only stable,

but also mesh–independent.

Δx	r	T_y at $y = 0$	x distance	Curve name
0.001	0.278	1.5213	1.5077	t_{71}
0.002	0.312	1.5139	1.5068	t_{72}
0.003	0.415	1.4858	1.5030	t_{73}
0.004	0.469	1.5077	1.5072	t_{74}

TABLE 5.8. Heat transfer obtained by the explicit method, case $T_w = 0$

The Crank–Nicolson scheme produced very similar results to those obtained by the simple explicit method. Although there was a small difference between the two methods we can say that they both predicted quite accurately the heat transfer across the wall. Figure 5.11 shows the results obtained when T_y was plotted against x for various combinations of Δx and Δy. As it may be seen all curves were very close to each other. The same observation can be said from the table 5.9, where these combinations were tabulated, together with the values of T_y. The Crank–Nicolson method seemed to produce results which were in a very good agreement with each other, independently of the ratios or the number of points in the mesh.

Δx	r	T_y at $y = 0$	x distance	Curve name
0.003	0.494	1.5006	1.5072	t_{82}
0.002	1.200	1.5085	1.5083	t_{81}
0.004	2.500	1.5003	1.4946	t_{83}

TABLE 5.9. Heat transfer obtained by the implicit method, case $T_w = 0$

Finally, we again compared the two numerical methods at a long distance downstream from the slot. For the explicit method (expl) it was used: Δx =0.004 and r = 0.469 and for the Crank–Nicolson scheme (cns): Δx = was taken to be 0.003 and r = 3.333. The graph of figure 5.12 shows the two curves obtained when T_y was plotted against x.

From figure 5.12 it may be seen that the heat fiux and the temperature gradient across the wall were decreasing as x was increasing. This was due to the decrease of the heat transfer coefficient, h', which is proportional to $\frac{1}{d^{0.22}}$, the x distance downstream

of the slot. At the trailing edge of the cavity, where the film thickness was small, the temperature near the wall rose quickly. However, further down from the slot h' decreased together with T_y.

If we attempt to relate Newton's law of cooling, $q = h'\Delta T$ (where q is the heat transfer and $\Delta T = T_w - T_f$), with Fourier's law of conduction, $q = kT_y$ (where k is the thermal conductivity of the fluid, defined in section 5.2), on $y = 0$ we obtain

$$h'\Delta T = kT_y \Rightarrow h' = \frac{kT_y}{\Delta T}.$$

From here, it may be seen that since ΔT is constant, independent of x as x increases, the heat transfer is reduced as the distance downstream from the slot increases. Thus the heat flux declines together with h' as x goes to infinity. This means that the temperature in the film will never reach the free stream temperature, since the wall is not insulated and a substantial amount of heat is absorbed by it.

x	Explicit Method	Implicit Method
1.000	0.0000	0.0000
1.068	0.5959	0.6049
1.110	1.0180	1.0210
1.239	1.4616	1.4587
1.418	1.5259	1.5153
1.609	1.4914	1.4764
1.856	1.4456	1.4254
2.006	1.4201	1.3981
2.090	1.4010	1.3882

TABLE 5.10. Comparison of the two numerical methods for the case $T_w = 0$

From the table 5.10 it may be seen that good agreement existed between the two methods and they both predicted an increase in the heat flux at the trailing edge of the slot, whereas further downstream from the cavity both numerical schemes estimated quite accurately that the heat flux would decrease.

5.10.2. Conclusions for the case $T_w = 0$

The problem considered in section 5.10 involved the investigation of heat transfer across the wall of a turbine blade in the presence of film cooling in a subsonic environment. The aim of this work was to calculate the heat flux across the face of the wall

when the wall temperature remained constant, $T_w = T_0$, where T_0 is the temperature of the injected flow.

The two finite difference schemes used in the previous problems were utilized again. We were able to implement the new boundary condition on the wall, $T_w = 0$, and used the existing programs, with some modifications, to calculate the heat flux at $y = 0$.

Many different runs were performed for both methods, simple explicit and Crank–Nicolson method. All the results showed that there was no mesh dependence, since the results produced from both methods were very similar (although different ratios and mesh points were used) and there was only a very small difference between the temperature calculations of the two finite difference schemes. It seemed that both methods predicted quite accurately the rapid increase of heat flux above the wall surface at the rear edge of the slot and the decline of T_y at the downstream region.

Another way to calculate the heat transfer across the wall surface could also be to investigate the film cooling effectiveness η of the slot arrangement. The parameter η is defined as

$$\eta = \frac{T_1 - T_{aw}}{T_1 - T_0},$$

where T_{aw} is the adiabatic wall temperature, the wall temperature of a perfectly insulated wall. The coefficient η depends only on the two flow temperatures and the position of the wall surface. Thus at the trailing edge of the slot η is 1, where downstream of the slot the film cooling effectiveness approaches zero since the adiabatic wall temperature approaches the mainstream temperature, because of the mixing of the primary and the secondary flows. In conclusion, the two numerical schemes would be possible to predict η for a range of slot configurations and conditions. The full details of the calculations may be found in Fitt and Stafanidis (1997).

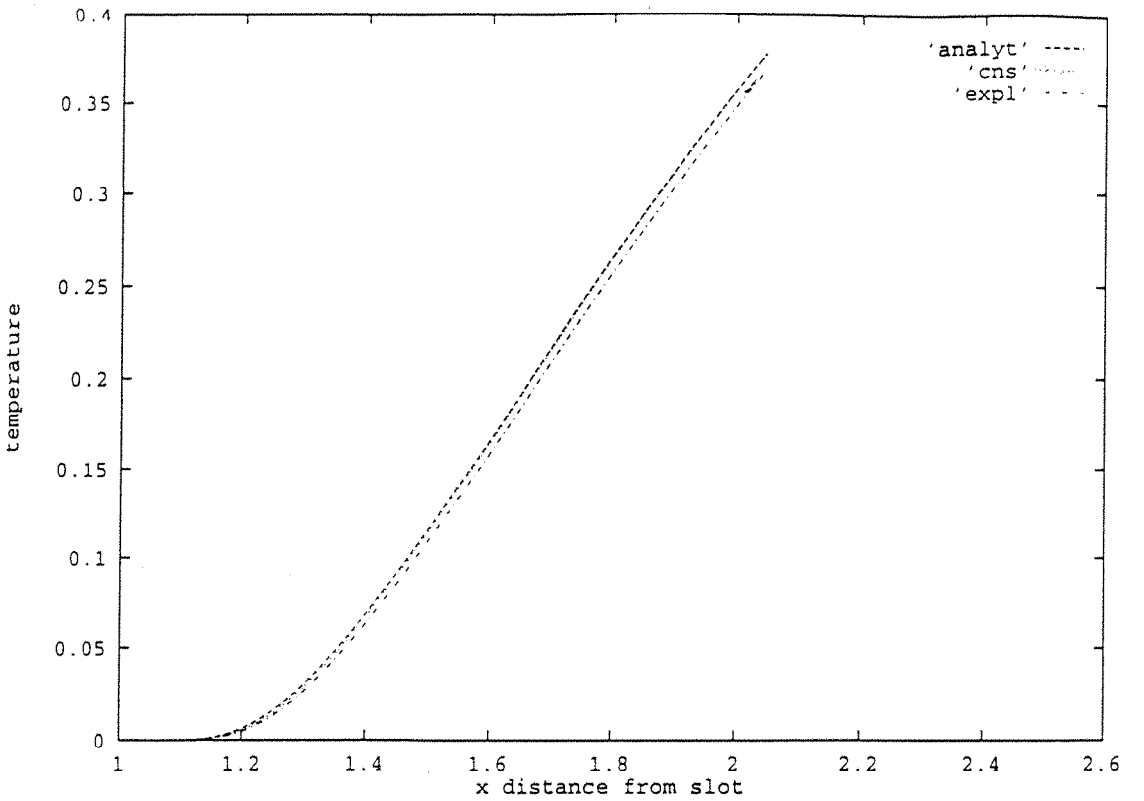

FIGURE 5.3. Temperature profiles on y=0 for the test problem for the numerical and analytical solutions

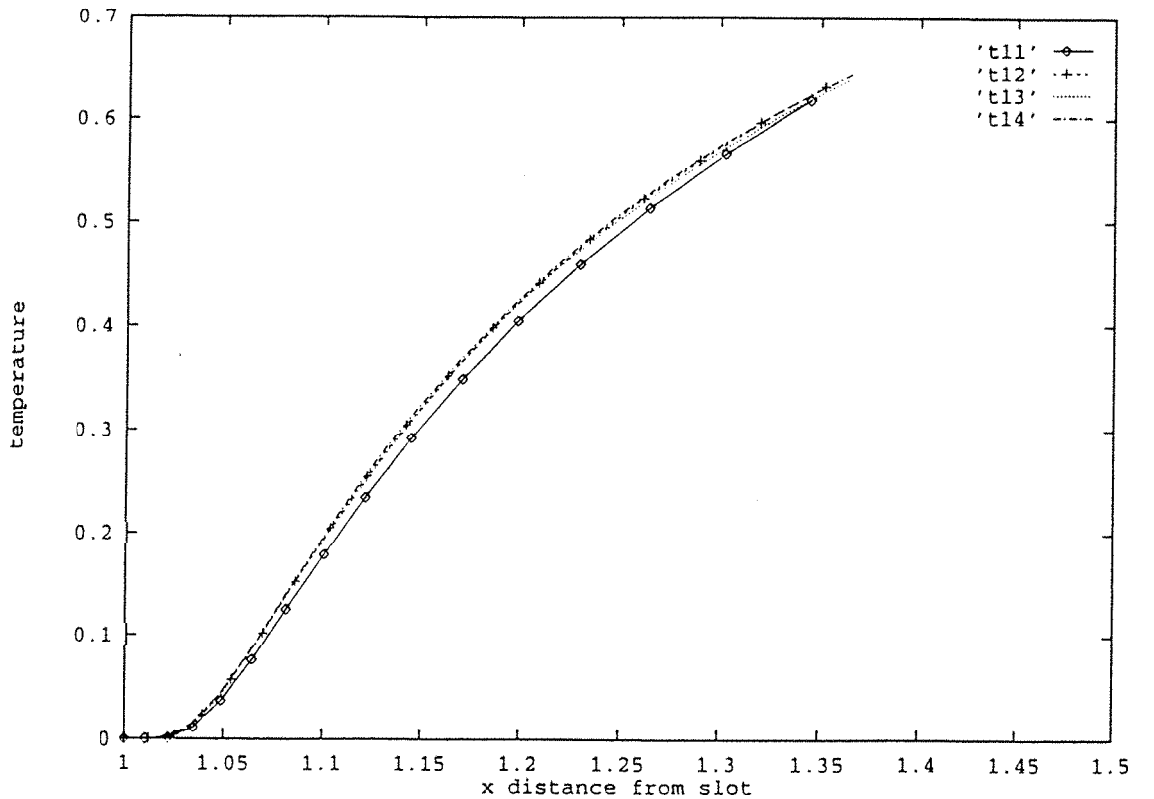

FIGURE 5.4. Graphical representation of the temperature away from the slot for the explicit method

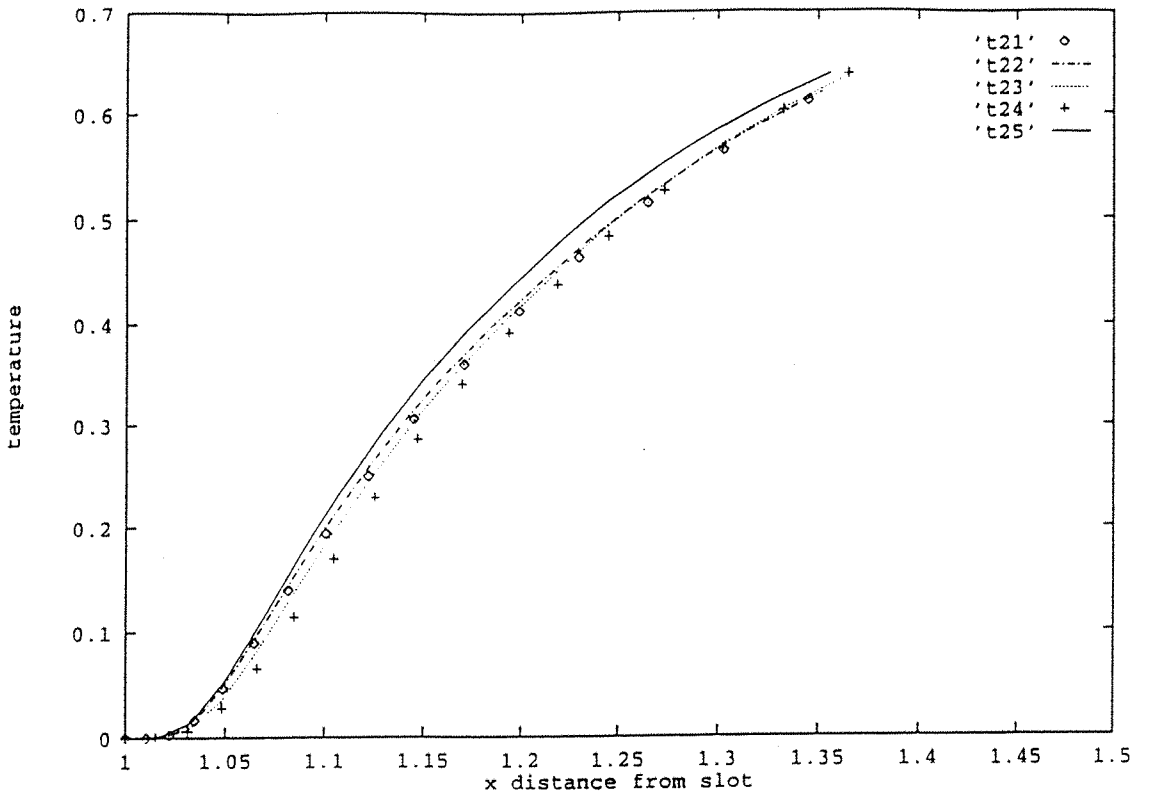

FIGURE 5.5. Graphical representation of the temperature away from the slot for the implicit method

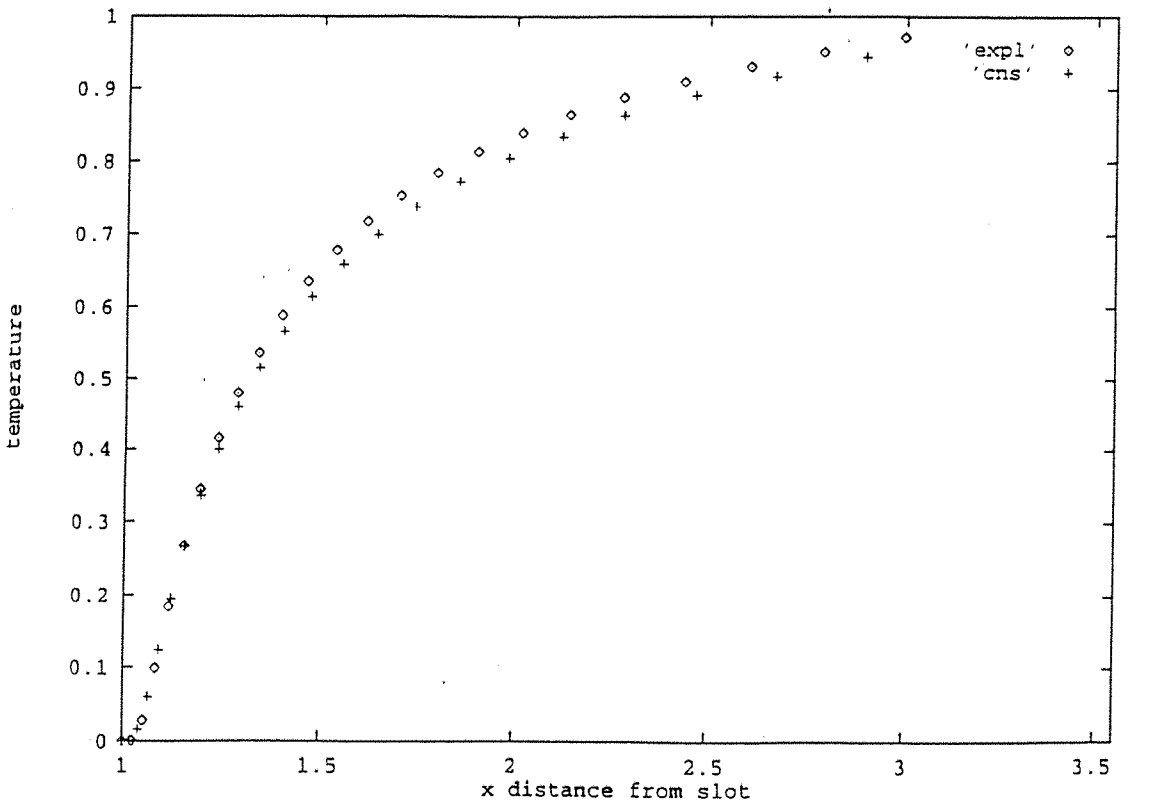

FIGURE 5.6. Graphical representation of the temperature away from the slot for both numerical schemes

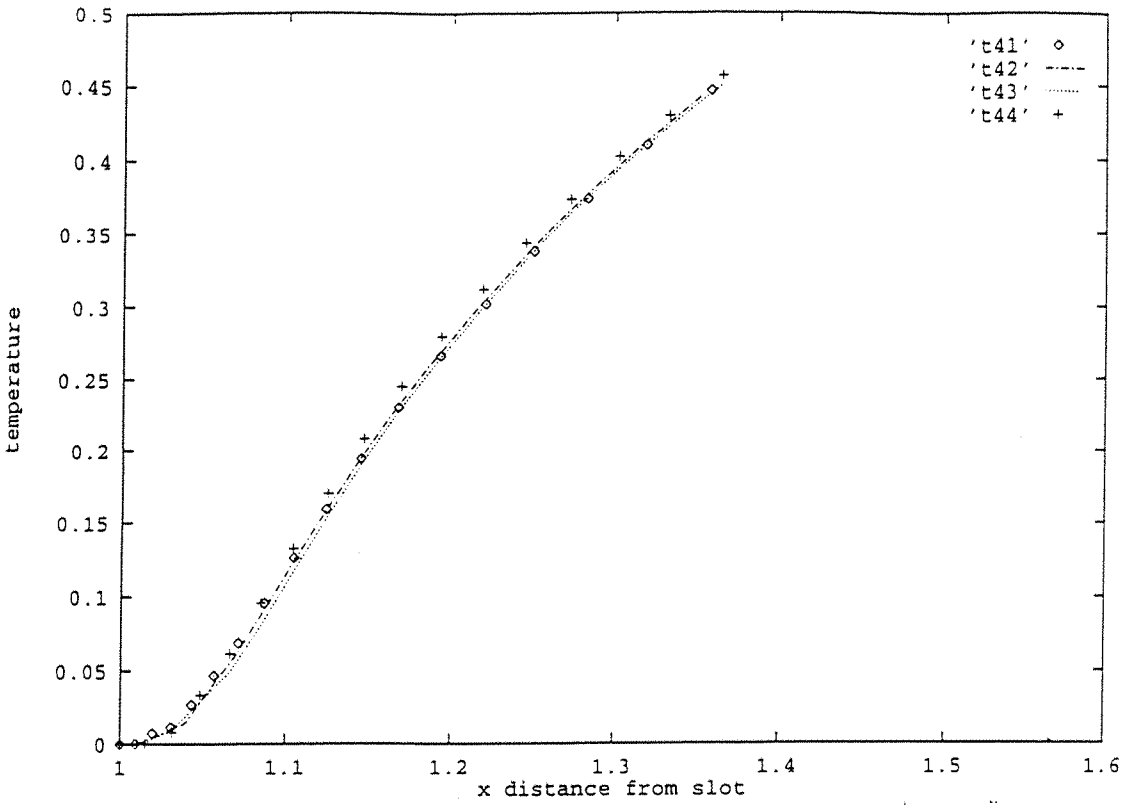

FIGURE 5.7. Graph of temperature against distance downstream from the slot for the explicit method, case $T_y \neq 0$

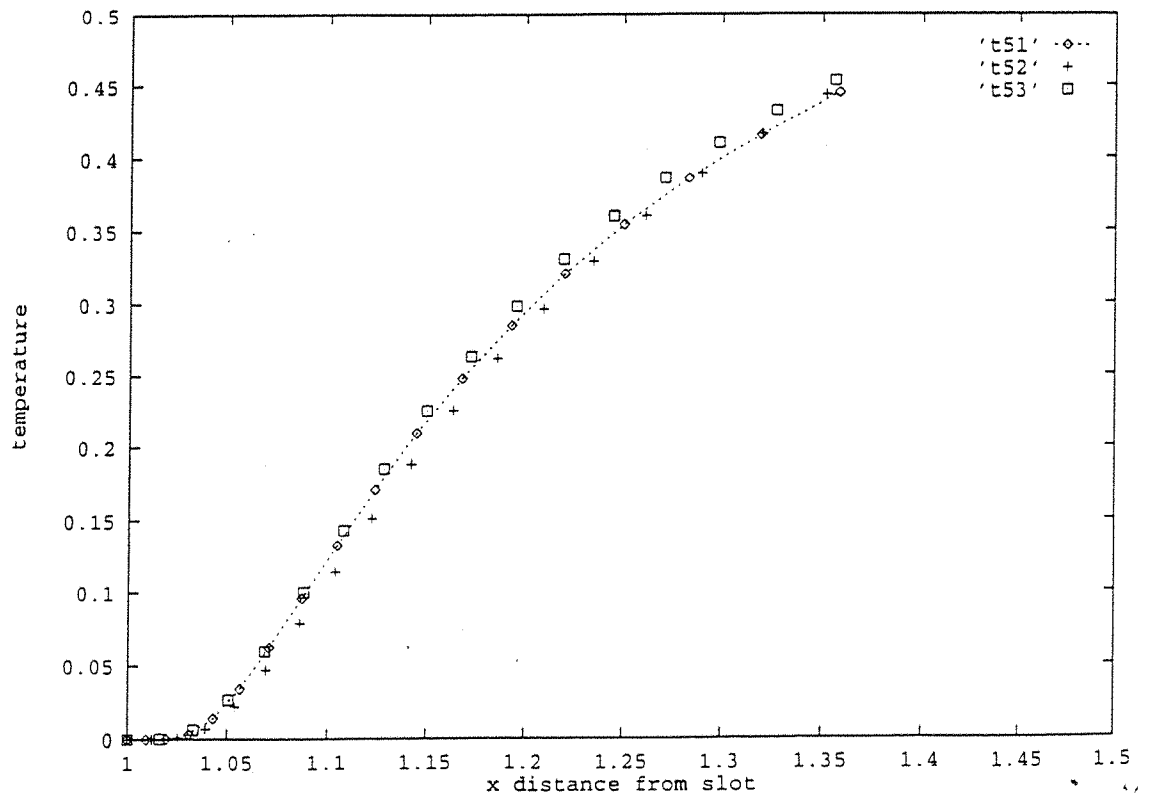

FIGURE 5.8. Graph of temperature against distance downstream from the slot for the implicit method, case $T_y \neq 0$

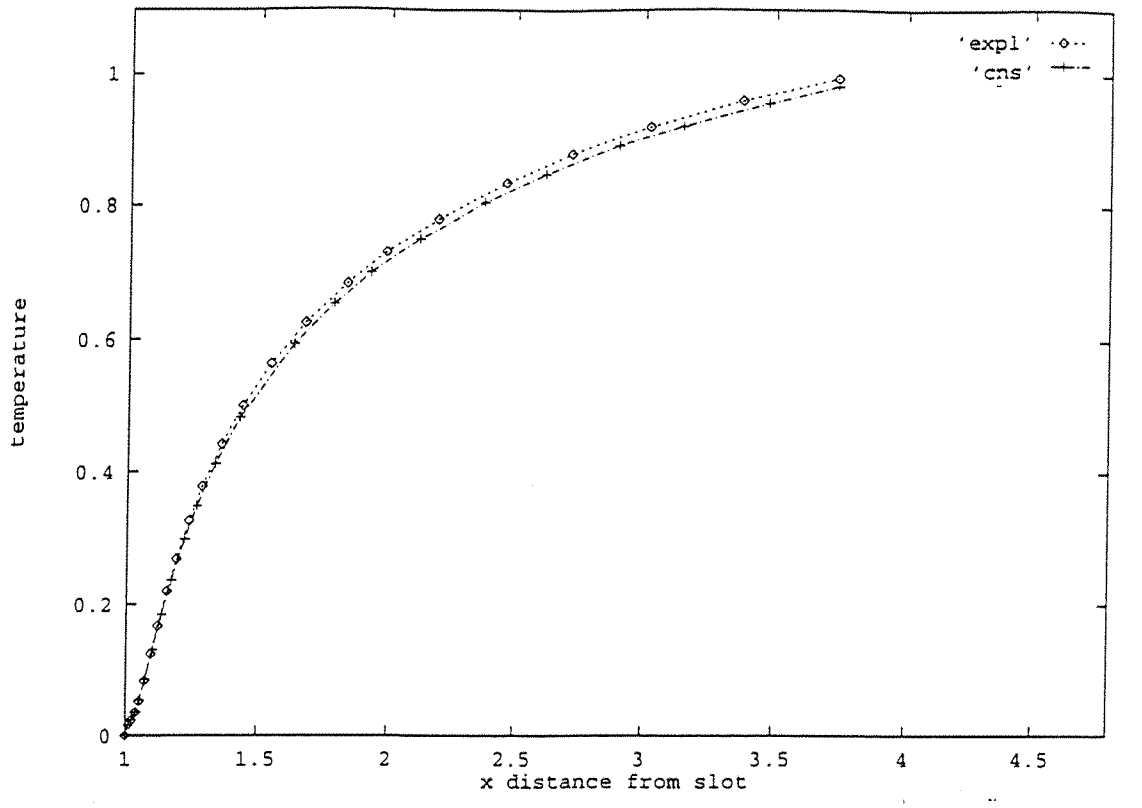

FIGURE 5.9. Comparison of the two methods for the case $T_y \neq 0$

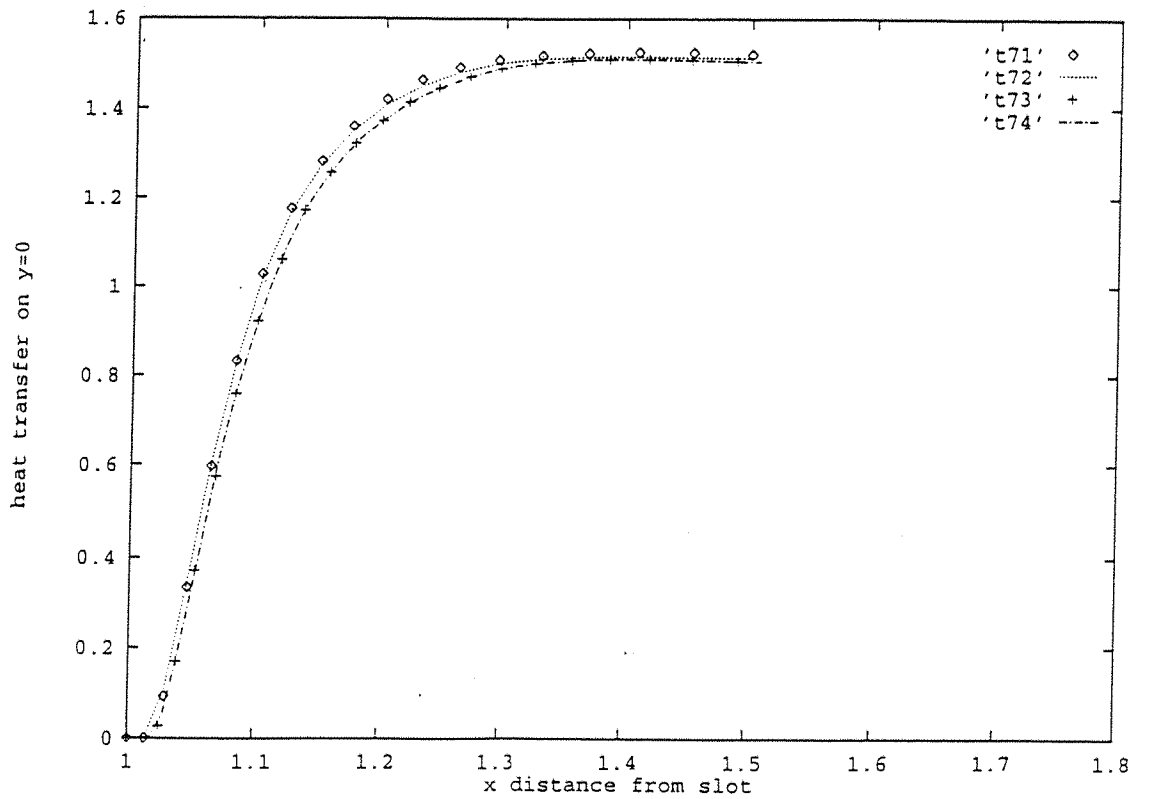

FIGURE 5.10. Graph of T_y at y=0 for the explicit method, case $T_w \neq 0$

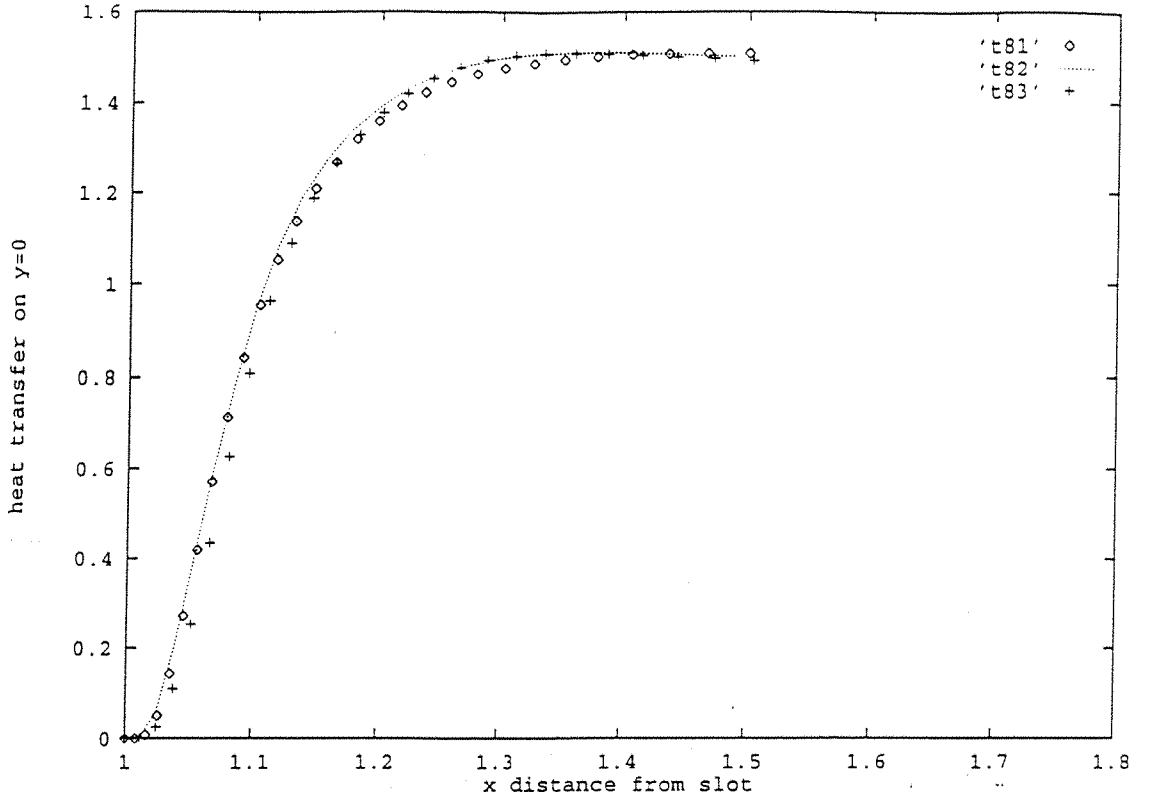

FIGURE 5.11. Graph of T_y at y=0 for the implicit method, case $T_w = 0$

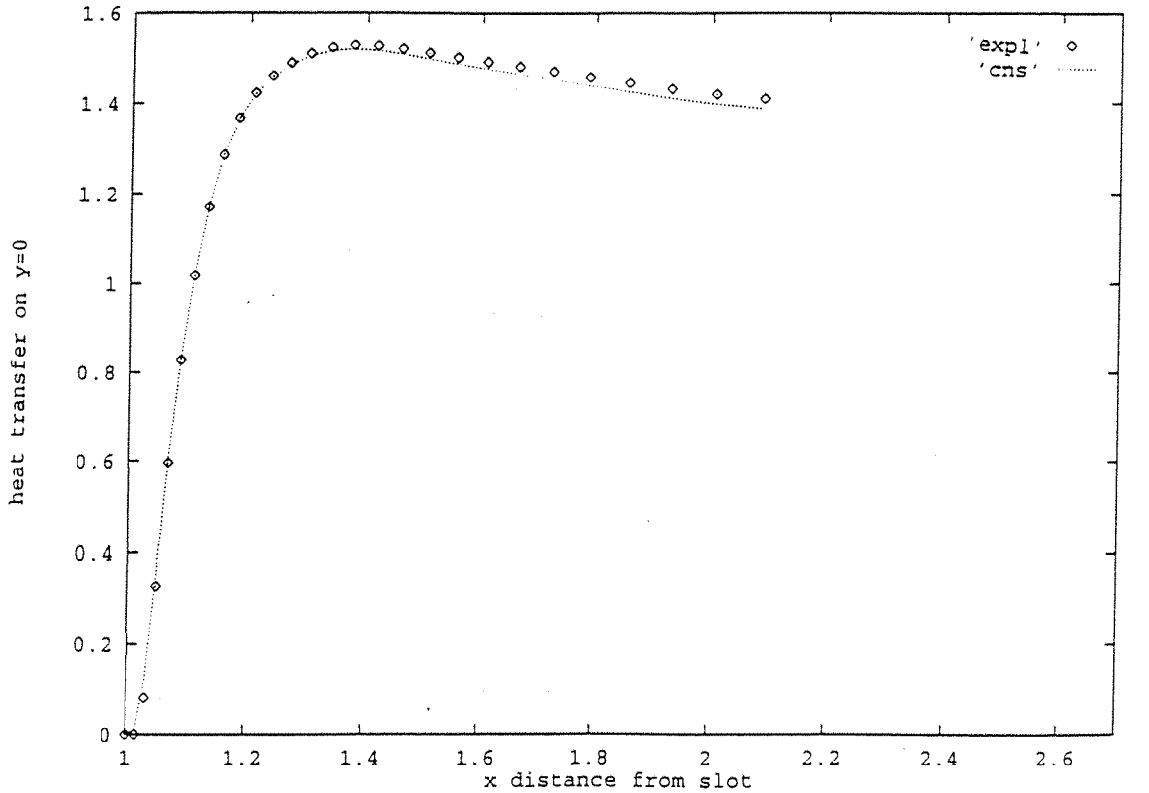

FIGURE 5.12. Comparison of the numerical methods for the case $T_w = 0$

CHAPTER 6
DISCUSSION AND FURTHER WORK

6.1. INTRODUCTION

The efficiency of aircraft gas turbine engines is strongly affected by maximum allowable turbine temperature, and the performance improvement that can be achieved by increases in this parameter are substantial. Such increases are limited by heat transfer considerations and, for this reason, many contemporary research efforts are directed at obtaining a better understanding of cooling schemes than can be incorporated into component designs in order to permit higher gas temperature operation.

The current research work represents investigations that were conducted, firstly, on the film cooling method in a supersonic regime in the turbine blade of an engine and secondly, on the effects of heat transfer on turbine components when the main flow is subsonic.

In the sections to follow we state the conclusions of the two problems analyzed and also suggest improvements and further work which might be carried out in order to get a more complete view of the problems.

6.2. THE SUPERSONIC CASE

A numerical investigation was performed on the problem of film cooling in a supersonic main flow, when a secondary flow was injected, from a slot, into the main stream. Both fluids were assumed inviscid and incompressible and the flow was time independent. Different numerical techniques were used to produce results which would

give us some idea about the process of film cooling in high speed flows. Our main aim was to calculate the mass flow across the slot by measuring the pressure difference across the streamline. The pressure difference was given by the difference of the averaged pressures of a set of points calculated on the dividing streamline by using the pressure equations for the outer flow and the film, for the area over the region of the slot. However, the results obtained seemed to be inconclusive due to the fact that a minimum Δp could not be found.

It was decided to model the unknown region of the free streamline between 0 and 1, by different polynomials. Then by comparing the pressure across the bounding streamline we would be able to find the value of mass flow that would produce the minimum pressure difference. At the beginning straight lines were used and, when this method failed, it was then decided to use smooth splines which would join the two ends of the boundary. However, after many tests it seemed that this method did not work either, since the results we were obtaining did not converge to a specific value of mass flow. Finally, an optimization technique was used, in an attempt to calculate the minimum pressure difference for a given mass flow. However, this method failed too.

It may be said that the model was very sensitive to changes in the number of grid points, especially in the region between 0 and 1. By changing the number of points, the pressure difference and the mass flow also changed. This mesh dependence was observed during all the various approaches used to solve the problem. Even test problems that were solved showed that mesh dependence existed.

It also seemed that the solution of the problem had been influenced by possible singularities in the region of the slot. The analytical solution showed us that in the inner region of the slot, very close to its edges, the boundary conditions did not hold. This phenomenon also existed in the subsonic case, but there we were able to ignore it, since it did not affect the final outcome. However, it affected the results of the supersonic case and it seemed that if further investigation on the problem had to be carried out, then these possible singularities should have been included in the formulation of the model.

It is possible that some experimental work must first be performed in order to be

able to compare the experimental results with the results obtained from the numerical investigation. Having done this, it will be easier to investigate the model in more detail and, especially, the region of great importance over the slot.

Finally, we can also take the problem forward by looking into other cases, such as the time dependent supersonic problem, the suction of air into the area of the slot ($p_\infty > p_s$, the main stream pressure is greater than the slot pressure) and also the case where, due to unsteadiness, the air can be sucked in, or injected out, as in a rim seal.

6.3. THE HEAT TRANSFER PROBLEM

The second problem that we looked into was the problem of heat transfer on the wall of a turbine blade in a subsonic environment, during the film cooling process. The temperature of the injected flow, T_0, was taken to be lower than the main cross flow temperature T_1. Three cases were examined: heat transfer in the region of the film when the wall was insulated, heat transfer in the area of the film when heat flux across the wall existed, and heat transfer across the wall surface when the wall temperature was taken to be constant. In the first two cases we were interested in calculating the wall temperature and in the last one we wanted to obtain results for the heat flux across the wall.

In order to solve the above three problems, two finite difference schemes were developed and then implemented into two computer codes. A simple explicit method and the Crank–Nicolson method were used.

For the first case, where there was no heat transfer across the wall, $T_y = 0$ at $y = 0$, the results obtained from both methods seemed to be in good agreement with each other. It was seen that both numerical methods were not sensitive to the number of mesh points, since all the different combinations used produced very similar results.

The model was not difficult to formulate, the meshes were relative easy to create and the numerical schemes very straightforward to implement on a computer. However, due to the fact that good accuracy could only be achieved with small x steps, many points were needed if we wanted to extent our mesh a long way downstream

from the slot. An exponential grid could be constructed by using a simple scaling factor to multiply it by the original Δx, the step in the x direction. Finally, the Crank–Nicolson method proved to be time consuming due to the large number of calculations that had to perform in order to estimate the temperature profiles.

The second problem was the case of heat transfer across the wall surface and the expression for the derivative boundary condition was now given by equation (5.16).

The same process as before was followed and both numerical schemes produced results which were in a very good agreement with each other. There was a slight difference between them, but, from the results produced in the previous case, we were confident that the two finite difference schemes were implemented correctly and the computer codes were written free of errors.

From the temperature profiles on $y = 0$, it may be seen that the temperature close to the rear edge of the slot rose quicker than before, but it took longer for T_w to reach the free stream temperature. This was due to the fact that the wall was not insulated anymore and a large amount of heat could pass across it. Near the trailing end of the slot, where the film thickness was small, the effect of the mainstream temperature on the blade surface was stronger than a long distance downstream of the cavity. Thus, along the wall the process of convection was slowed down.

The final case that we looked at was the problem of heat transfer in a subsonic environment when the wall surface downstream from the slot was kept at a constant temperature, $T_w = T_0$, where T_0 was the temperature of the secondary fluid and T_w the wall temperature. In this case we were able to investigate the heat flux across the surface of the turbine blade and calculate T_y at y =0.

To solve this problem the two numerical schemes developed above were employed again. It was found that both methods gave results which were mesh independent and it seemed that they predicted quite accurately the variation of the heat flux at $y = 0$ as the temperature of the film changed.

In this case T_w was constant, ΔT (where $\Delta T = T_w - T_f$) was also constant, which meant that as x increased h' decreased (since h' was proportional to $\frac{1}{x^{0.22}}$, described in section 5.9) and the temperature gradient together with the heat flux declined too.

Also a large amount of heat was absorbed by the wall surface in the inner regions of the turbine blade. This meant that the temperature of the film was seriously affected and it could never reach the free stream temperature as long as the mixing of the main and injected flows was not strong.

The Crank–Nicolson scheme is, in general, considered a more reliable numerical method than the simple explicit method, possibly because it is stable over a wider range of ratio values. Nevertheless, both numerical schemes used are very easy to implement and provide a very economical means of calculating heat transfer problems.

Finally, by using the above two numerical methods it is possible to estimate the distance on the turbine blade where the film temperature starts to reach the main stream temperature. It is essential for the designer to know the distance downstream of the slot of which the film temperature rises significantly and causes material problems to the blade. By determining this distance the engineer can improve the life expectancy of the turbine components (in our case the turbine blade) by injecting into the free stream more cooling fluid from another slot, situated downstream of the first one.

Another way to improve the life expectancy of a turbine is to investigate the effectiveness of a particular slot arrangement by looking at the film cooling effectiveness η, defined in section 5.10.2. Usually, designers and engineers prefer to use η instead of temperature readings on the wall surfaces, because in this way they can quickly obtain more information by just changing the main flow and the film temperatures T_1 or T_0 respectively,so to obtain a different η value and be able to calculate the cooling effectiveness of a particular slot arrangement.

For the same geometric situation it would be possible to investigate all the above three cases for the problem where the flow is not steady but time dependent. Also we can carry out experiments and numerical investigation for the second case ($T_y \neq 0$) when a different heat transfer coefficient is used, or in the expression for the derivative boundary condition T_1 is changed, i.e. different scaling, $T_1 \neq 1$.

Another interesting problem is the supersonic heat transfer problem. However, we would have difficulties defining the boundaries of the model, due to the fact that

the supersonic problem examined did not produce the results that we wanted, thus the position of the dividing streamline is still unknown.

APPENDIX I
REFERENCES

I.1. REFERENCES

AMANO, R. S., WANG, K. D., & PAVELIC, V. 1994, *A Study of Rotor Cavities and Heat Transfer in a Cooling Process in a Gas Turbine.* Trans. ASME *J. Turbomach.*, **116**, *pp.* 333–338.

BARNARD, R. H., PHILPOTT, D. R., 1989, *Aircraft Flight, a Description of the Physical Principles of Aircraft Flight*, Singapore: Longman Scientific & Technical, second edition 1995.

BARRY, B. 1976, *The Aerodynamic Penalties Associated With Blade Cooling*, VKI LS83.

BOYLE, R. J. 1991, *Navier–Stokes Analysis of Turbine Blade Heat Transfer.* Trans. ASME *J. Turbomach.*, **113**, *pp.* 392–403.

BROWN, S. N., CHENG, H. K., & SMITH, F. T. 1988, *Nonlinear Instability and Breakup of Separated Flow . J. Fluid Mech.*, **193**, *pp.* 191–216.

CARAFOLI, E., 1969, *Wing Theory in Supersonic Flow*, Braunschweig: Pergamon Press.

CHEW, J. W., GREEN, T., & TURNER, A. B. 1994, *Rim Sealing of Rotor–Stator Wheelspaces in the Presence of External Flow.* Trans. ASME *J. Turbomach.*, **114**, *pp.* 1–12.

CHO, H. H., GOLDSTEIN, R. J. 1995, *Heat (Mass) Transfer and Film Cooling Effectiveness With Injection Through Discrete Holes: Part II–On the Exposed*

Surface. Trans. ASME *J. Turbomach.*, **117**, *pp.* 451–459.

COLE, J. D., AROESTY, J. 1967, *The Blowhard Problem—Inviscid Flows With Surface Injection.* Trans. ASME *J. Heat Mass Transf.*, **11**, *pp.* 1176–1183.

CONTE, S. D., de BOOR, C., 1965, *Elementary Numerical Analysis, an Algorithmic Approach*, New York: McGraw–Hill Inc.

DADKHAH, S., TURNER, A. B., & CHEW, J. W. 1992, *Performance of Radial Clearance Rim Seals in Upstream and Downstream Rotor–Stator Wheelspaces.* Trans. ASME *J. Turbomach.*, **114**, *pp.* 439–445.

DANIELS, W. A., JOHNSON, B. V., GRABER, D. J. & MARTIN, R. J. 1992, *Rim Seal Experiments and Analysis for Turbine Applications.* Trans. ASME *J. Turbomach.*, **114**, *pp.* 426–432.

FITT, A. D., OCKENDON, J. R. and JONES, T. V. 1985, *Aerodynamics of Slot-Film Cooling: Theory and Experiments. J. Fluid Mech.*, **160**, *pp.* 15–27.

FITT, A. D. & STEFANIDIS, V. 1997, *Film Cooling Effectiveness for Subsonic Slot Injection into a Cross Flow. Acta Mechanica* (in press).

FOX, L. & WILKINSON, J. H., 1993 *NAG Fortran Library Manual, Mark 16*, Oxford: published by NAG Ltd.

HARASGAMA, S. P., & BURTON, C. D. 1992, *Film Cooling Research in the Endwall of a Turbine Nozzle Guide Vane in a Short Duration Annular Cascade: Part 1—Experimental Techniques and Results.* Trans. ASME *J. Turbomach.*, **114**, *pp.* 734–740.

ITO, S., GOLDSTEIN, R. G., & ECKERT, E. R. G. 1978, *Film Cooling of a Gas Turbine Blade.* Trans. ASME *Journal of Engineering for Power*, **100**, *pp.* 476–481.

JACOB, M. the Late, 1959, *Heat Transfer*, vol. I, New York: J. Wiley & Sons Inc.

JANNA, W. S., 1986, *Engineering Heat Transfer*, Boston: PWS Publishers.

KERREBROCK, J. L., 1977, *Aircraft Engines and Gas Turbines*, Cambridge, Massachusetts: The MIT Press.

McMILLIN, R. D., & LAU, S. C. 1994, *Effect of Trailing-Edge Ejection on Local Heat (Mass) Transfer in Pin Fin Cooling Channels in Turbine Blades.* Trans. ASME *J. Turbomach.*, **116**, *pp.* 159–168.

METZGER, D. E., CARPER Jr., J. H., & WARREN, J. M. 1972, *Predicted Film Cooling Near Flush Slots—Comparison With Experiment.* Trans. ASME *J. Aircraft*, **9**, *pp.* 857–863.

METZGER, D. E., & FLETCHER, D. D. 1971, *Evaluation of Heat Transfer for Film Cooled Turbine Components.* Trans. ASME *J. Aircraft*, **8**, *pp.* 33–38.

OATES, G. C., 1985, *Aerodynamics of Aircraft Engine Components*, New York: AIAA education series.

O'CONNOR, J. R., & HAJI–SHEIKH, A. 1992, *Numerical Study of Film Cooling in Supersonic Flow.* AIAA Paper, **30**, *pp.* 2426–2433.

ÖZIŞIK, M. N., 1977, *Basic Heat Transfer*, New York: McGraw–Hill.

RIZZETTA, D. P. 1992, *Numerical Simulation of Slot Injection Into a Turbulent Supersonic Stream.* AIAA Paper, **30**, *pp.* 2434–2439.

ROLLS-ROYCE LTD, 1966, *The Jet Engine*, Derby: issued by Rolce–Royce Ltd, 2nd edition.

SINHA, A. K., BOGARD, D. G., & CRAWFORD, M. E. 1991, *Gas Turbine Film Cooling: Flowfield due to a Second Row of Holes.* Trans. ASME *J. Turbomach.*, **113**, *pp.* 450–456.

SMITH, G. D., 1965, *Numerical Solution of Partial Differential Equations: Finite Difference Methods*, Oxford: Oxford University Press, 2nd edition 1978.

VAN DYKE, M., 1964, *Perturbation Methods in Fluid Mechanics*, Stanford, California: The Parabolic Press, second edition 1975.